ERROR ANALYSIS OF EXPERIMENTS

A Manual for Engineers

S.E. Nickols III

Diablo Moutain Reasearch ,LLC

Contents

PREFACE

Students are required to perform error analyses of results obtained from experiments in engineering laboratory courses. Laboratory manuals and standard texts on engineering experimentation usually contain a chapter or two on error analysis: also, students have had prior experience in lower division physics and chemistry laboratory courses. In addition, laboratory instructors are available to answer questions concerning errors in a particular experiment. Notwithstanding, when asked, nearly all students will say that they have more difficulty with error analyses than any other aspect of experimental procedures and reporting, and at the end of the course they feel that they have learned little about error analysis. I(AFM) have been an instructor in engineering laboratory courses for more than forty years, and must share the blame for this sorry state of affairs. But, better late than never, so we have undertaken the preparation of this manual on error analysis for engineering students. Because of our background, the examples and case studies presented are from the fields of heat transfer and fluid mechanics: however, the principles and methodology advocated have broad application to most aspects of engineering experimentation.

What are possible reasons for the difficulties reported by students? We can suggest three, as follows.

1. Texts on engineering experimentation emphasize statistical methods for error analysis. The only proper use for statistical methods is for the analysis of precision (random) errors: however, in most experiments performed by students, precision errors are insignificant due to the use of modern electronic instrumentation, data acquisition systems, and computers to control and process data. When there are significant precision errors, it is usually quite obvious that these errors can be reduced with an investment of more time and/or more funds for better instrumentation. To support our argument we note that standard texts often use examples from production technology to illustrate statistical concepts: why are real experimental data not used? Also, in the case studies that are presented, the precision error is very often negligible, as we claim is the rule. Of course, statistical analysis does yield results of consequence to the experimentor—but often texts fail to properly recognize the most important results, for example, the uncertainty of a sample mean and the corresponding concept for curve fits. In this manual we will introduce statistical analysis of precision errors, with an emphasis on the really pertinent results.
2. Texts do not present much material on bias errors: some sources are listed and one or two quantitative examples given. The most common example given is bias error in an instrument, which is seldom a real problem: if the bias error is significant and known, it should be incorporated in the data processing; if it is possibly significant and unknown, a different instrument should be used. The bias errors that cause students headaches are of the conceptual type. Is the sensor measuring the correct quantity? Or are the models used to explain the experimental results faithful to the real situation? The beginning student has little experience in these matters and needs to be educated. The problem is compounded by the turnover of instructors in laboratory courses. Experiments are, by their nature, challenging and often new instructors do not spend significant time mastering an experiment before attempting to teach students. An all too frequent complaint from students is that an experiment "didn't work." What this usually means is the instructor did not take the time to understand the bias errors present and take steps to eliminate the causes or develop appropriate correction procedures. Students need to see many case studies that show how bias errors were identified, and either corrected for or eliminated. Such studies should give the student ideas on how to proceed when faced with new situations.
3. Lastly, there is the recent practice of presenting rules for combining precision and bias uncertainties, based on procedures that are now *de riguer* for publication of papers in research journals, and that have been adopted by standards organizations. As most workers familiar with error analysis are aware, these rules have no scientific basis. No real attempt is made to explain this peculiar situation to the student, which is unfortunate. But, at the risk of being branded as heretics, we will go further and claim that there is seldom even a good pragmatic reason for the use of these rules. Indeed, the examples of their use given in standard texts invariably only demonstrate the folly of attempting their use. If advocates of these rules protest, let them try to explain to a bright student how to estimate a bias error at 95% coverage. Once upon a time there was perhaps a pragmatic justification for treating bias errors statistically so that the dominant precision error could be "corrected" for a smaller bias error. But if precision errors are small and the major concern is bias errors, is not this procedure a case of the tail wagging the dog? In this manual we will make the case that evaluation and intelligent discussion of possible bias errors are of more value than rules based on invalid premises.

It should now be clear to the reader that this manual will advocate some departures from current practice that will not be kindly received by some. But we hope the potential critic will keep in mind our major objective, which is to introduce students to error analysis in the context of experiments that are typical of laboratory courses and routine research. In so doing we hope the students will develop a good understanding of error analysis so that they can later appreciate the special needs of more complex experimental procedures. In addition, we hope that they will develop sufficient confidence to report their error analy-

ses in a meaningful manner, rather than simply following some rules that may not be appropriate to the particular situation.

1 Introduction

This manual presents the more elementary aspects of error analysis of experiments that students in undergraduate engineering laboratory courses should be able to master. Throughout are many examples based on real experiments that should satisfactorily illustrate the theory and procedures. Section 2 defines types of errors with the important distinction between precision (random) and bias (systematic) errors. Section 3 introduces concepts associated with a sample, such as the mean and standard deviation, and Section 4 introduces least-squares curve-fitting of data. Section 5 carefully defines how experimental uncertainty should be reported. Sections 6 and 7 deal with propagation of errors from measurements to final results, first for bias errors and then for precision errors. Section 8 discusses the use and misuse of error bars and related concepts. Sections 9, 10 and 11 go more deeply into the statistical theory used to handle precision errors. Section 9 presents features of the normal (Gaussian) probability distribution, while Sections 10 and 11 deal, respectively, with samples and curve-fitting data from parent normal populations. Section 12 briefly discusses the role of statistical inference in engineering experiments. Section 13 deals with the controversial topic of whether and how to combine precision and bias errors. Section 14 discusses sampling of time dependent data. The manual closes with a selection of case studies in Section 15, which reports in detail the development of a variety of experiments.

2 Types of Errors

Physical quantities measured in experiments, e.g., velocity, temperature, concentration, heat or neutron fluxes, etc., are subject to error. It is the custom to classify errors into two broad categories, (i) *precision* errors, and (ii) *bias* errors.

Precision Errors. Precision errors, also called *random* errors due to their nature, can have various sources. They are often associated with the "least count" of the scale on an analog instrument. For example, if a manometer has graduations at intervals of 1 mm (a *least count* of 1 mm), we can expect precision errors of about 1 mm in readings of the manometer due to the way we eye the scale. Precision errors also arise in analog to digital conversions of signals. For example, an 8-bit A/D converter can record 256 voltage levels: if it is to have a range of 10V, precision errors of about $10/256 = 0.04$V can be expected. Precision errors associated with an instrument are also called *repeatability* errors. Precision errors often result from fluctuating experimental conditions. Flow of water through a pipe system can be very steady with negligible fluctuations in flow rate; on the other hand, when an automobile engine is tested on a dynamometer, there can be significant fluctuations in the measured r.p.m. and torque.

Precision errors cause scatter in experimental data. They are amenable to statistical analysis and the theory of statistics has many powerful and useful results that facilitate a satisfactory treatment of precision errors.

Bias Errors. Bias errors, also called *systematic* errors, have many sources. The source most often mentioned in texts is a calibration error in a measuring instrument. Calibration errors may be a *zero-offset* error that causes a constant absolute error in all readings, or a scale error in the slope of output versus input that causes a constant percentage error in all readings. Scale errors are also called *sensitivity* or *span* errors. Some instruments have a bias error associated with hysteresis, that is, the output differs depending on whether the input is increasing or decreasing. Also, there can be a bias error due to local nonlinearity in the instrument response. Figure 1 illustrates calibration errors. Often a measurement technique is chosen even though it is known to have a significant bias error. A correction is then made to eliminate this bias error on the assumption that secondary bias errors associated with the correction calculation are much smaller than the primary bias error. An example is the use of an unshielded thermocouple to measure the temperature of a hot gas flow where the thermocouple temperature is lower than the gas temperature due to radiation heat losses to the cooler duct wall (see Example 4). To make a correction the thermocouple emittance and convective heat transfer coefficient must be known, and both of these quantities have some degree of uncertainty. Similarly, Example 2.6 of BHMT [1] shows how bias errors in thermocouple measurements that occur due to conduction along the leads can be corrected.

Unfortunately, there are frequently "hidden" bias errors in an experiment, that is, significant bias errors that the experimentor is unaware of. The situation is usually one where the quantity being measured is not what the experimentor thinks it is, and for this reason such errors are often called *conceptual* errors. For example, a temperature sensor attached to a surface will not read the surface temperature unless there is a good thermal contact between the sensor and surface; if not, the sensor will give a value somewhere between the true surface temperature and the ambient temperature. Even when aware of a possible problem the experimentor may choose not to correct the sensor temperature because it would be a difficult calculation to make. The literature of science and engineering has numerous examples of experimental results that are practically worthless because the experimentors were unaware of, or did not correct for, gross bias errors. It is imperative for an experimentor to attempt *quantitative* estimates of all suspected bias errors and determine the effect of such errors on the desired results. Often a significant bias error in a particular measurement can have a negligible impact on the desired result, and hence can be ignored. For example, if the radiation heat loss from a very hot object to cold

surroundings is to be determined (see Eq. 1.18 of BHMT), the surroundings temperature need not be accurately measured since the precise value has little effect on the heat loss: it is the temperature of the hot object and its emittance that must be accurately known.

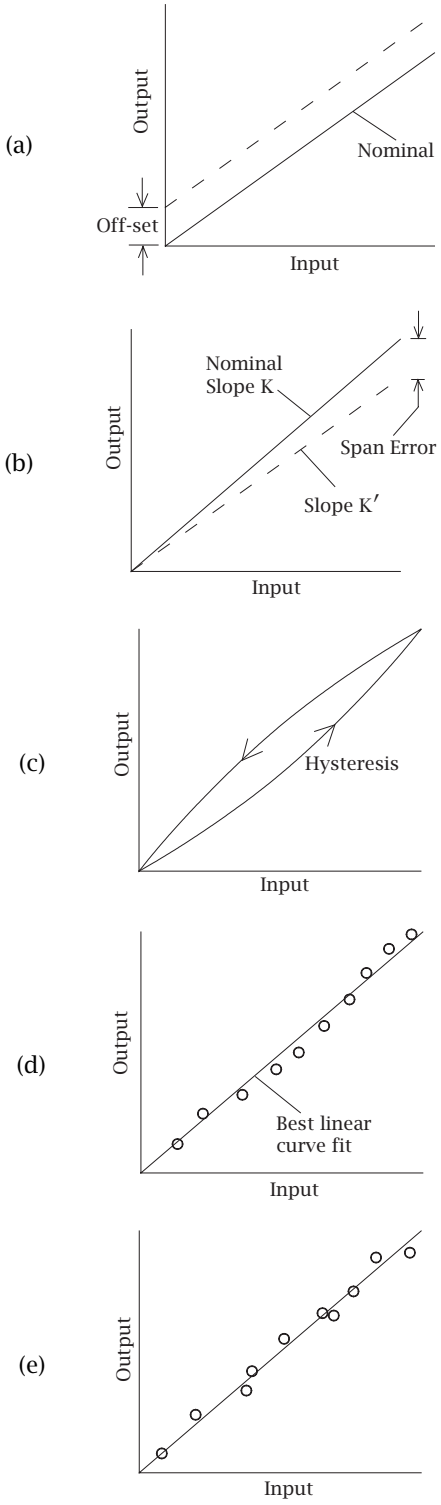

Figure 1 Instrument errors: (a) zero-offset, (b) sensitivity, (c) hysteresis, (d) nonlinearity, (e) repeatability.

Hidden bias errors are seldom encountered in frequently used test facilities using well established techniques. Examples include the use of sophisticated testing machines to measure the ultimate tensile strength of metal samples, or a wind-tunnel facility for measuring lift and drag on aerofoils. After many years of use and development, such facilities seldom give unreliable results. Problems arise when new, one-off, test rigs are designed and built. For example, there has been recently many studies of friction and heat transfer for fluid flow in microchannels to support emerging MEMS technologies. Adapting experimental techniques used successfully for macroscale components to microscale components introduces unforeseen problems and hidden bias errors in measurements. In such situations the experimentor must make a thorough numerical evaluation of all possible bias errors, initially when the test rig is designed, and later when test data are available. On the other hand, in most engineering experimentation the precision of data is of secondary concern. If more precise data are required, they usually can be obtained by investing more man-hours and more funds to purchase better equipment and instrumentation. Precision errors can be a nuisance, a gross bias error can be a catastrophe!

Often a comparison is made between theoretical and experimental results. When there are discrepancies between these results, the beginning student tends to believe that the experimental results are somehow less reliable. The student refers to errors in the experimental results when preparing a report. Of course, theoretical results do not have significant precision errors (round-off errors in numerical computations should be orders of magnitude less than precision errors in experimental data); thus, precision errors are only associated with the experimental results. Likewise, bias errors associated with sensors and instruments are also associated only with the experimental results. However, most often the largest discrepancies are due to the fact that the physical system does not exactly match the theoretical model, or conversely, the theoretical model does not exactly match the physical system. For example, when we test an automobile engine and compare the measured efficiency with the Otto-cycle efficiency of thermodynamics theory, the discrepancy is an error in the theoretical model: the test engine is reality. On the other hand, if we use theory to predict heat transfer rates for fluid flow through microchannels in an IC chip cooling system, the discrepancies between theoretical and experimental results could well be due to difficulties in making measurements on such a small scale. Then the discrepancies are appropriately viewed as errors in the experimental results. The student should always be careful to ascertain whether discrepancies between theory and experiment should be considered as errors in the theory, errors in the experiment, or perhaps in both.

Accuracy. Often instrument manufacturers quote an "accuracy" for their instrument, for example ±0.5%. Of course, a maximum error of ±0.5% is implied (the instrument is 99.5% accurate). The concept of accuracy is used

rather loosely, but usually can be taken to include errors from all sources such as bias errors associated with scale nonlinearity, and precision errors associated with repeatability of values. In essence the manufacturer is prepared to guarantee that a measurement will never have a total error greater than 0.5%.

Some important rules. Having defined the various types of errors encountered in experiments, it is now possible to introduce some rules, or guiding principles, for error analysis of engineering experiments.

Rule 1: As soon as an error from a particular source is seen to be significantly smaller than other errors present, it is given no further consideration.

Rule 2: The major concern of most error analyses is the quantitative estimate of bias errors, and correction of data accordingly when possible.

Rule 3: Whenever feasible, precision errors should be estimated from repeated tests or from observed scatter in graphed results.

Rule 4: In planning an experiment where it appears that significant bias errors will be present, an effort should be made to ensure that precision errors are much smaller.

The significance of these rules will become clear as we proceed through this manual. They are presented here so that the student can more clearly understand the motivation behind the material and examples that follow.

Example 1. Measurement of Air Temperature and Relative Humidity

The moisture content of ambient air has a critical effect on the manufacturing processes of various silicon based products, such as chip wafers and optical fibers. Thus, the air condition in experimental and production facilities needs to be measured and tightly controlled. A measurement unit that is used in production facilities is the Vaisala HMP 233 Humidity/Dewpoint Transmitter. It uses a platinum RTD to measure temperature, and the humidity sensor uses the effect of moisture on the dielectric properties of a solid polymer to measure relative humidity. The following specifications are given by the manufacturer:

Relative Humidity	
Measurement range	0–100%
Accuracy	±1% RH, 0–90% RH
(including nonlinearity	±2% RH, 90–100% RH
and repeatability)	
Temperature	
Measurement range	−40 ℃ to +80 ℃
Accuracy at 20 ℃	±0.2 ℃

The output on the computer screen is simply two columns of figures giving temperature and relative humidity at intervals of 1 second (1 Hz frequency). For example, a measurement of the laboratory ambient air gives:

T (℃)	RH (%)	T (℃)	RH (%)
21.8	50.5	21.8	50.5
21.8	50.5	21.7	50.5
21.8	50.5	21.8	50.6
21.8	50.5	21.8	50.6
21.8	50.5	21.8	50.5
21.8	50.5	21.8	50.5
21.8	50.5	21.8	50.5

What does these data tell us? Clearly, the precision errors are very small, less than 0.1% RH and 0.1 ℃. The claimed accuracy of the RH measurement accounting for both bias and precision errors is ±1.0%. Clearly, the 0.1% observed possible precision errors are negligible compared to the 1.0% (the values of 50.6% could be due to precision error or due to a fluctuation in the ambient air condition). The claimed accuracy of the temperature measurement is ±0.2 ℃. The 0.1 ℃ observed possible precision error is one-half this value: if an additional figure were displayed the possible precision error may even be smaller. Clearly the manufacturer expects a bias error approaching ±0.2 ℃. Indeed, the common wisdom is that one does not claim a total error less than 0.2 ℃ for any temperature sensor unless a very special effort is made to calibrate the sensor and process the output.

We conclude that the precision error in these measurements will be negligible for usual experimental practice.

Example 2. A Turbine Flowmeter

Turbine flowmeters are popular because of their accuracy and convenient output. Similar to the familiar anemometer used by weather stations to measure wind speed, the rotor rotational speed, proportional to flow rate, is sensed by a reluctance-type pick-up coil to give a voltage pulse rate that can be sensed by a frequency meter. The frequency can be converted to flow rate using a calibration constant for the meter, and shown on a digital display. Using the manufacturer supplied calibration constant, and accuracy of 0.5% or 1.0% may be claimed for a flow range down to 1/10 of the maximum flow rate. At lower flow rates the response becomes increasing nonlinear. If the standard accuracy is not sufficient, the manufacturer will supply a calibration, and perhaps specify a 0.25% accuracy. A sample calibration is shown in Table 1.

We see that the deviation has a maximum of 0.2% and only occurs for two of the ten tests. The manufacturer claims that the "true" flow is within ±0.15% of NIST flow standards. Due to its regular variation with flow rate we suspect that the calibration error is a bias error, and we really do not know whether the ±0.15% is a bias or precision error, or both. These errors are small and we are not likely to ever know their true nature. The manufacturer also claims a repeatability of ±0.02% of the reading: clearly this precision error is of no consequence since it is an order of magnitude less than the significant figures of

the data used in the calibration. We can certainly accept the manufacturer's claim that use of a constant K factor of 2715 will ensure an error no greater than 0.5%. On the other hand, use of the calibration table will not necessarily ensure an error less than 0.25% because of the additional 0.15% uncertainty in the "true" flow.

Table 1 Calibration of a turbine flow meter.

.

True Flow gpm	Frequency Hz	K-factor Hz/gpm $\times$ 60	Deviation[a] %
27.94	1262.2	2710.8	−0.1
19.90	899.6	2713.0	0
19.90	899.51	2712.6	−0.1
14.91	673.7	2711.8	−0.1
10.067	454.6	2709.4	−0.2
7.484	338.35	2712.6	−0.1
5.464	247.74	2720.4	0.2
3.508	158.87	2717.3	0.1
3.505	158.76	2717.8	0.1
2.309	104.47	2714.7	0.0

[a]The deviations are from an average K factor of 2717.04.

Comments:

1. Errors of less than 0.5% in a flow rate are usually of no consequence in a fluid flow or heat transfer experiment. Thus, for practical purposes, we can assert that there is negligible error in the flow rate measurement and not concern ourselves further.
2. When used in test rig there may be flow fluctuations large enough to give a significant random variation in the flow rate. In a steady state experiment, a sample of measurements over a chosen time period should be taken and averaged: such a process should eliminate any concern of a precision error due to this random fluctuation. In a time dependent experiment the flow rate data can be smoothed using a least squares technique (similar to curve fitting as described in Section 5).

Example 3. Flow Rate Measurement using a Laboratory Burette.

A simple laboratory burette is used to measure condensate flow rate in a condensation experiment. Just prior to making a measurement the valve is closed, and subsequently the time required for the meniscus to pass from the 0 ml to the 10 ml graduation, say τ s. The condensate flow rate is then calculated as $10/\tau$ ml/s. But this value is too high because the liquid film on the burette inside wall reduces the volume being filled below 10 ml. Let us estimate the resulting bias error for water at 300K and a measured flow rate of 3.1 ml/s. The burette inside diameter is 12.00 mm.

The water is seen to wet the wall well to give a film on wall. To estimate the error the liquid film is assumed to be in laminar flow and uniformly distributed around the circumference. Then the film thickness δ is related to the mass flow per unit width of film Γ as

$$\delta = \left[\frac{3\nu_\ell \Gamma}{\rho_\ell g}\right]^{1/3}$$

which can be derived from Eq. (7.5) of BHMT for $\rho_v << \rho_\ell$.

$$\begin{aligned}\Gamma &= \left[\frac{(3.1\times10^{-6}\mathrm{m^3/s})(996\,\mathrm{kg/m^3})}{(\pi)(12\times10^{-3}\mathrm{m})}\right]\\ &= 8.19\times10^{-2}\,\mathrm{kg/m\,s}\\ \delta &= \left[\frac{(3)(0.87\times10^{-6}\,\mathrm{m^2/s})(8.19\times10^{-2}\,\mathrm{kg/m\,s})}{(996\,\mathrm{kg/m^3})(9.81\,\mathrm{m/s^2})}\right]^{1/3}\\ &= 2.8\times10^{-4}\,\mathrm{m}(0.28\,\mathrm{mm}).\end{aligned}$$

The volume fraction occupied by the film is

$$\frac{\pi D\delta L}{(\pi D^2/4)L} = \frac{4\delta}{D} = \frac{4(0.28)}{12} = 0.093(9.3\%).$$

Thus, the bias error in the flow rate is about +10% and should be corrected for.

Comments: Once we have corrected for a bias uncertainty in our data processing, it is no longer an uncertainty. However, we may have introduced secondary bias errors due to uncertainty in our calculation procedure. For example, at higher flow rates Eq. (7.5) becomes inaccurate due to waves appearing on the surface of the film. We always try to ensure that these secondary errors are negligible.

Example 4. Temperature of a Hot Air Flow.

A thermocouple is used to measure the temperature of a hot air flow in the center of a large duct. The thermocouple reads 255 ℃ when the duct walls are at 100 ℃. The emittance of the thermocouple is estimated as 0.85, and the calculated convection heat transfer coefficient between the thermocouple and air flow is calculated to be 110W/m^{2}K. We wish to estimate the true temperature of the air and the associated bias error in the thermocouple reading.

The thermocouple must be at a lower temperature than the air in order for the radiation heat lost to the duct walls to be balanced by convective heat gain from the air. Since the duct is large we will neglect conduction along the thermocouple leads to the duct wall. An energy balance on the thermocouple junction requires that

$$\varepsilon\sigma A_{tc}\left(T_{tc}^4 - T_w^4\right) = h_c A_{tc}\left(T_e - T_{tc}\right)$$

where T_{tc}, T_w and T_e are the thermocouple, duct wall and air temperatures, respectively. A small gray body in large,

Table 2 Manufacturer specified errors for a pressure transducer.

Pressure	Full Scale Span		Linearity and Hysteresis		Temperature effect one Full Scale Span		Total	
kPa	kpa	%	kpa	%	kpa	%	kpa	%
200, Typical	±7.5	3.75	0.1	0.05	1	0.5	8.6	4.3±
Maximum	±7.5	3.75	0.5	0.25	2	1	10	5.0±
100, Typical	±3.75	3.75	0.1	.10	0.5	0.5	4.35	4.35±
Maximum	±3.75	3.75	0.5	.50	1	1	5.25	5.25±
50, Typical	±1.88	3.75	0.1	.20	0.25	0.5	2.23	4.46±
Maximum	±1.88	3.75	0.5	1.0	0.5	1.0	2.88	5.76±
20, Typical	±0.75	3.75	0.1	0.5	0.1	0.5	0.95	4.75±
Maximum	±0.75	3.75	0.5	2.5	0.2	1.0	1.45	7.25±
10, Typical	±0.375	3.75	0.1	1.0	0.1	0.05	0.5	0.525±
Maximum	±0.375	3.75	0.5	5.0	0.1	1.0	0.975	9.75±
5, Typical	±1.88	3.75	0.1	2.0	0.025	0.5	0.313	6.26±
Maximum	±1.88	3.75	0.5	10.0	0.05	1.0	0.738	14.8±

nearly black, surroundings has been assumed to calculate the radiation loss. Substituting,

$$(0.85)(5.67\times10^{-8})(528^4-373^4)=(110)(T_e-528).$$

Solving, T_e = 552K (281 °C) and the bias error in the thermocouple measurement is therefore $(528-552)=-26$K.

Comments: At the experiment design stage it may be decided that this bias error is too large for an accurate correction (see Example 11 for the effect of uncertainties in ε and h_c on the error estimate). A simple solution is to use a radiation shield or multiple radiation shields to reduce the radiation heat loss to an acceptable level (see BHMT Exercise 6-22).

Example 5. Accuracy of a Pressure Transducer.

Silicon piezoresistive pressure sensors are widely used. The Omega PX200-030DV sensor consists of a single monolithic silicon diaphragm with a strain gage and film resistor network on each chip. The chip is laser trimmed to give a precise span, offset and temperature calibration. The voltage response is linear to high accuracy. Pertinent specifications are as follows (refer to Figure 1 for error definitions):

Operating temperature: 0 – 85 °C
Differential pressure range: 0 – 200 kPa
Full scale span: 40 ± 1.5 mV
Zero pressure offset: 0.05 mV typical, 1 mV maximum
Linearity and hysteresis, % full scale: ±0.05 typical, 0.25 maximum
Temperature effect on full scale span, % full scale: 0.5 typical, 1 maximum
Temperature effect on offset, % full scale: 0.5 typical, 1 maximum

The transducer output is fed to a computer controlled data acquisition system and the pressure displayed on the screen and/or used in further calculations. Before each test the transducer is zeroed by a command to the data acquisition system. Hence, the specified offset errors are of no real practical importance. The key issue is the specified errors in the full-scale span. Notice that no error is specified in the sensitivity: instead an error of ±1.5 mV is specified for the full scale span. Let us now examine the error in pressure measurements over the range 5 to 200 kPa.

The manufacturer does not state whether the specified errors are precision, bias or combined errors. However, we will consider a set-up consisting of a data acquisition system coupled to a PC. Data are sampled at 5 Hz and averaged over 2s: new values are displayed as available. Since the displayed value is a running average of 10 measurements, the precision error associated with the instrumentation should be negligible, and the errors stated by the manufacturer will be taken as bias errors. Table 2 shows these errors assuming the nominal sensitivity of 0.2 mV/kPa is programmed into the data acquisition software.

The summed "maximum" error is the absolute maximum bias error that could be present and would occur with an anomalous transducer. The summed "typical" error is the maximum bias error that could occur with a typical

transducer. Since the errors can be positive or negative, the actual net error can be anywhere in the ranges specified. We cannot be more specific. Notice that at the high end of the pressure range the full-scale span error is dominant, while at the low end the linearity and hysteresis are also important. From Table 2 we see that use of the transducer below 20 kPa usually should not be recommended: 20 kPa is 10% of full scale, and an operating range of 90% of full scale is quite reasonable. If pressures below 20 kPa are to be measured, a transducer with a much smaller full scale span should be used. In the range 20–200 kPa the typical errors are reasonable ($\cong$ 5%) considering that this model transducer is relatively cheap(about $30). A decision to use the transducer for a particular task will depend on the needs of the task (see Case Study No. 2 of §15).

3 Data Samples

If we repeat a measurement a number of times we obtain a sample of values. If the variable being measured is x, we obtain $x_1, x_2, \ldots, x_n$ for a sample of size n. The mean value of the sample is

$$\overline{x} = \frac{1}{n}\sum_{i=1}^{n} x_i. \tag{1}$$

The measured values scatter around the sample mean. The commonly used measure of the scatter is the standard deviation S_x,

$$S_x = \left[\frac{1}{n-1}\sum_{i=1}^{n}(x_i - \overline{x})^2\right]^{1/2}. \tag{2}$$

The reason for dividing by $(n-1)$ rather than n will become apparent later. Figure 2 shows a *histogram* of the data: each bar has a height corresponding to the number of measurements in the intervals of size Δx. Notice that the shape of the histogram is similar to the familiar normal (Gaussian) probability distribution. Indeed, most precision errors have the characteristic that, as the sample size becomes large, the shape of the histogram tends to that of the normal distribution. This characteristic allows many powerful methods of statistical analysis to be applied to the analysis of precision errors. We shall see that by taking a sample of measurements we can usually find all we need about the precision errors in a measurement. For example, we are almost always more interested in the sample mean than in individual measurements. If we were to take a number of samples the resulting mean values are also normally distributed, and it will be shown that the standard deviation of the mean can be estimated as

$$S_{\overline{x}} \cong \frac{S_x}{n^{1/2}}. \tag{3}$$

This is a very useful result: it tells us that there is always less precision error in a sample mean than in the individual measurements, and if the sample size is large enough the error can be negligible. (Remember Rule 1: when one error is much smaller than other errors it can be ignored.)

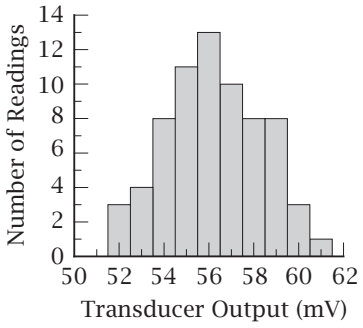

Figure 2 Histogram of a large data sample.

Whereas statistical analysis of a sample tells us a lot about precision errors, having a sample tells us nothing about *bias* errors. The *total error* in a measurement is the difference between the measured value and the true value. Figure 3 shows the total error in the k^{th} and $(k+1)^{th}$ measurements of the variable x. The total error is the sum of the fixed bias error and random precision error. If we take a large enough sample we could say that a good estimate of the bias error is $\overline{x} - x_{\text{true}}$. But the catch is that we do not know x_{true} *a priori*: x_{true} is the unknown we seek to determine. Thus, determination of bias errors has nothing to do with samples of data and statistical analysis. Bias errors are determined by engineering analysis or by comparisons with data from alternative instruments, or test rigs that have been reliably validated.

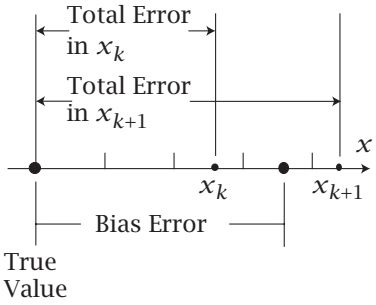

Figure 3 Total and bias errors in a measurement.

Example 6. Boiling Heat Transfer Peak Heat Flux.

A laboratory experiment involves quenching a copper sphere in liquid nitrogen contained in a Dewar flask. The sphere has a diameter of 1.27 cm and a 30 gage copper–constantan thermocouple is located at the center of the sphere. The thermocouple is connected to a signal conditioning unit that transforms the analog signal to a digital signal, which is then transmitted to a PC. In a particular experiment temperatures are sampled at 50 Hz and averaged over 0.2 s: the resulting temperature–time response is displayed and stored by the computer. As the sphere cools down, the boiling regimes change following the usual "boiling curve." See, for example, BHMT Fig. 7.15. Initially there is film boiling followed by transitional boiling, the

peak heat flux, nucleate boiling, and finally free convection. Application of the first law of thermodynamics in the form of a lumped thermal capacity model (BHMT Section 1.5) relates the surface heat flux to the instantaneous temperature-time derivative.

$$qA = -\rho cV\frac{dT}{dt}.$$

After the temperature–time response has been obtained, the derivative dT/dt is calculated using a central-difference finite difference approximation: at the n^{th} step,

$$\left.\frac{dT}{dt}\right| = \frac{T_{n+1} - T_{n-1}}{2\Delta t}.$$

The heat flux so obtained is used to prepare a boiling curve, that is, a graph of q versus $(T - T_{\text{sat}})$. Of particular interest is the peak heat flux, also called the "burn-out" heat flux since exceeding this flux can cause failure of the heat transfer surface.

Ten trials of the experiment yielded the values for the peak heat flux shown in Table 3.

Table 3 Boiling heat transfer peak heat flux.

Trial	$q_{\max} \times 10^{-5}, \text{W/m}^2$
1	1.3063
2	1.3187
3	1.2578
4	1.2873
5	1.3068
6	1.2837
7	1.2724
8	1.2303
9	1.2831
10	1.2964

The mean value of the sample from Eq. (1) is

$$\overline{q}_{\max} = \frac{1}{n}\sum_{i=1}^{n} q_{\max,i} = 1.284 \times 10^5\,\text{W/m}^2.$$

From Eqs. (2) and (3) the standard deviations are

$$S_{q_{\max}} = \left[\frac{1}{n-1}\sum_{i=1}^{n}\left(q_{\max,i} - \overline{q}_{\max}\right)^2\right]^{1/2} = 2744\,\text{W/m}^2$$

$$S_{\overline{q}_{\max}} = 2744/10^{1/2} = 868\,\text{W/m}^2.$$

Comments:

1. Although the physical phenomena involved are complex, the $q_{\max}$ value is surprisingly reproducible. The standard deviation is only 2.1%
2. Established correlations can be used to estimate a value of $q_{\max} = 1.34 \pm 0.06 \times 10^5 \text{W/m}^2$. The difference between the measured and expected results is less than the uncertainty in the correlation value.

4 Least-Squares Curve Fits

The usual engineering experiment involves two or more variables. For example, in testing an automobile engine we may determine how brake horsepower output varies with air-fuel ratio. Or in a heat transfer experiment we may determine the convective heat transfer coefficient as a function of flow velocity. Once having obtained a data set $(x_i, y_i) = 1, 2, \ldots, N$, where x_i and y_i may themselves be sample averages, we find it useful to curve-fit the data. That is, we put a "best" line through the data, and the equation of this line is a *functional relationship* between the two variables, that is, a *correlation* of the data in analytical form. In general, we can attempt to curve-fit the data with a polynomial of any order, an exponential function, or whatever we deem appropriate. Most often we attempt a linear (first order) curve-fit, that is, we fit a straight line to the data,

$$y = mx + C. \tag{4}$$

Let us now restrict our attention to this simple case, and further assume that y has significant precision error, while for x the precision error is negligible.

Our data set will now be written $(x_i, Y_i); i = 1, 2, \ldots, N$ with capital Y_i denoting a random variable, as shown in Fig. 4. Equation 4 becomes

$$\hat{Y} = mx + C \tag{5}$$

where use of the hat on $\hat{Y}$ recognizes that the values of Y will generally not fall on the curve-fit.

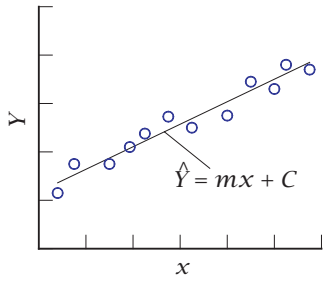

Figure 4 A least squares straight line curve fit of a data set (x_i, Y_i).

The "best" line is found by minimizing the sum of the squares of the deviations between the actual data and values given by Eq. 5. Since the deviation is $D_i = Y_i - \hat{Y}$, we seek to minimize

$$\sum D_i^2 = \sum (Y_i - \hat{Y}_i)^2 = \sum (Y_i - mx_i - C)^2 \tag{6}$$

by choosing appropriate values of m and C. To obtain these values we differentiate Eq. (6) with respect to m and C and equate the resulting expressions to zero,

$$\frac{\partial \sum D_i^2}{\partial m} = \sum x_i Y_i - C\sum x_i - m\sum x_i^2 = 0$$

$$\frac{\partial \sum D_i^2}{\partial C} = \sum Y_i - NC - m\sum x_i = 0.$$

Solving for m and C and noting that $\overline{x} = (1/N)\sum x_i$, $\overline{Y} = (1/N)\sum Y_i$

$$m = \frac{\sum x_i Y_i - N\overline{x}\,\overline{Y}}{\sum x_i^2 - (\sum x_i)^2/N};$$

$$C = \frac{\overline{Y}\sum x_i^2 - \overline{x}\sum x_i Y_i}{\sum x_i^2 - (\sum x_i)^2/N} = \overline{Y} - m\overline{x}. \quad (7)$$

Why should the least squares line be the "best" line through the data points? A simple justification is that the sample mean defined by Eq. (1) has the attribute that the sum of squares of deviations of the sample members from the mean is a minimum (check!). This idea is then extended to data correlated by a straight line where $\hat{Y}$ represents a "mean" Y value. Analogous to the standard deviation of a sample Eq. (2) we define a *standard error* for the curve-fit as

$$S_Y = \left[\frac{1}{N-2}\sum D_i^2\right]^{1/2}. \quad (8)$$

Statistics theory shows why the factor $(N-2)$ is appropriate. (Clearly, for $N = 2$ there can be no error in a straight line curve-fit.)

There are a number of issues related to curve-fitting that the student should be aware of: a brief discussion of the more important issues follows.

1. We have assumed that all the random error is associated with variable y, which was therefore written Y. If we instead assume that the random error is associated only with x, that is, we consider a data set (X_i, y), then a least squares curve-fit will give a different "best" line. But, more generally, both x and y can have random error, and then more advanced analysis is required.
2. When a data plot in rectangular coordinates is seen to be nonlinear, it is sometimes possible to obtain a linear relation on a semi-log or log–log plot. Often theory will indicate which plot is more appropriate. If we expect $y = ae^{-bx}$, a semi-log plot is appropriate, or if we expect $y = ax^n$, a log–log plot is appropriate. If a straight line is subsequently deduced, it is then the sum of squares of the deviation of the logarithm of y that is minimized, not the actual deviations. A different and more correct result is obtained by minimizing the actual deviations.
3. One has to choose a form of the functional relationship, e.g., linear, exponential, power law, etc.. Preferably there is some theoretical basis to the choice (an underlying model), but sometimes it must be a guess. A given set of data points can be fitted to more than one functional form.
4. Sometimes a data point appears incorrect, as shown in Fig. 5. The cause could be a system malfunction or human error. Often these *outlier* data points can be eliminated by inspection. If there is doubt then Chauvenent's principle can be used: this principle is described in §10.
5. Routines for straight line curve-fitting are found on most hand-held calculators and spreadsheets. In addition there are many software products for advanced curve-fitting tasks. The software is usually intended for *regression analysis* as practiced by statisticians. The difference between regression analysis and seeking a functional relationship will be discussed in §11. However, there is no difference in the least squares curve fitting methodology.
6. Sometimes the precision error depends on the value of the variable x: then the concept of a standard error can be too simplistic. The data should be graphed and checked for such anomalies.

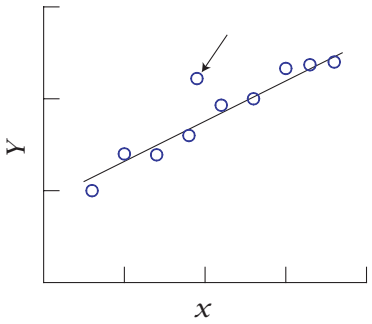

Figure 5 An "outlier" data point.

Example 7. Stagnation Line Convective Heat Transfer.

A laboratory study of convective heat transfer to a cylinder in cross-flow was conducted in a small wind tunnel. A thin film heat flux sensor is bonded to a 35.3 mm diameter thick wall copper test cylinder, as shown in Fig. 29. The heat flux sensor has a manufacturer specified calibration constant of 0.405μV/(Btu/hr ft^2). The sensor also contains a type T thermocouple that is used to obtain the sensor surface temperature. The free-stream air temperature is also measured by a type T thermocouple. Upstream of the test section is a 4 to 1 area contraction through which ambient air enters the tunnel. Pressure taps are located at the ends of the contraction and the pressure differential used to determine the air velocity in the working section: an OMEGA PX-160 series pressure transducer is used for this purpose. Data acquisition is performed by a Strawberry Tree connection Mini-16 system, with the data fed to a PC for further processing and display.

The sensor was located at the forward stagnation line and tests performed over a range of air speeds. For each test, the Reynolds and Nusselt numbers are calculated using

$$\mathrm{Re}_D = \frac{VD}{\nu}$$

$$h_c = \frac{q}{T_s - T_c};$$

$$\mathrm{Nu}_D = \frac{h_c D}{K}.$$

Table 4 and Fig. 6 show the experimental results. The figure is a plot of $\log \mathrm{Nu}_D$ versus $\log \mathrm{Re}_D$.

Table 4 Comparison of experimental and theoretical stagnation line Nusselt numbers for flow of air across a cylinder

Re_D	Nu_D Experiment	Nu_D Theory	Difference %
15025	117.1	120.6	-2.90
17527	127.1	130.2	-2.38
20007	133.6	139.1	-3.95
23331	143.3	150.2	-4.59
24880	148.8	155.1	-4.06
27196	153.8	162.2	-5.18
30008	161.1	170.4	-5.46
32583	168.1	177.6	-5.35
35026	174.2	184.1	-5.38
37215	178.9	189.8	-5.74
40003	185.9	196.7	-5.49
42500	192.0	202.8	-5.33
44998	197.4	208.7	-5.41
47463	202.7	214.3	-5.41
49992	208.8	219.9	-5.05

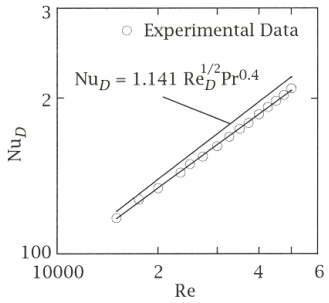

Figure 6 Comparison of experimental and theoretical stagnation line Nusselt numbers.

Since the data appear to fall on a straight line, a linear relation between $\log \nu_D$ and $\log \mathrm{Re}_D$ is suggested. A least squares linear curve-fit yields

$$\log \mathrm{Nu}_D = 0.1813 + 0.476 \log \mathrm{Re}_D$$

or,

$$\mathrm{Nu}_D = 1.199\, \mathrm{Re}_D^{0.476}.$$

The standard error of the curve-fit is defined by Eq. (8) of §4, and is

$$S_Y = 0.968.$$

Since Nu_D varies from 117.1 to 208.8, S_Y varies between 0.46% to 0.83%.

Also shown in the table and figure is the theoretical result obtained from laminar boundary layer theory, namely

$$\mathrm{Nu}_D = 1.141\, \mathrm{Re}_D^{0.5}\, \mathrm{Pr}^{0.4}; \quad \mathrm{Pr} \approx 1.$$

The discrepancy between theory and experiment varies from 2.9% to 5.7%. Since these values are considerably larger than the standard error of the curve-fit, it is clear that precision error is a minor issue. Then following Rule 1 of §2, no further consideration of precision error is justified. The discrepancy between theory and experiment should be viewed as a bias error: however this bias error is relatively small and should not be of concern for usual engineering purposes. Whether the bias error should be attributed to the instrumentation and experiment technique, or to an inadequacy of the theoretical result will be discussed in Case Study No. 1.

Since the experiment used only one fluid, namely air with a Prandtl number $\mathrm{Pr} = 0.69$, the results cannot be used to deduce the Prandtl number dependence of the Nusselt number (see BHMT §4.2.3). We can however accept the theoretical dependence of Nu_D or $\mathrm{Pr}^{0.4}$ for $\mathrm{Pr} \approx 1$, and for $\mathrm{Pr} = 0.69$ rewrite the correlation of our data as

$$\mathrm{Nu}_D = 1.391\, \mathrm{Re}_D^{0476}\, \mathrm{Pr}^{0.4}; \quad \mathrm{Pr} \approx 1.$$

Notice that the 22% discrepancy in the constants in the previous two equations is meaningless because the exponents on the Reynolds numbers are different. An alternative approach would be to assume that a one-half power dependence on Reynolds number is correct, and perform a least squares curve-fit of the data accordingly. Then the discrepancy in the constants will be of a similar magnitude to the errors shown in the Table 4.

5 Uncertainty

The terms "error" and "uncertainty" are often used interchangeably when discussing experimental results, which can be confusing to the beginning student. We need to be more precise and will follow the practice described below. We have already defined the errors in a measurement to be the difference between the measured value and the true value. However, as noted in §3, we never know the true value, so that the actual error is a rather elusive quantity. Thus, instead of actual error, we must work with estimated errors.

Precision Uncertainty. For the precision uncertainty in a measurement we estimate a *probable error* in the measurement. We need to say that we are C% confident that the true value X_{true} of a measurement X_i lies within the interval $X_i \pm P_X$: then P_X is called the *precision uncertainty* at a *confidence level* of C%. This means that if we specify a 95% confidence level estimate of P_X, we would expect X_{true} to be in the interval $X_i \pm P_X$ about 95 times out of a 100. If our sample comes from a normal population and the sample is large, the statistics theory in §10 gives that P_X can be taken to be approximately twice the standard deviation at the $C = 95\%$ level,

$$P_X \cong 2S_X(C = 95\%, N > 10). \tag{9}$$

In practice we almost always assume a normal population and use Eq. (9) for $N > 10$. In §10 we will see that Eq. (9) can be corrected for smaller samples; however if we are truly concerned about precision error we should avoid small samples—which is often quite feasible.

The probable error in a sample mean is less than in the individual measurements because $S_{\overline{X}} \cong S_X/N^{1/2}$ for N large. Then the precision uncertainty of the sample mean is

$$P_{\overline{X}} \cong 2S_{\overline{X}} (C = 95\%, N > 10). \tag{10}$$

Equation (10) is very important: it is the result of the very powerful central limit theorem of mathematical statistics and will be discussed further in §10. It is important for two reasons:

1. When we use modern data acquisition systems for steady state experiments, we usually automatically average measurements over an interval of time before even recording data. For example, we may sample a sensor signal at a frequency of 5 Hz over an interval of 2s and display a "running" mean of 10 measurements.
2. When we do have scatter due to precision errors, we are only really concerned with the mean value—that is why we take a sample average. It is always the precision of the mean that is pertinent to further data processing.

The importance of Eq. (10) has not been properly appreciated in many engineering experimentation texts. Figure 7 illustrates Eqs. (9) and (10).

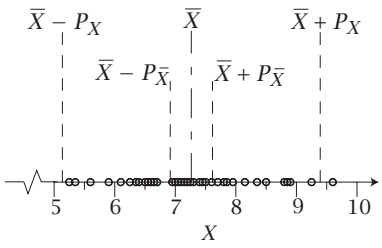

Figure 7 Precision uncertainties for a single measurement P_X, and for a sample mean, $P_{\overline{X}}$.

Now consider the situation where we have only one measurement X_1. What can we say about the precision uncertainty? We do not have a sample standard deviation to use for this purpose. All we can do is estimate (often, very roughly) a precision error from the nature of the measurement. For example, if we have a temperature given on a digital readout to 0.1°C and the temperature is not fluctuating by more than about 0.1°C, we can take $P_X \cong 0.1$°C. Obviously, we cannot make a precise statistical statement at a specified confidence level. If precision errors are of concern we should make every effort to obtain a data sample, and should not rely on a single measurement. On the rare occasion that we must rely on a single measurement, it must be understood that a precise statement about precision error cannot be made.

Our major concern for a sample was the uncertainty of the sample mean. Similarly, when we consider precision errors for a curve-fit of data (x_i, Y_i), our major concern is the probable error, or uncertainty of the curve-fit: $\hat{Y}$ for a curve-fit is like a "mean" value analogous to $\overline{X}$ for a sample of values of a single variable. The precision uncertainty for the straight-line curve-fit is

$$P_{\hat{Y}} = 2\left\{S_Y^2\left[\frac{1}{N} + \frac{(x-\overline{x})^2}{S_{xx}}\right]\right\}^{1/2} \tag{11}$$
$$(C = 95\%, N > 10)$$

where S_Y is the standard error defined by Eq. (8), and

$$S_{xx} = \sum x_i^2 - \left(\frac{1}{N}\right)\left(\sum x_i\right)^2.$$

Figure 8(a) shows that $P_{\hat{Y}}$ depends on how far x is away from $\overline{x}$: it is a minimum at $x = \overline{x}$. Equation (11) is said to give the 95% *confidence interval*, and gives the range where the curve fits will fall 95% of the time for repeated sets of measurements, as shown in Fig. 8(b). If the purpose of the experiment is to validate a theoretical model, and if the theoretical relation $Y(x)$ lies within the 95% confidence interval, we would conclude that we are 95% sure that the model is correct (or conversely, our experiment was valid: we seldom know which viewpoint to take!).

Of less importance is the uncertainty associated with a single measurement. Again suppose we have a curve-fit of data (x_i, Y_i) and we take one additional data point x_{N+1}, Y_{N+1}. The 95% *prediction interval* gives the range in which we are 95% confident this data point will fall, and is given by

$$P_Y = 2\left\{S_Y^2\left[1 + \frac{1}{N} + \frac{(x-\overline{x})^2}{S_{xx}}\right]\right\}^{1/2} \tag{12}$$
$$(C = 95\%, N > 10)$$

which is shown in Fig. 8(c). Notice that P_Y is always larger than $P_{\hat{Y}}$, analogous to P_X being greater than $P_{\overline{X}}$ for a sample. As for a sample, we seldom have use for P_Y; it is $P_{\hat{Y}}$ that is of major concern (see Example 9).

(a)

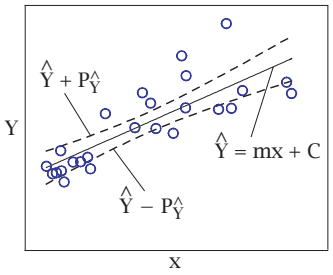

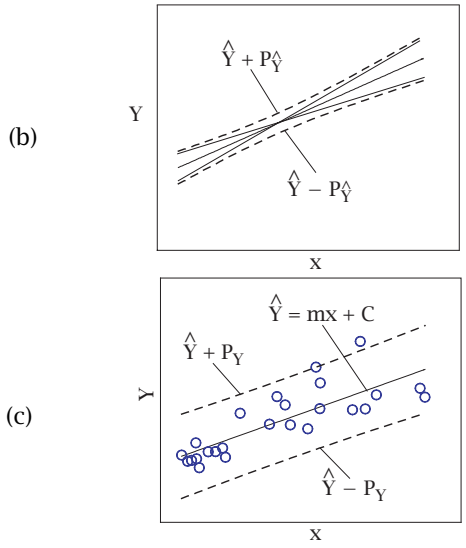

Figure 8 (a) Precision uncertainty of a straight line curve fit—the confidence interval. (b) Illustration of curve fits within the confidence interval. (c) Precision uncertainty of a single data point—the prediction interval.

Bias Errors. For a bias error we should estimate a reasonable *upper bound* as best we can, based on our knowledge of the test rig, instrumentation and technique, our understanding of the physical phenomena involved and check tests, eg. a mass or energy balance.. We shall call this estimate *bias uncertainty B*. If there is more than one source of bias error, then we should sum arithmetically to obtain the upper bound (worst case).[1] Specification of bias uncertainties is always difficult and can be quite controversial: beginning students are often understandably confused when faced with the problem of specifying a bias uncertainty. One of the main objectives of this manual is to show the student how bias errors can be handled (see Rule No. 2 in §2). At the end of the day you cannot say more than that your experimental result may have a bias error as large as *B*. It is up to the user of the result to judge whether this uncertainty is acceptable or not. A design engineer who needs to use the result for an engineering design, with its customary generous safety factors, is less demanding than a research engineer who seeks to validate a test rig or publish a paper in an engineering science journal.

The best way to identify a bias error is by *benchmark testing*, if possible. Indeed, it is good practice to design an experimental rig to facilitate benchmark testing. For example, consider building a flow loop to determine friction factors for a rectangular cross-section duct with one surface having parallel ribs to enhance heat transfer (e.g., BHMT Fig. 4.48). We should "benchmark" the rig by first obtaining friction factors for a smooth-wall duct or tube, for which accurate friction factor data are available. Such testing will indicate if there is a significant bias error that could be attributed to the sensors, data acquisition unit, or the design of the rig and sensor installations.

It is most important to understand that bias uncertainty differs from precision uncertainty in the following sense. We are usually concerned with the precision uncertainty of a sample mean or a curve-fit: these precision uncertainties can be reduced by increasing the number of data points used. On the other hand, a bias uncertainty is independent of sample size: it is the same for one data point as for a sample of 100 data points.

Example 8. Turbulent Flow in a Smooth Tube.

In an experiment to determine the friction factor for turbulent flow of water in a smooth wall tube, the pressure drop ΔP over a length L was measured over a range of flow rates. Table 5 shows the calculated results as friction factor $f = (L/D)\Delta P/(1/2\rho V^2)$ versus Reynolds number $\mathrm{Re}_D = \rho VD/\mu$. Previous experimental work has shown that a simple power low $f = C\mathrm{Re}^m$ should calculate such data well. Thus we seek a best squares linear curve fit of $\log f (= \hat{Y})$ versus $\log \mathrm{Re}_D (= x)$, to obtain

$$\hat{Y} = -0.208x - 0.6985.$$

Then $m = -0.208$ and $C = 10^{-0.6985} = 0.200$, and the power law is

$$f = 0.200\mathrm{Re}_D^{-0.208}.$$

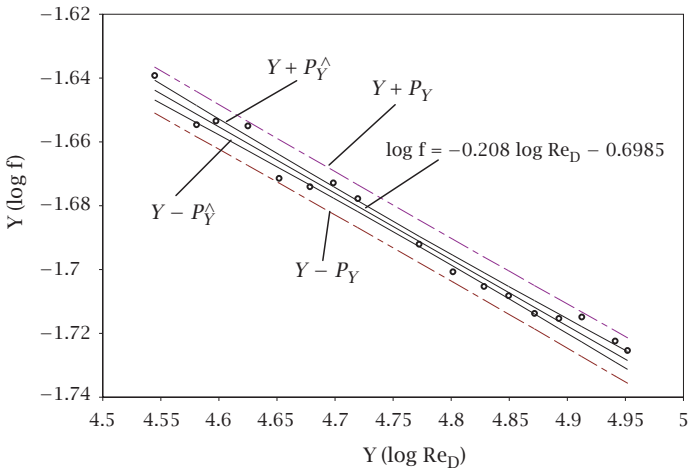

Figure 9 Log f versus log Re_D: least squares curve fit, and 90% prediction and confidence intervals.

Figure 9 shows $\log f$ versus $\log \mathrm{Re}_D$ and the least squares straight line curve fit. Also shown are the 95% prediction interval $\pm P_Y$ calculated from Eq. (12), and the 95% confidence interval $\pm P_{\hat{Y}}$ calculated from Eq. (11). Values of P_Y and $P_{\hat{Y}}$ are as given in Table 5. The precision of the data looks good, but we should give a meaningful quantitative evaluation. Once the data have been curve fitted, it is the precision of the curve fit that is of concern, not the

[1] This recommendation differs from current common practice: in §13 we will discuss other conventions.

precision of individual data points. Thus we must examine the 95% confidence interval for the curve fit. Consider $\mathrm{Re}_D = 3.505 \times 10^4$; pertinent results include

$$\hat{Y} = \log \hat{f} = -1.6438 \qquad P_{\hat{Y}} = 0.003071.$$

Then $\hat{Y} - P_{\hat{Y}} = -1.6438 - 0.003071 = -1.64751$. Taking antilogs,

$$\begin{aligned} \hat{f} &= 0.022709; \\ \hat{f} - P_{\hat{f}} &= 0.022516 \\ \frac{\hat{f} - (\hat{f} - \hat{P}_f)}{\hat{f}} &= 8.5 \times 10^{-3} = 0.85\%. \end{aligned}$$

A check of the data shows that this is the worst case, i.e., the largest deviation on a percentage basis. This result tells us that if we were to repeat the experiment, we would be 95% confident that the new least squares curve fit will not deviate from $f = 0.200\,\mathrm{Re}_D^{-0.208}$ by more than 0.85%. We conclude that our data is indeed very precise: the precision uncertainty in our result is very small.

Comments:

1. Notice that we compared f values, not $\log f$ values. Since the effect of taking logarithms is to reduce the ranges of the variable, so too are errors reduced. Check that

   $$\frac{\hat{Y} - (\hat{Y} - P_{\hat{Y}})}{\hat{Y}}$$

   is considerably smaller than

   $$\frac{\hat{f} - (\hat{f} - P_{\hat{f}})}{\hat{f}}.$$

2. We very often do least squares curve fits on a logarithmic basis in order to take advantage of the fact that power laws become straight lines. Linear curve fits can be done by all simple computational aids. From the viewpoint of rigorous statistical analysis, minimizing sums of squares of deviations on a logarithmic basis is not quite the same as when the original variables are used. This rather subtle point is ignored in general engineering practice.
3. Our least squares curve fit assumed that the precision error was contained in f through ΔP, and that the Reynolds number calculated from the flow rate was much more precise. This choice resulted from the observation that the flow rate, measured by a turbine flow meter, showed much smaller fluctuations than did the pressure drop measured using a pressure transducer with A/D conversion.
4. Notice in Table 5 that four significant figures have been given for f. No more than three are justified based on the least count of the ΔP measurement: the extra figure is given to aid further data processing. Values of f calculated from the curve fit should not be specified to more than three figures.

Table 5 Friction factors and 95% confidence and prediction intervals for a power law least squares curve fit.

$\mathrm{Re}_D \times 10^4$	f	$\hat{Y} = \log \hat{f}$	P_Y	$P_{\hat{Y}}$
3.505	0.02295	−1.6438	0.0072	0.0031
3.809	0.02215	−1.6513	0.0071	0.0027
3.958	0.02221	−1.6548	0.0070	0.0025
4.217	0.02213	−1.6605	0.0069	0.0023
4.486	0.02131	−1.6661	0.0068	0.0021
4.769	0.02118	−1.6716	0.0068	0.0019
4.995	0.02124	−1.6758	0.0068	0.0018
5.243	0.02100	−1.6802	0.0067	0.0017
5.922	0.02032	−1.6912	0.0067	0.0016
6.332	0.01992	−1.6972	0.0067	0.0017
6.735	0.01971	−1.7028	0.0067	0.0018
7.071	0.01958	−1.7072	0.0068	0.0019
7.443	0.01933	−1.7118	0.0068	0.0021
7.812	0.01926	−1.7162	0.0069	0.0023
8.176	0.01928	−1.7203	0.0070	0.0024
8.734	0.01895	−1.7263	0.0071	0.0027
8.951	0.01882	−1.7285	0.0071	0.0028

Example 9. A Natural Convection Thermosyphon.

Oil-cooled high voltage transformers can be modelled as a stack of heated plates characterized by the plate width and thickness, and the gap width. The oil is confined to move upward around the stack by natural convection: oil leaving the top of the stack is piped back to the bottom to form a thermosyphon loop. For design purposes it is necessary to have correlations for heat transfer from the plates, which are presented in the form

$$\mathrm{Nu} = f(\mathrm{Ra}, \text{geometric parameters})$$

where the Nusselt and Rayleigh numbers are usually based on a characteristic length L_c equal to flow surface area divided by flow perimeter. For long plates $L_c = 2a + t$, where a is the plate half-width, and t is the plate thickness as shown in Fig. 10. The Rayleigh number is also based on the isothermal plate temperature and the average of the upstream and downstream temperatures.

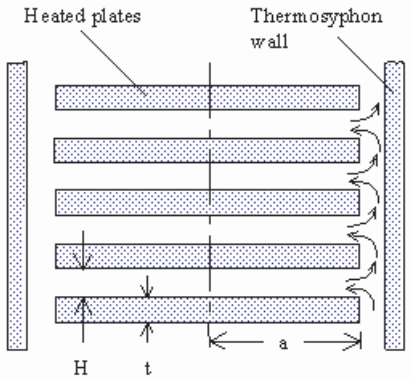

Figure 10 Natural convection thermosyphon system.

Typical results are shown in Fig. 11 for a plate gap $H = 1.27\,\text{cm}$, giving a gap to the plate half-width ratio $H/a = 0.314$. The figure shows experimental data points and the following lines:

- The least squares linear curve fit for $\log \text{Nu}$ versus $\log \text{Ra}$ giving $\text{Nu} = 0.031\text{Ra}^{0.399}$.
- The 95% confidence interval for the regression line.
- The 95% prediction interval for the data.

The scatter in the data is seen to be relatively large giving a 95% prediction interval of about ±20% . However, since there are many data points, the 95% confidence interval for the regression line is much smaller: it is less than ±4% in the middle of the Rayleigh number range.

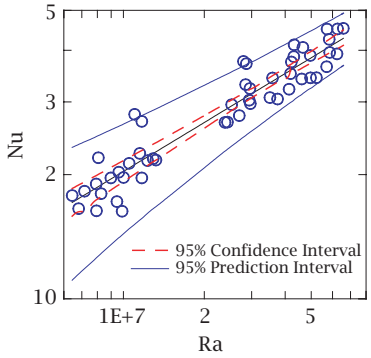

Figure 11 Experimental results of Nusselt numbers for the thermosyphon system.

From the point of view of the user of these results it is only the 95% confidence interval that is relevant because it indicates the uncertainty of the correlation given by the least squares regression line. The indicated confidence interval, typical of heat transfer correlations, is quite adequate for engineering purposes. The 95% prediction interval may be of interest to the experimentor. The relatively large value, indicating considerable scatter in the data, is due to difficulties in performing these experiments. The stack of copper plates has a large time constant that makes it difficult to obtain a true steady state when laboratory conditions vary. Also, the flow in the natural convection thermosyphon is characterized by a variety of minor instabilities that possibly causes the flow pattern to vary depending on how parameter values are changed, e.g., if the Rayleigh number is increased or decreased to reach a new test condition. Improvements in the conduct of the experiments may yield more precise data and the same confidence level with fewer data points, which may have some merit.

Example 10. A Pressure Transducer.

Let us return to the silicon piezoresistive pressure sensor described in Example 5. The set-up considered involved a data acquisition system coupled to a PC. Data are sampled at 5 Hz and averaged over 2s: the displayed value is a running average of 10 measurements, and the precision errors in this mean value will usually be negligible. (But see Example 15, which deals with the quantitization error associated with analog to digital signal conversion in a data acquisition system.) Thus we decide that the errors specified by the manufacturer should be taken as bias errors. For example, consider a measurement at 50% of full scale. The sum of bias errors due to various sources was found to be ±4.35% for a "typical" sensor and ±5.25% maximum. That is, the manufacturer is giving a guarantee that the maximum bias error will never be larger than ±5.25%. Since manufacturers tend to be conservative in their specifications (in order to avoid law suits!), the actual bias error will very seldom approach this value. Nevertheless, all we can say is that the bias uncertainty in the pressure measurement could be as large as ±5.25% and concerned parties must decide whether this value is acceptable or not. Section 6 will show how such bias uncertainties propagate to give a bias uncertainty in the final result.

Comments: These transducers are mass-produced and the manufacturer tests a sample in order to arrive at the error specifications. Thus the 4.35% value for a "typical" transducer is related to a standard deviation for the sample. But it is important to understand that a given transducer has a unique bias uncertainty that will be somewhere between ±5.25%—no other statements should be made.

6 Propagation of Bias Error

Experiments usually involve measurement of a number of variables that are then used to calculate the desired experimental result. Such calculations are termed *data reduction*, and can be accomplished using analytical formulas, spreadsheets or computer programs. Often a number of parameter values are also needed—such as geometrical dimensions and thermophysical properties. An important issue is how an error or uncertainty in a particular measured variable affects the final result. The usual practice in texts is to develop the concept of error propagation in connection with precision (random) errors—the term "random error analysis" is often seen. Indeed, the student should have already seen such analyses in lower division physics laboratory courses. Here we will introduce the concept of error propagation for bias errors, owing to the critical importance of bias error analysis to the design of experiments. Random error propagation will be dealt with in Section 7.

Let the calculated result y be a function of n independent measured variables and parameters $x_1, x_2, \ldots, x_n$.

$$y = y(x_1, x_2, \ldots, x_n). \tag{13}$$

Suppose x_i has a bias error Δx_i. Then the resulting error in y is

$$\begin{aligned} \Delta y_i &= y(x_1, x_2, \ldots, x_i + \Delta x_i, \ldots, x_n) \\ &\quad - y(x_1, x_2, \ldots, x_n). \end{aligned} \tag{14}$$

It is good practice to prepare a spreadsheet or computer program to process experimental data. Then one simply obtains y for a nominal input value of x_i and then $y + \Delta y_i$ for an input $x_i + \Delta x_i$: subtraction gives Δy_i. If the error is small we can use a Taylor series expansion of Eq. (14) and retain the first derivatives only to obtain

$$\Delta y_i = \frac{\partial y}{\partial x_i} \Delta x_i. \tag{15}$$

When the functional relationship is simple enough, the derivative can be found analytically. If not, it can be found numerically using a first order differencing scheme, but this latter numerical approach is usually redundant. Rather, one should always prepare a spreadsheet or computer program to reduce experimental data, unless the data reduction is very simple. It ensures reliable computations and is the basic tool for propagating bias errors. It can also be used to propagate uncertainty associated with random errors, if necessary.

Example 11. Bias Error in a Hot Gas Stream Temperature

Let us return to the situation described in Example 4, which involved the error in a hot gas stream temperature due to radiation heat loss from the thermocouple. We wish to consider two issues: (i) if over time the emittance of the thermocouple increases from 0.85 to 0.9 due to soot-like deposits, how does the bias error in the measured air temperature change? and (ii) the duct wall temperature is not conveniently controlled: how does the bias error in the air temperature change if the wall is at 90 °C rather than 100 °C?

As shown in Example 4, the data reduction formula for the air temperature is

$$\begin{aligned} T_e &= T_{tc} + \frac{\varepsilon\sigma}{h_c}\left(T_{tc}^4 - T_w^4\right) \\ \frac{\partial T_e}{\partial \varepsilon} &= \frac{\sigma}{h_c}\left(T_{tc}^4 - T_w^4\right) \\ &= \frac{5.67\times10^{-8}}{110}(528^4 - 373^4) = 30.1\,\mathrm{K} \\ \Delta T_e &= \frac{\partial T_e}{\partial \varepsilon}\Delta\varepsilon = (30.1)(0.05) = 1.5\,\mathrm{K}. \end{aligned}$$

$$\begin{aligned} \frac{\partial T_e}{\partial T_w} &= -4\frac{\varepsilon\sigma}{h_c}T_w^3 \\ &= -4\frac{(0.85)(5.67\times10^{-8})}{(110)}(373)^3 = 0.091 \\ \Delta T_e &= \frac{\partial T_e}{\partial T_w}\Delta T_w = (0.091)(10) = 0.91\,\mathrm{K} \cong 1\,\mathrm{K}. \end{aligned}$$

Comments: We see that T_e is relatively insensitive to T_w; a 10 K uncertainty in T_w gives only a 1 K uncertainty in T_e.

Example 12. Pressure Drop in an Enhanced Surface Duct

Measurements of pressure drop for flow through smooth tubes is a standard undergraduate laboratory experiment. To expand the scope of the experiment, it is planned to add an enhanced surface duct. The surface enhancement is in the form of parallel square ribs, which is a configuration that has been studied extensively in connection with enhancing heat transfer in gas-cooled nuclear reactors. A rib height of 0.0305 mm and pitch of 3.08 mm is chosen. An aluminum plate is machined with this profile, cut into four strips and welded to form a square duct of nominal inside dimensions of 10 mm by 10 mm. The duct is connected to inlet and outlet sections to be fitted with pressure taps and machined to give smooth walls and 10 mm square inside dimensions. If the flow area in the inlet and outlet sections are not equal, the flow will either accelerate or decelerate and there will be an associated pressure change. Our objective is to determine the allowable tolerance on the inside dimensions to meet a specified allowable error in the pressure drop measurement.

The nominal test condition is water at 300 K at a hydraulic Reynolds number of 10^5, for which the expected pressure drop in the test duct is 100 kPa. We first calculate the nominal velocity,

$$\mathrm{Re} = 10^5 = VD_h/\nu$$

$$V = 10^5\nu/D_h = (10^5)(0.87\times10^{-6})/0.01 = 8.7\,\mathrm{m/s}$$

and the volume flow rate is

$$\dot{Q} = VA_c = (8.7)(0.01)^2 = 8.7\times10^{-4}\mathrm{m}^3/\mathrm{s}.$$

The extended Bernouli's equation applied to the flow between the pressure taps is,

$$P_1 + \tfrac{1}{2}\rho V_1^2 = P_2 + \tfrac{1}{2}\rho V_2^2 + f\,(L/D_h)\,\tfrac{1}{2}\rho V^2$$

where $V = (V_1 + V_2)/2$. If we view the change in velocity as causing an error in the measured pressure drop,

$$dP = -\rho V dV.$$

Substituting $V = \dot{Q}/D_h^2$ gives

$$dP = -\tfrac{1}{2}\rho\dot{Q}^2\left(-4D_h^{-5}\right)dD_h$$

or

$$\begin{aligned} \Delta D_h &= \frac{D_h^5}{2\rho\dot{Q}^2}\Delta P \\ &= \frac{(0.01)^5}{(2)(997)\,(8.7\times10^{-4})^2}\Delta P \\ \Delta D_h &= 6.62\times10^{-8}\Delta P. \end{aligned}$$

The table gives the tolerance on $D_h = W$ the side of the duct for specified bias errors in ΔP.

ΔP kPa	ΔP% %	ΔD_h mm	ΔD_h mils
1	1	0.066	2.6
2	2	0.132	5.2
3	3	0.198	7.8

Comments:

1. This duct is a replacement for one that proved to be unsatisfactory. The original design was simpler in that the aluminum plate had smooth wall portions at each end: after cutting and welding, pressure taps were inserted at each end in the smooth wall sections of the duct. When tested the results were suspect and after considerable effort it was found that the inside dimensions of the pressure tap sections were substantially different. It was not possible to maintain a close tolerance when welding the four strips together due to distortion resulting from uneven thermal expansion. Hence the need to have machined pressure tap sections to control dimensional tolerances.
2. This example well illustrates the critical importance of making careful calculations when designing an experimental rig. Sample data processing calculations must be made to identify bias errors that may propagate to give significant errors in the final results.

Example 13. Air–fuel Ratio of an Automobile Engine

The most direct method for measuring the air–fuel ratio at a specific operating condition of an automobile engine is to measure the fuel and air flow rates directly. Even when the engine is on a test bed coupled to a dynamometer, these measurements are not straightforward. An alternative method is based on measuring the CO_2, CO and O_2 content of the exhaust, provided the elemental composition of the gasoline is known. For example, a typical gasoline may contain 83.3% C, 14.7% H and 2% O by mass. Consider combustion of 100 kg of fuel; then, since air contains 23.2% O and 76.8% N by mass,

$$\begin{aligned} &83.3\,\text{kg C} + 14.7\,\text{kg H} + 2\,\text{kg O} \\ &\quad + \phi(23.2\,\text{kg O} + 76.8\,\text{kg N}) \\ &\longrightarrow 44b\,\text{kg CO}_2 + 28d\,\text{kg CO} \\ &\quad + 18e\,\text{kg H}_2\text{O} + 28f\,\text{kg N}_2 \\ &\quad + 32g\,\text{kg O}_2 \end{aligned}$$

where ϕ is the air–fuel ratio, and b, d, e, f and g are numbers of kmols of each exhaust constituent. The small amounts of unburnt hydrogen and nitrogen oxides in the exhaust have been ignored. Balance equations for the chemical elements are as follows:

$$\begin{aligned} &\text{H}: && 14.7 = 2e, \text{ thus } e = 7.35 \\ &\text{N}: && 76.80 = 28f, \text{ thus } f = 2.742\phi\,\text{k mol} \\ &\text{C}: && 83.3 = 12(b + d) \\ &\text{O}: && 2 + 23.2\phi = 32b + 16d + 16e + 32g. \end{aligned}$$

The ratios b/d and g/b can be obtained from the exhaust gas analysis.

In a test on a Toyota 5S-FE engine at full throttle and 6200 rpm, the measured exhaust gas composition was 7.2% CO, 10.92% CO_2 and 1.05% O_2 by volume. Thus the ratios b/d and g/b are

$$\begin{aligned} b/d &= 10.92/7.2 = 1.517 \\ g/b &= 1.05/10.92 = 0.0962. \end{aligned}$$

From the carbon balance

$$83.3 = 12(1.517d + d); \quad d = 2.758.$$

Also,

$$\begin{aligned} b &= (1.517)(2.758) = 4.168; \\ g &= (0.0962)(4.168) = 0.401. \end{aligned}$$

Solving for the air–fuel ratio

$$\begin{aligned} \phi &= \frac{32b + 16d + 16e + 32g - 2}{23.2} \\ &= \frac{133.4 + 44.1 + 117.6 + 12.8 - 2}{23.2} \\ &= 13.2. \end{aligned}$$

It is difficult to obtain reliable accuracy specifications for gas analysis equipment. Thus it is pertinent to explore the effects of possible bias errors in the measured gas composition. For example, how does a 1% bias error in the CO% affect ϕ? In a typical test situation ϕ must be calculated for a large amount of test data. Using a modern computer controlled dynameter complete complete performance curves may include 50–100 tests. Thus the above hand calculation should be automated using a spreadsheet or computer program. Then error propagation can be simply effected by varying the relevant input to the calculations. Table 6 shows the results of such calculations. Of particular interest is the % O_2 in the exhaust. The instrumentation used obtained the % O_2 indirectly and hence is most prone to bias error. The table shows how the fuel/air ratio is affected by the uncertainty in % O_2.

Table 6 Propagation of bias errors in exhaust and fuel composition. Reference data of Example 13.

Parameter	Perturbed value,%	ϕ	$\Delta\phi$
% CO,	6.2	13.44	0.201
exhaust	8.2	13.03	−0.180
% CO_2	9.92	13.13	−0.079
exhaust	11.92	13.28	+0.070
% O_2,	2.05	13.47	0.26
exhaust	1.55	13.74	0.53
	0.55	12.95	−0.26
	0.05	12.68	−0.53
% O	1	13.47	0.27
	0	13.74	0.53
% C,H	83.8, 14.2	13.89	−.123
	84.3, 13.7	12.96	−.248

7 Propagation of Precision Uncertainties

Since precision uncertainties are random in nature, the propagation of precision uncertainties in measurements through to calculated results is governed by the laws of statistics. Consider a calculated result Y that is a function of N independent measurements X_i. If the uncertainties P_i are small enough we can use a first order Taylor expansion of Y to write

$$Y(X_1 + P_1, X_2 + P_2, \ldots, X_N + P_N)$$

$$\cong Y(X_1, X_2, \ldots, X_N) + \frac{\partial Y}{\partial X_1}P_1 + \frac{\partial Y}{\partial X_2}P_2 + \cdots + \frac{\partial Y}{\partial X_N}P_N.$$

Now Y is a *linear* function of the independent variables and a theorem of mathematical statistics can be used to write

$$P_Y = \left[\sum_{i=1}^{n}\left(\frac{\partial Y}{\partial X_i}P_i\right)^2\right]^{1/2} \tag{16}$$

where in Eq. (16) all the uncertainties in the X_i must be at the same confidence level. As was noted for bias uncertainties in §6, the preferred method for propagating precision uncertainties is by using a spreadsheet or computer program. Then Eq. (16) is replaced by

$$P_Y = \left[\sum_{i=1}^{N}\Delta Y_i^2\right]^{1/2} \tag{17}$$

where ΔY_i is the change in Y resulting from a change P_i in X_i.

If Y depends only on a product of the independent measurements X_i, for example

$$Y = CX_1^{m_1}X_2^{m_2}\ldots$$

it is then possible to derive a convenient form of Eq. (16), namely

$$\frac{P_Y}{Y} = \left[\sum_{i}\left(m_i\frac{P_i}{X_i}\right)^2\right]^{1/2} \tag{18}$$

which is particularly easy to use since fractional uncertainty in the result is directly related to the fractional errors in the individual measurements.

The propagation of precision uncertainties has received more attention than any other aspect of error analysis of experiments. However, in this manual we make the case that useful information is seldom derived by carrying out a precision error propagation calculation. There are two reasons underlying this conclusion:

1. Use of modern electronic instrumentation, computer control of experiments, and computer based data acquisition and processing, often reduces precision errors to a negligible level.
2. When precision errors are not negligible, the processed experimental data usually allows a direct determination of the precision error that is more reliable than values obtained by propagating the errors in individual measurements. This is because we usually generate parametric data in an experiment, e.g., convective heat transfer coefficient as a function of flow velocity, $h_c(V)$. After curve-fitting the data, the standard error of the curve-fit is a much more reliable indicator of the uncertainty than an estimate obtained by propagating the uncertainties in individual measurements used to calculate h_c. The scatter seen in a graph of h_c versus V is the precision error in the measurement of h_c (see Rule No. 3 in §2).

Example 14. A Coaxial Tube Heat Exchanger.

A test is performed to determine the performance of a two-stream counterflow water–to–water heat exchanger at nominal flow conditions. The measured temperatures are:

$$T_{H,\text{in}} = 44.8\,^\circ\text{C}, \qquad T_{H,\text{out}} = 31.3\,^\circ\text{C},$$
$$T_{C,\text{in}} = 23.5\,^\circ\text{C}, \qquad T_{C,\text{out}} = 30.0\,^\circ\text{C},$$

and measured flow rates are

$$\dot{m}_H = 0.0562\,\text{kg/s}; \quad \dot{m}_C = 0.121\,\text{kg/s}.$$

The precision error in the temperature is taken to be the least count of the digital thermometer, and is ± 0.1 °C. The precision error in the flow rates is taken to be the least count of the rotameter scales and is $\pm 1.5\times10^{-3}$ kg/s. Let us propagate these precision errors to determine the precision uncertainty in the effectiveness, the number of transfer units, and the exchanger energy balance.

From Eq. (8.42) of BHMT, the number of transfer units for a counterflow exchanger is

$$N_{tu} = \frac{1}{1-R_C}\ln\frac{1-\varepsilon R_C}{1-\varepsilon}$$

where $R_C = C_{\min}/C_{\max}$, $C = \dot{m}c_p$, $N_{tu} = UA/C_{\min}$, and $\varepsilon = (T_{H,\text{in}} - T_{H,\text{out}})/(T_{H,\text{in}} - T_{C,\text{in}})$, since $\dot{m}_H c_{pH} = C_{\min}$. For equal specific heats $c_{pC} = c_{pH}$, hence

$$R_C = \dot{m}_H/\dot{m}_C = 0.464.$$

The effectiveness ε is

$$\varepsilon = \frac{44.8 - 31.3}{44.8 - 23.5} = \frac{13.5}{21.3} = 0.634$$

and

$$N_{tu} = \frac{1}{1-0.464}\ln\frac{1-(0.634)(0.464)}{1-(0.634)} = 1.225.$$

We will first propagate the precision errors in temperature to the effectiveness.

$$\varepsilon = \frac{T_{H,\text{in}} - T_{H,\text{out}}}{T_{H,\text{in}} - T_{C,\text{in}}}$$

$$\frac{\partial\varepsilon}{\partial T_{H,\text{in}}} = \frac{1}{T_{H,\text{in}} - T_{C,\text{in}}} - \frac{T_{H,\text{in}} - T_{H,\text{out}}}{(T_{H,\text{in}} - T_{C,\text{in}})^2}$$

$$= \frac{1}{21.3} - \frac{13.5}{21.3^2} = 1.72\times10^{-2}\text{K}^{-1}$$

$$\frac{\partial \varepsilon}{\partial T_{H,\text{out}}} = -\frac{1}{T_{H,\text{in}} - T_{C,\text{in}}}$$
$$= -\frac{1}{21.3} = -4.69 \times 10^{-2}\text{K}^{-1}$$

$$\frac{\partial \varepsilon}{\partial T_{C,\text{in}}} = \frac{T_{H,\text{in}} - T_{H,\text{out}}}{(T_{H,\text{in}} - T_{C,\text{in}})^2}$$
$$= \frac{12.5}{21.3^2} = 2.97 \times 10^{-2}\text{K}^{-1}$$

$$P_\varepsilon = \left[\sum_{i=1}^{3}\left(\frac{\partial \varepsilon}{\partial x_i}P_i\right)^2\right]^{1/2}$$
$$= \left[\left(1.72 \times 10^{-2} \times 0.1\right)^2 + \left(-4.60 \times 10^{-2} \times 0.1\right)^2 + \left(2.97 \times 10^{-2} \times 0.1\right)^2\right]^{1/2}$$
$$= 5.81 \times 10^{-3}.$$

Thus, $\varepsilon = 0.634 \pm 5.81 \times 10^{-3} = 63.4\% \pm 0.58\%$. Next we propagate the precision errors in flow rate to the capacity rate ratio

$$R_C = \frac{C_{\min}}{C_{\max}} = \frac{C_H}{C_C} = \frac{\dot{m}_H}{\dot{m}_C}, \text{ since } c_{pH} \approx c_{p_C}$$
$$\frac{\partial R_C}{\partial \dot{m}_H} = \frac{1}{\dot{m}_C} = \frac{1}{0.121} = 8.26;$$
$$\frac{\partial R_C}{\partial \dot{m}_C} = -\frac{\dot{m}_H}{\dot{m}_C^2} = -\frac{0.0562}{0.121^2} = 3.84$$
$$P_{R_C} = \left[\left(8.26 \times 1.5 \times 10^{-3}\right)^2 + \left(3.84 \times 1.5 \times 10^{-3}\right)^2\right]^{1/2}$$
$$= 1.37 \times 10^{-2}.$$

Thus $R_C = 0.464 \pm 0.014$. Then we can propagate the errors in ε and R_C to the number of transfer units,

$$N_{tu} = \frac{1}{1 - R_C}\ln\left(\frac{1 - \varepsilon R_C}{1 - \varepsilon}\right)$$

$$\frac{\partial N_{tu}}{\partial R_C} = \frac{-\varepsilon}{(1 - R_C)(1 - \varepsilon R_C)} + \ln\left(\frac{1 - \varepsilon R_C}{1 - \varepsilon}\right)\frac{1}{(1 - R_C)^2}$$
$$= \frac{-0.634}{(1 - 0.464)(1 - (0.634)(0.454))} + \ln\left(\frac{1 - (0.634)(0.464)}{1 - 0.634}\right)\frac{1}{(1 - 0.464)^2}$$
$$= 0.610$$

$$\frac{\partial N_{tu}}{\partial \varepsilon} = \frac{1}{(1 - \varepsilon R_C)(1 - \varepsilon)}$$
$$= \frac{1}{(1 - (0.634)(0.464))(1 - 0634)} = 3.87$$

$$P_{N_{tu}} = \left[\left(3.87 \times 5.81 \times 10^{-3}\right)^2 + \left(0.61 \times 1.37 \times 10^{-2}\right)^2\right]^{1/2}$$
$$= 2.4 \times 10^{-2}.$$

Thus, $N_{tu} = 1.225 \pm 0.024 (2.0\%)$. We can also propagate the precision errors to the exchanger energy balance. From Eq. (8.4) of BHMT the exchanger energy balance is

$$\dot{Q}_H = \dot{Q}_C$$
$$\dot{Q}_H = \left(\dot{m}c_p\right)_H (T_{H,\text{in}} - T_{H,\text{out}});$$
$$\dot{Q}_C = \left(\dot{m}c_p\right)_C (T_{C,\text{out}} - T_{C,\text{in}}).$$

For $c_{pH} \approx c_{pC} = 4175\,\text{J/kg K}$,

$$\dot{Q}_H = (0.0562)(4175)(44.8 - 31.3) = 3168\,\text{W};$$
$$\dot{Q}_C = (0.121)(4175)(30.0 - 23.5) = 3284\,\text{W}.$$

$$\frac{\dot{Q}_H - \dot{Q}_C}{\dot{Q}_H} = \frac{3168 - 3284}{3168} = -3.7\%.$$

Let us estimate the precision uncertainty in $\dot{Q}_C$

$$\frac{\partial \dot{Q}_C}{\partial \dot{m}_C} = c_{pC}(T_{C,\text{out}} - T_{C,\text{in}})$$
$$= (4175)(30.0 - 23.5) = 2.71 \times 10^4$$
$$\frac{\partial \dot{Q}_C}{\partial T_{C_{\text{out}}}} = \left(\dot{m}c_p\right)_C = (0.121)(4175) = 505;$$
$$\frac{\partial \dot{Q}_C}{\partial T_{C_{\text{in}}}} = \left(\dot{m}c_p\right)_C = -505.$$

$$P_{\dot{Q}_C} = \left[\left(\left(2.71 \times 10^4\right)\left(1.5 \times 10^{-3}\right)\right)^2 + (505 \times 0.1)^2 + (-505 \times 0.1)^2\right]^{1/2} = 82.2\,\text{W}$$

$$\frac{P_{\dot{Q}_C}}{\dot{Q}_C} = \frac{82.2}{3284} = 2.5\%.$$

Similarly,

$$P_{\dot{Q}_H} = 90.9\,\text{W}$$
$$\frac{P_{\dot{Q}_H}}{\dot{Q}_H} = \frac{90.9}{31.68} = 2.9\%$$
$$P_{(\dot{Q}_H - \dot{Q}_C)} = \left[(82.2)^2 + (90.9)^2\right]^{1/2} = 123,$$

which can be compared with $|\dot{Q}_H - \dot{Q}_C| = 116$.

As mentioned in §7, the preferred method for propagating precision uncertainties is by using a spreadsheet or computer program; then Eq. (17) is used, namely

$$P_Y = \left[\sum_{i=1}^{N}\Delta Y_i^2\right]^{1/2}.$$

Table 7 Computer propagation of precision uncertainties.

X_i	ΔX_i	$Y_i(X_i+\Delta X_i)$	$Y_i(X_i-\Delta X_i)$	$\Delta\overline{Y}_i$	$\Delta\overline{Y}_i^2$
$T_{H,\text{in}}$	± 0.1 K	1.231	1.218	0.0065	4.23×10^{-5}
$T_{H,\text{out}}$	± 0.1 K	1.206	1.243	0.0185	3.42×10^{-5}
$T_{C,\text{in}}$	± 0.1 K	1.236	1.213	0.0115	1.32×10^{-5}
$\dot{m}_H$(kg/s)	$\pm 1.5\times10^{-3}$	1.232	1.217	0.0075	5.73×10^{-5}
$\dot{m}_C$(kg/s)	$\pm 1.5\times10^{-3}$	1.221	1.228	0.0035	1.23×10^{-5}

A computer program was written to process the data for this experiment, and, in addition to calculating the experimental value of N_{tu}, also calculates the expected values using correlations for the hot- and cold-side heat transfer coefficients. The results are as shown in Table 7 and

$$\begin{aligned} P_Y &= \Big[4.23\times10^{-5}+3.42\times10^{-5}+1.32\times10^{-5} \\ &\qquad +6.73\times10^{-5}+1.23\times10^{-5}\Big]^{1/2} \\ &= \pm 0.0242 \end{aligned}$$

which is to be compared with the value of ± 0.024 obtained by partial differentiation.

Comments:

1. Notice that $\partial\varepsilon/\partial T_{H,\text{in}}$ is relatively small due to way $T_{H,\text{in}}$ appears in both numerator and denominator of the formula for ε.
2. The important results are that
$$\begin{aligned} \frac{P_\varepsilon}{\varepsilon} &= 0.92\% \\ \frac{P_{Ntu}}{Ntu} &= 2\%, \text{ and} \\ \frac{P_{\dot{Q}_C}}{\dot{Q}_C} &= 2.5\%. \end{aligned}$$
3. Since $P_{(\dot{Q}_H-\dot{Q}_C)}$ is about the same as $(\dot{Q}_H-\dot{Q}_C)$, we might argue that the 3.7% discrepancy in the energy balance can be attributed to precision errors. However, such a conclusion would be premature. We must first obtain a number of data sets and ascertain that the discrepancy does vary in a random manner.
4. When using the computer program to propagate precision errors, our choice of $\Delta\overline{Y}_i = \frac{1}{2}\left(\Delta Y_i(X_i+\Delta X_i)+\Delta Y_i(X_i-\Delta X_i)\right)$ is arbitrary. We have not linearized the equations as is done when using partial differentiation: thus positive and negative values of a given $\Delta\overline{X}_i$ can give different values of $\Delta\overline{Y}_i$. In an extreme case the difference can be large—but of no concern because then the precision error is too large to have a meaningful experiment.
5. The purpose of this example was to demonstrate how precision errors are propagated. We will return to this heat exchanger experiment in Case Study No. 4, where a more complete error analysis will be presented.

Example 15. Analog/Digital Signal Converter Quantization Error.

Let us return to the boiling heat transfer experiment described in Example 6, where the heat flux is calculated using a lumped thermal capacity model for the temperature–time response,

$$qA = -\rho cV\frac{dT}{dt}.$$

Using a central difference numerical approximation for the derivative and $V/A = D/C$ for a sphere gives

$$q = -C\frac{T_{n+1}-T_{n-1}}{2\Delta t};\quad C=\rho cD/6.$$

The analog to digital (A/D) converter in the data acquisition system replaces the continuous voltage signal from the thermocouple by a sequence of discrete values. For example, an 8-bit A/D converter can record $2^8 = 256$ voltage levels. If it is to have a range of 10 mV, then its least count is necessarily $10/256 - 0.04$ mV. The quantization error is a precision error; when designing the experiment it is of value to predict the effect of this error on the calculated heat flux, by propagating the error through the heat flux calculation.

We can assume that C and Δt are precisely known, then

$$\frac{\partial q}{\partial T_{n+1}} = -\frac{C}{2\Delta t};\qquad \frac{\partial q}{\partial T_{n-1}} = \frac{C}{2\Delta t}.$$

Using Eq. (16)

$$\begin{aligned} P_q &= \left[\left(\frac{-C}{2\Delta t}P_{T_{n+1}}\right)^2+\left(\frac{C}{2\Delta t}P_{T_{n-1}}\right)^2\right]^{1/2} \\ &= \frac{C}{2\Delta t}\left[P_{T_{n+1}}^2+P_{T_{n-1}}^2\right]^{1/2}. \end{aligned}$$

For a numerical example consider a sampling frequency of 10 Hz ($\Delta t = 0.1$ s), a least count for the temperature data acquisition of 0.025 K, and a cooling rate of 2 K/s (corresponding to film boiling). Then

$$P_q = \frac{C}{(2)(0.1)}\left(0.025^2+0.025^2\right)^{1/2} = 0.177\,C.$$

For a cooling rate of 2 K/s, $q = 2C$, then

$$\frac{P_q}{q} = \frac{0.177}{2} = 8.85\%.$$

When the experiment is performed we would expect to see noise of at least this magnitude in q in the film boiling regime.

8 Use of Error Bars

Graphical presentation of experimental results is useful to show trends in the data and to indicate the precision of the data: you have seen graphs of experimental data in textbooks and must have prepared such graphs in physics or chemistry laboratory courses. A recent trend is to show *error bars* on a graph. At first sight it seems like a good way to show uncertainty on the graph; however, often error bars are inappropriately used and can be quite misleading. In this section we focus on the use of error bars to display bias uncertainties, and the related concepts of error rectangles and error vectors. We will also briefly discuss why error bars should not be used for precision errors.

First consider a set of data points (x_i, y_i) where x_i is assumed to have negligible error, while y_i has negligible precision error but is suspected to have a significant bias error over part of the x_i range. For example, x_i could be a pressure differential across a combination of pipe fittings, and y_i the resulting flow rate. The flow meter used to measure flow rate has a linear response and has been calibrated over a specified range (see Example 2): in this range the bias error is negligible. However, some of the data were obtained at lower flow rates outside the calibration range and it is known that the response of this type of flow meter may become significantly nonlinear below the calibrated flow rate range. The purpose of the experiment is to compare the measured flow rate with the value predicted by using standard pipe fitting loss coefficients for the individual fittings. Such data is found in fluid mechanics texts and handbooks.

Figure 12(a) shows the results obtained. At higher flow rates the data shows a small uniform deviation from the predicted values, but at lower flow rates the deviation increases significantly. The question is whether these large deviations are real, or are they caused by bias error in the flow meter. Figure 12(b) shows the data again with the calibration range of the flow meter indicated: the data in question do lie outside the calibration range. Based on information on the type of flow meter the bias uncertainty is estimated: in this case it is not symmetrical and is actually one-sided from the known behavior of calibration constants of such flow meters. The error bars show the magnitude of the estimated bias uncertainty, and it is seen that bias error could indeed explain the increased deviations. The small uniform deviation is attributed to an inadequacy in the prediction procedure.

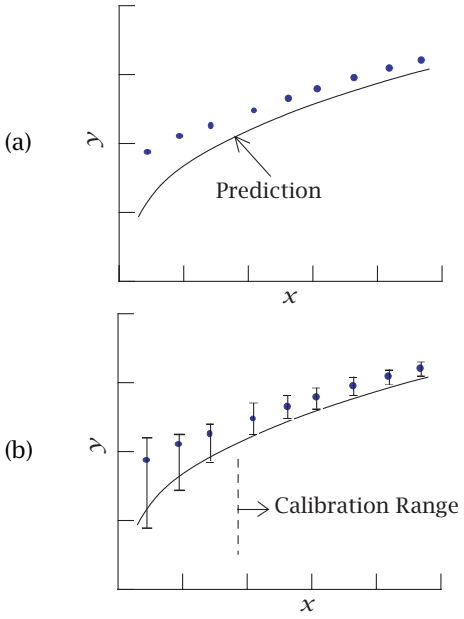

Figure 12 Flow rate y versus pressure drop x for a combination of pipe fittings (a) Data and predicted variation. (b) Error bars showing estimated bias uncertainty in the flow rate measurements.

Next, consider a set of data points of independent variables (x_i, y_i) where x_i and y_i have negligible precision error and where both are suspected to have a bias error. The purpose is to evaluate the theory that predicts $y = mx+C$. In this case our best estimation of the upper bound of the bias errors yield symmetrical uncertainties in both variables. Figure 13 shows the data and the theory. Since the variables x and y are independent we can draw *error rectangles* that display the bias uncertainty for each data point. We conclude that the model underlying the theory does not give accurate predictions and, if greater accuracy is desired, an effort should be made to refine the model.

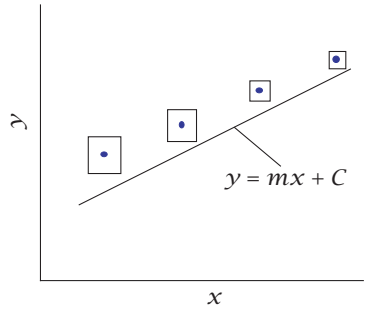

Figure 13 Use of error rectangles to show bias uncertainty when x and y are independent variables.

Finally we consider a situation that too often appears in reports on experiments. Engineers prefer to graph results in terms of dimensionless variables in order to obtain the greatest generality (see, for example, BHMT Section 4.2.3). In fluid mechanics we often plot a drag coefficient, friction factor or Euler number versus Reynolds number to

present results of a pressure drop experiment. Consider data presented in terms of Euler number, Eu $= \Delta P/\rho V^2$ versus Reynolds number $\mathrm{Re}_{d_h} = V d_h/\nu$ for pressure drop across a perforated plate.

The hole diameters are d_h, and V is the gas velocity based on free-flow area, i.e., the bulk velocity through the holes. Figure 14(a) shows some test data together with a theoretical prediction. The precision uncertainty is seen to be negligible, which is due to the design of the test rig: the experiment is computer controlled and all data is obtained using a computer based acquisition system. Again we see a significant deviation at low flow rates (low Reynolds numbers), and ask the question whether this deviation could be due to bias error in the flow measurements. At first we might be tempted to draw error rectangles as shown in Figure 14(b) and conclude that bias error could indeed explain the deviation of the data point from the theory. But this would be incorrect because the variables (x, y) of the graph are *correlated*—the velocity V appears in both variables. Thus we need to use an *error vector* to indicate the impact of bias error in V. Figure 14(c) shows the effect of recalculating the data point accounting for a bias error estimate of ±10%: notice that Eu decreases and Re increases as a result (and vice-versa). We would now conclude that the theory is inaccurate at this Reynolds number.

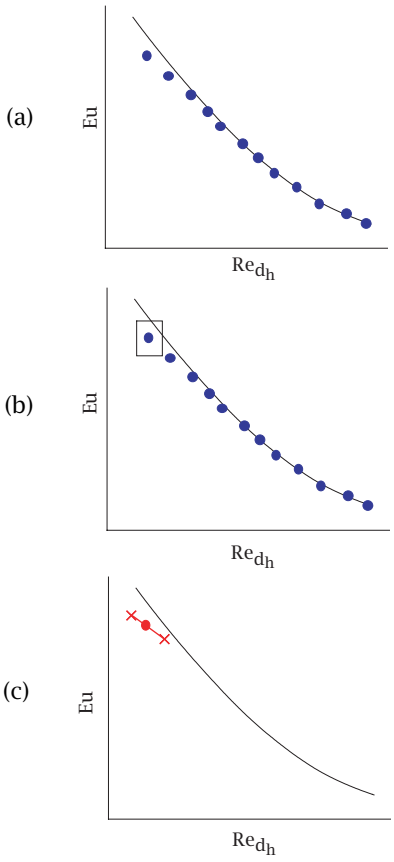

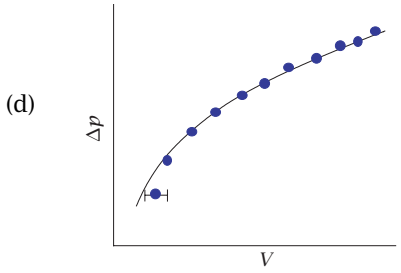

Figure 14 Euler number versus Reynolds number for flow through a perforated plate. (a) Experimental data and a theoretical prediction. (b) Error rectangles showing estimated bias uncertainties in Eu and Re_{d_h}. (c) An error vector for estimated bias uncertainties in Eu and Re_{d_h}. (d) Replot in terms of the primitive variables pressure drop and velocity with an error bar showing the bias uncertainty in V.

Because of the difficulties presented by correlated variables it is good practice to examine errors on graphs of primitive, not derived, variables. In the foregoing example a graph of ΔP versus V could be prepared for this purpose: then the effect of bias error in V only affects the abscissa variable, as shown in Figure 14(d). Unfortunately, in attempts to shorten reports to journal papers, graphs in terms of primitive variables are usually omitted in favor of graphs in terms of dimensionless groups. Such graphs are important and useful, but not for examining issues relating to errors.

So far we have focused on situations where precision errors are negligible and only bias errors are of concern. Now consider a situation where precision errors are significant and bias errors are negligible. Figure 15 shows a data set (x_i, Y_i) where x_i has negligible total error and Y_i has a significant precision errors: also shown is a least squares curve-fit. Often one sees error bars on such data points, but does this practice have value? The precision error of the data is already indicated by the scatter about the least squares curve-fit. This scatter could be quantified by indicating the prediction interval P_Y defined by Eq. (12) as shown in Figure 15. But we are not really interested in the precision of individual data points: we are concerned with the precision of the curve-fit, which has an uncertainty given by Eq. (11). Thus, it would be more appropriate to indicate $P_{\hat{Y}}$ as shown in Figure 15. The displayed band then covers the precision uncertainty of the curve-fit at the 95% level. It is Figure 15 that shows the users what they need to know. Error bars on individual data points are of no real interest, unless there are too few data for statistical analysis.

Finally, what about the situations where bias and precision errors are both significant? (situations to be avoided if at all possible!). The essential problem is that there is no rational way to combine random bias errors governed by statistical laws and fixed bias errors governed by physical laws. In simple situations a pragmatic approach can be used, remembering Rule 2 of § 2, which can be paraphrased "talk sense about bias errors." For example, if in the previous case the variable Y_i had an estimated bias un-

certainty of $+B$, we could replace Figure 15 by Figure 16. Figure 16 tells the user that our experiment has yielded the correlation indicated by the curve-fit, with the precision uncertainty shown, but that the true result may also deviate as much as the bias uncertainty shown. We have done our best to correct for bias errors but there is possibly a remaining bias uncertainty as indicated. Again, users must decide whether this result is acceptable for their particular needs. The foregoing recommendation is not in accord with the current practice of engineering professional societies and journals, and of standards organizations. Further discussion of this conflict is deferred to § 13.

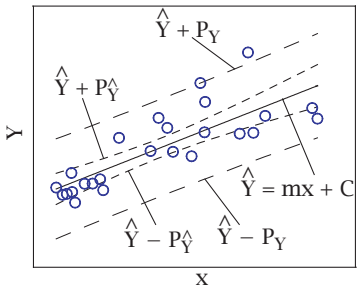

Figure 15 Confidence and prediction intervals for a straight-line least squares curve fit.

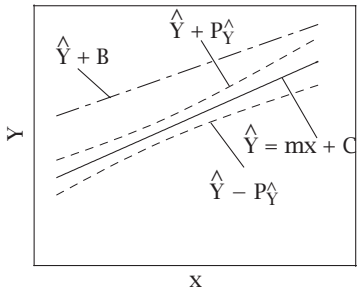

Figure 16 A possible display of uncertainty when both precision and bias errors are of concern for a least square straight-line curve fit.

Example 16. Precision Errors for Convective Heat Transfer in an Oscillatory Flow.

Gopinath and Harder [2] report the results of an interesting study of convective heat transfer from a cylinder in a low amplitude zero-mean oscillatory flow. Figure 17 shows some typical data for Nusselt number versus the streaming Reynolds number $R_s = a^2\omega/\nu$, where a is the displacement amplitude of the fluid oscillation and ω is the angular frequency of the oscillation. The solid line is a $R_s^{1/2}$ least square fit of the data for higher values of R_s. The precision of the data is indicated by the scatter about the least squares fit. It can be quantified by indicating the prediction interval P_Y defined by Eq. (12). But since we are not really interested in the precision of individual data points, we should rather indicate the confidence interval $P_{\hat{Y}}$ given by Eq. (11), which is the precision uncertainty of the curve fit (see also Fig. 15).

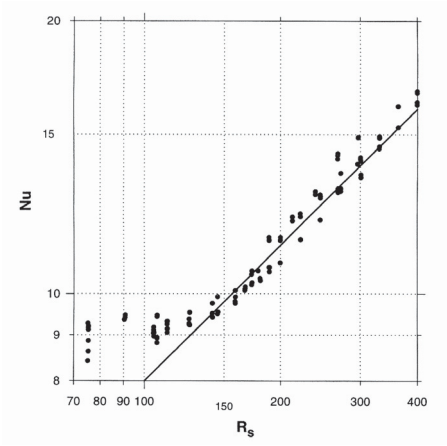

Figure 17 Nusselt number versus the streaming Reynolds number.

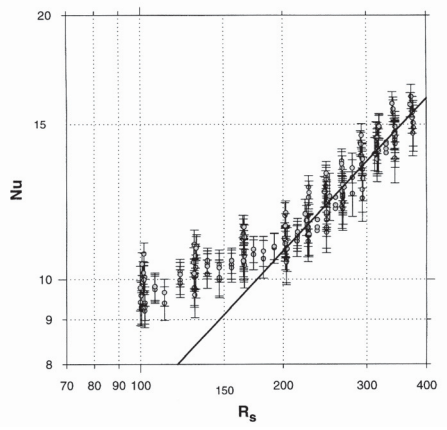

Figure 18 Precision uncertainty of Nusselt number from random error uncertainty analysis.

However, the authors chose to indicate the precision uncertainty using error bars, as shown, for example, in Fig. 18. The error bars indicated are stated to be "from a random error uncertainty analysis." It is doubtful whether the error bars convey any useful information. Firstly, since a relatively large number of experimental data points were obtained, the precision uncertainty P_Y calculated from the scatter in the data is the true measure of random error uncertainty. No attempt to predict the precision uncertainty in the Nusselt number from the expected precision errors in the primitive measurements can be more accurate or reliable. Secondly, the precision uncertainty of the curve-fit should be shown, as in Fig. 15, not on the individual data points as shown in Fig. 18. If they had only measured one data point, then an error bar on that data point would have been appropriate since that value would have been a best estimate of the true value. But, when there are many data points, the curve-fit is the best estimate of the true values, and a random error only makes sense in terms of the curve-fit. Thus the "spread" of the superimposed error bars in Fig. 18 gives a false impression of the precision uncertainty of the result: it is in fact far less.

Thus, as stated in § 8, the use of error bars to indicate precision uncertainty is not advised (unless it is a *single sample* experiment, which is rarely the case).

9 The Normal Probability Distribution

The normal (or Gaussian) probability distribution plays a central role in the analysis of precision errors. When we repeat a measurement a number of times we obtain a finite *sample* of values, as shown by the histogram in Fig. 19. As noted in § 3, the shape of the histogram is similar to the familiar bell-shape of the normal probability distribution, and this is true for most measurements made in usual laboratory experiments. We can regard the sample as coming from a *population* of values that would be obtained when the sample size approaches infinity. Two samples taken from this population will, in general, have different mean values; but each approximates the population mean at some level of uncertainty. Clearly, the difference between sample characteristics and the population characteristics will decrease as the sample becomes larger.

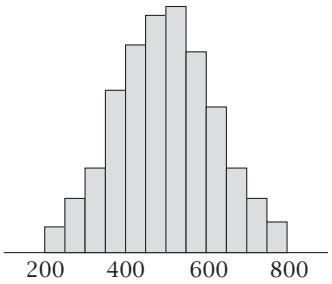

Figure 19 A histogram of a sample from a normal population.

We will assume that precision errors cause the measured value to vary randomly: hence our use of the notation X to represent the measurement in line with the usual practice in probability theory. The probability density function for a random variable X having a normal distribution is defined as

$$f(X) = \frac{1}{\sigma\sqrt{2\pi}} e^{-(X-\mu)^2/2\sigma^2} \tag{19}$$

where $f(X)dX$ is the probability that a single measurement of X will lie between X and $X + dX$. Equation (19) is in normalized form, that is

$$\int_{-\infty}^{\infty} f(X)\, dX = 1.0. \tag{20}$$

The parameters of the distribution are the *mean* value μ, defined as

$$\mu = \int_{-\infty}^{\infty} X f(X)\, dX \tag{21}$$

and the *variance* σ^2 defined as

$$\sigma^2 = \int_{-\infty}^{\infty} (X-\mu)^2 f(X)\, dX. \tag{22}$$

The *standard deviation* of the distribution is defined as the square root of the variance and indicates the width of the distribution.

Let us consider a single measurement that is assumed to be from a normal parent population. The probability P that this value will fall in a specified range $\pm\Delta X$ about the mean value is given by

$$P(\mu - \Delta X \le X \le \mu + \Delta X) = \int_{\mu-\Delta X}^{\mu+\Delta X} \frac{1}{\sigma\sqrt{2\pi}} e^{-(X-\mu)^2/2\sigma^2}. \tag{23}$$

Evaluation of the integral is simplified if we introduce a new variable z that is a normalized deviation from the mean value,

$$z = \frac{X-\mu}{\sigma} \tag{24}$$

and $dz = dX/\sigma$. Then Eq. (23) becomes

$$P(-z_1 \le z \le z_1) = \frac{1}{\sqrt{2\pi}} \int_{-z_1}^{z_1} e^{-z^2/2}\, dz \tag{25}$$

where $dz = dX/\sigma$. Since $f(X)$ is symmetrical about μ, we can write

$$\frac{1}{\sqrt{2\pi}} \int_{-z_1}^{z_1} e^{-z^2/2}\, dz = \text{erf}\left(\frac{z_1}{\sqrt{2}}\right) \tag{26}$$

where erf is the *error* function,

$$\text{erf}\, z_1 = \frac{2}{\sqrt{\pi}} \int_0^{z_1} e^{-z^2}\, dz. \tag{27}$$

BHMT Table B4 is a tabulation of the complementary error function erfc(erfc = 1 − erf).

We are often interested in the probability that a measurement will fall within one or more standard deviations (σ's) of the mean. Referring to Eq. (25), for one standard deviation we must evaluate

$$P(-1 \le z \le 1) = \frac{1}{\sqrt{2\pi}} \int_{-1}^{+1} e^{-z^2/2}\, dz. \tag{28}$$

Using Table A.1 the right side of the equation is evaluated to be 68.3%. Alternatively, we can calculate the interval corresponding to a specified probability which requires iteration using an error function table. Some results are listed below.

Probability	Range about mean value
50	$\pm 0.675\sigma$
68.3	$\pm 1.0\sigma$
95	$\pm 1.96\sigma$
99.7	$\pm 3\sigma$
99.99	$\pm 4\sigma$

Suppose we have a normal parent population of a measurement X. If we take a single measurement X_1, we can be 95% confident that it will fall within a $\pm 1.96\sigma$ interval about the mean: that is, $\pm 1.96\sigma$ is the 95% confidence limit. In practice we often round off 1.96 to 2.0 and specify $\pm 2\sigma$ as the 95% *confidence limit*. Alternatively, we can be 95% confident that the mean of the parent distribution μ will fall within $\pm 1.96\sigma$ of the single measurement X_i.

10 Samples From a Normal Parent Population

Consider a sample of measurements from a parent population that is assumed to be normal. The mean of a sample was defined by Eq. (1) as

$$\overline{X} = \frac{1}{N}\sum_{i=1}^{N} X_i$$

for a sample of size N. The standard deviation of a sample was defined by Eq. (2) as

$$S_X = \left[\frac{1}{N-1}\sum_{i=1}^{N}\left(X_i - \overline{X}\right)^2\right]^{1/2}.$$

The factor $(N-1)$ rather than N appears in Eq. (2) because it can be shown that S_X is then an unbiased (best) estimate of the population standard deviation σ: $(N-1)$ is called the *degrees of freedom*, denoted ν.

The precision uncertainty P_X of an individual measurement at a confidence level C% is defined such that we are C% sure that the population mean μ lies in the interval $X_i \pm P_X$. Since we do not know the population standard deviation σ we cannot use Eqs. (23)–(26) to obtain P_X. Instead we use a result for a parent normal population from statistics theory, namely that

$$P_X = t_{\nu,\%} S_X \tag{29}$$

where $t_{\nu,\%}$ is the *Student t-distribution* variable. The value of t depends on the degrees of freedom, $\nu = (N-1)$, and the confidence level, %. For $\nu \geq 30$ the t-distribution is identical to the z-distribution, as shown in Figure 20. Selected values for are shown below

ν	$t_{95\%}$	ν	$t_{95\%}$
4	2.770	15	2.131
5	2.571	20	2.086
7	2.365	30	2.042
10	2.228	60	2.000

As $N \to \infty$, $t_{95\%} \to 1.96$ the value given in §9 for a normal population. Also the general use of $t_{95\%} = 2$ for $N > 10$ advocated in §5 is seen to a reasonable approximation. After all, there is always some uncertainty in error analysis!

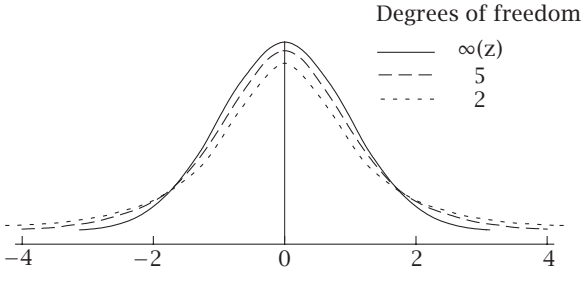

Figure 20 The Student t-distribution for various degrees of freedom.

Let us now suppose that we take a number of samples of size N from the population. We would not expect the mean values of the samples to be the same. The *central limit theorem* of mathematical statistics states that the sample means are also normally distributed with mean μ and standard deviation

$$\sigma_{\overline{X}} = \frac{\sigma}{N^{1/2}}. \tag{30}$$

In fact, sample means are normally distributed even when the parent population is not Gaussian! This is a very powerful result because, in steady state experiments, measurements are usually averaged over some time period before even recording the data. Notice that the scatter in data for $\overline{X}$ is only $1/N^{1/2}$ times that for X.

We now come to an important question: how well does the sample mean $\overline{X}$ estimate the population mean μ? The standard deviation of the sample mean can be estimated from the standard deviation of a single finite data set as

$$S_{\overline{X}} = \frac{S_X}{N^{1/2}}. \tag{31}$$

Then, since the sample means are normally distributed, the t-distribution can be used to write

$$\overline{X} = \mu \pm t_{\nu,\%} S_{\overline{X}}(C\%). \tag{32}$$

This is a very important result since we are most often primarily interested in estimating the sample mean. We can say with $C\%$ confidence that the population mean is within $\pm t_{\nu,\%} S_{\overline{X}}$ of $\overline{X}$.

Sometimes when a sample of N measurements are examined, one or more values appear to be out of line with the rest of the values: such data points are called *outliers*. If there is some good reason, based on our knowledge of how the test was carried out, to suspect the validity of the point, it can be discarded. For example, your laboratory notebook might indicate that the rig was left unattended for that test, or the ambient air condition had a significant variation. Otherwise, one can use a statistical criterion to identify data points that can be discarded. *Chauvenet's criterion* is recommended for this purpose. It states that points should be discarded if the probability of obtaining their deviation from the mean is less than $1/2N$. The probability is calculated from the normal distribution (not the t-distribution as may have been expected), and the following table results in which the ratio of the maximum acceptable deviation to the standard deviation is given as a function of N.

N	$\frac{(X_{\max} - \overline{X})}{S_X}$
5	1.65
7	1.80
10	1.96
15	2.13
20	2.24
50	2.57
100	2.81

One often sees a simpler criterion, namely $(X_{\max} - \overline{X}) = 3S_X$. The table shows that this should only be used for very large samples. For smaller samples Chauvenet's principle is more stringent.

Example 17. Gas Inventory of a Gas-Loaded Heatpipe.

BHMT Section 7.5.3 gives an analysis of gas-loaded heat pipe performance. A key parameter is the mass of gas loaded into the heatpipe, w_g. When testing such a heatpipe it is useful to check the amount of gas present. A simple check involves use of measured adiabatic section and heat sink temperatures and the length of the active portion of the condenser, L_a. This length can be estimated from plots of the axial temperature variation along the condenser due to the sudden temperature decrease into the inactive portion of the condenser (see Fig. 7.32 of BHMT). Due to axial conduction and diffusion the temperature change is not a step function and a precision error is introduced in "eyeballing" the temperature profile. Typical data are tabulated below.

Test	L_a, cm	w_g, μg
1	33.3	4.99
2	27.1	5.32
3	20.6	5.51
4	16.2	5.98
5	8.4	4.33

$$\overline{w}_g = \frac{1}{N}\sum_{i=1}^{N} w_{g,i} = 5.23\,\mu g$$

$$S_{w_g} = \left[\frac{1}{N-1}\sum_{i=1}^{N}\left(w_{g,i} - \overline{w}_g\right)^2\right]^{1/2} = 0.616\,\mu g.$$

From Eq. (30) the standard deviation of the sample mean is

$$S_{\overline{w}_g} = \frac{S_{w_g}}{N^{1/2}} = \frac{0.616}{\sqrt{5}} = 0.275\,\mu g.$$

The precision uncertainty of $\overline{w}_g$ is obtained from Eq. (32) as

$$P_{\overline{w}_g} = t_{4.95\%} S_{\overline{w}_g} = (2.770)(0.275) = 0.762\,\mu g$$

at the 95% confidence level.

Comments: Notice that the precision uncertainty in at the 95% level is actually greater than the standard deviation of the measurements because the sample is too small. In larger samples the precision uncertainty of the population mean at the 95% level is always smaller than the standard deviation of the measurements.

11 Curve-Fitting Samples from a Normal Population

In §4 we introduced the concept of least squares curve-fitting. In particular we showed how to obtain the slope m and intercept C of a straight-line curve-fit. Equation (8) gave the *standard error* of the fit as

$$S_Y = \left[\frac{1}{N-2}\sum_{i=1}^{N}(Y_i - \hat{Y}_i)^2\right]^{1/2} \tag{33}$$

where $\hat{Y} = mx + C$ was the curve-fit. Recall that all the precision error was assumed to be concentrated in the variable Y_i; x_i was assumed to have negligible precision error. Thus Y_i is a random variable and can be taken to have normal distribution for each value of x_i. Implicit in the theory we use is the assumption that the variance of these normal distributions does not vary with x_i, which may be inappropriate in many situations. The regression line is essentially a relationship between a "mean" value of Y, $\hat{Y}$, and x shown in Figure 21. The precision uncertainty of $\hat{Y}$ is the range that contains the parent population mean μ_Y, with C% confidence, and is

$$P_{\hat{Y}} = t_{\nu,\%}\left\{S_Y^2\left[\frac{1}{N} + \frac{(x_i - \overline{x})^2}{S_{xx}}\right]\right\}^{1/2} \tag{34}$$

where $S_{xx} = \sum x_i^2 - (1/N)\left(\sum x_i\right)^2$, and $\nu = N - 2$ (see, for example, [3]).

For N large and a 95% confidence level, we set $t_{\nu,\%} \cong 2$ to obtain Eq. (11). Equation (34) gives the 95% *confidence interval*, and gives the range where the regression lines will fall 95% of the time for repeated measurements, as shown in Fig. 8(b). There is a corresponding result for the 95% prediction interval, from which Eq. (12) is obtained.

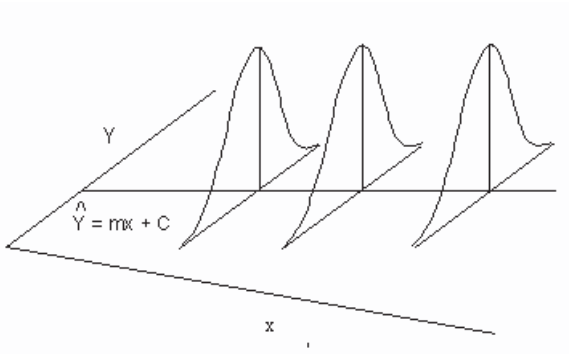

Figure 21 A straight-line best squares curve fit for a set of data (x_i, Y_i) where Y_i has a normal distribution at each value of x_i.

We are also interested in the precision uncertainty of the slope of curve-fit line m and the intercept C. The standard error in m is

$$S_m = \left(\frac{S_Y^2}{S_{xx}}\right)^{1/2} \tag{35}$$

and for the intercept

$$S_C = \left[S_Y^2 \left(\frac{1}{N} + \frac{\overline{x}^2}{S_{xx}} \right) \right]^{1/2}. \tag{36}$$

The corresponding precision uncertainties are

$$P_m = t_{\nu,\%} S_m \tag{37}$$
$$P_C = t_{\nu,\%} S_C. \tag{38}$$

Again, for N large and a 95% confidence level, we set $t_{\nu,\%} \cong 2$.

The Correlation Coefficient. Hand-held calculators, spreadsheets and a great variety of computer software are available for least squares curve-fitting and statistical analysis of the results—an activity usually called *regression analysis*. The correlation coefficient r plays a central role in statistical analysis of straight line curve-fits; it is defined as

$$r = \frac{1}{N-1} \sum \frac{(X_i - \overline{X})}{S_X} \frac{(Y_i - \overline{Y})}{S_Y} \tag{39}$$

and, in its general form, applies to data where X_i and Y_i are random variables. A value of $r = \pm 1$ indicates a perfect correlation of X and Y, that is, there is no scatter about the curve-fit and the standard error is zero. In statistics practice a straight-line curve-fit is considered reliable for $\pm 0.9 \le r \le \pm 1$ (the sign indicates that Y increases or decreases with X). Figure 22 shows how data appears at different values of r. The correlation coefficient thus give a useful quick check on whether a straight-line curve-fit makes sense. However, the correlation coefficient is only really useful when precision errors are large, as is often the case in experiments in the life sciences and medicine. Then the central question concerns whether there is any correlation whatsoever. In engineering experiments the precision errors are usually much smaller and the precision uncertainties of $\hat{Y}$, m and C are much more useful.

Higher Order Curve-fits. Straight-line (first order) curve-fits are used whenever possible. In general we can fit any function to data, often guided by theoretical modeling. In the absence of such guides we can use a polynomial of the form

$$Y(X) = a_0 + a_1 X + a_2 X^2 + a_3 X^3 + \cdots \tag{40}$$

where we prefer to use as few terms in the series as required to obtain an acceptable standard error. The algebra required to obtain the coefficients can be found in standard texts, but is not really required since there are many computer software products available to do the task. Although it is relatively simple to obtain a higher order curve-fit, the theory required for statistical analysis of the result is much less developed than for first order curve-fits.

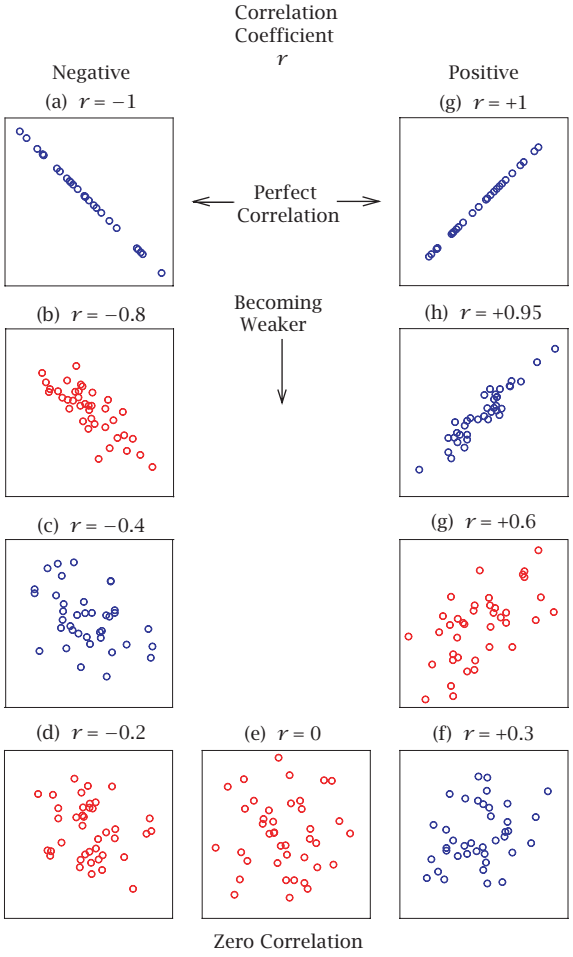

Figure 22 Data sets having different values of the correlation coefficient r.

Multivariable Curve-fits. We are often concerned with a dependent variable Y that is a function of a number of independent variables,

$$Y = f(X_1, X_2, X_3, \ldots). \tag{41}$$

For example, in forced convection heat transfer, we often seek a power law dependence of the Nusselt number or the Reynolds and Prandtl numbers,

$$\mathrm{Nu} = C\,\mathrm{Re}^m\,\mathrm{Pr}^n \tag{42}$$

(see, for example BHMT, Section 4.23). Again, computer software is available for this purpose, though for some functional relationships it may be desirable to write a new computer program.

Regression Analysis. Engineers usually obtain a least-squares curve fit of experimental data in order to estimate a functional relationship between the variables, for example, the relationship between friction factor and Reynolds number for pipe flow. In principle, with appropriate choice of instrumentation and careful execution of the experiment, the random error can be made to be negligibly small

(a correlation coefficient of ±1 to some specified tolerance). The underlying physical laws imply that there is a unique functional relationship between the two variables, for which the curve fit is an excellent estimate. However, in fields such as education, the life sciences, sociology, etc., the situation is usually different. For example, consider a sample of students who have their height and weight measured. The data is least-squares fitted to yield a *regression* line. If the measurements are made very precisely, the random error due to the measuring techniques can also be made to be negligibly small. But, since there is no physical law relating height to weight, a residual random error remains that is quite large—maybe a standard error of 50% or more.

The technique of performing least-squares curve fits is the same for both estimating a functional relationship, and performing a regression analysis. Owing to the critical importance of statistical analysis in these other fields, textbooks and software are usually primarily concerned with regression analysis. What is different between these two applications of curve fitting is how the curve fit is used, and the statistical procedures used to test hypotheses related to the data.

Example 18. Determination of Heatpipe Wick Parameters.

A test of a fixed conductance ammonia heat pipe is described in Example 7.12 of BHMT. In the test the burnout heat load is determined as a function of inclination angle. Theory indicates a linear relationship between $\dot{Q}_{\max}$ and $\sin\theta$ (= θ for small inclinations). The test procedure involves fixing the angle of inclination, and increasing $\dot{Q}$ in finite increments until burnout is observed (a rapid increase in the evaporator temperature due to dryout of the wick). $\dot{Q}_{\max}$ is then taken as the average of the $\dot{Q}$ values before and after burnout. Since testing is time consuming, the increment in $\dot{Q}$ cannot be too small—usually 2–4 W and hence a precision error results that is of this order. Precision and bias error in the power measurement are negligible in comparison. The angle of inclination is obtained by measuring the height of the evaporator above the condenser using a dial gage and the associated precision and bias errors are negligible. The table below show typical data.

Angle, radians	$\dot{Q}_{\max}$, W	Angle, radians	$\dot{Q}_{\max}$, W
0.0105	90.5	0.0209	43.0
0.0122	87.4	0.0227	27.52
0.0140	78.4	0.0244	18.15
0.0157	72.7	0.0262	15.46
0.0175	56.9	0.0279	10.74
0.0192	47.4		

With the angle denoted x and the burnout heat load denoted Y, the least squares curve fit for the data is

$$Y = mx + C = -5061x + 147$$

and is shown in Fig. 23, along with the data. If the only significant error is the precision error in $\dot{Q}_{\max}$, i.e., Y, a statistical analysis yields the following

$$\sum x_i = 0.211; \quad \sum Y_i = 548.17; \quad \overline{x} = 0.0192$$
$$\sum x_i^2 = 4.39 \times 10^{-3}$$
$$\frac{1}{N-2}\sum (Y_i - \hat{Y}_i)^2 = 14.93.$$

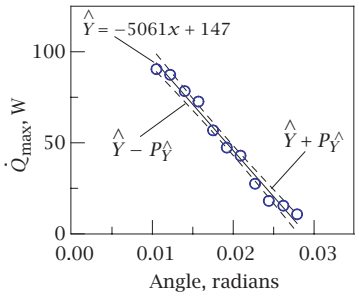

Figure 23 Heat pipe data, curve fit, and confidence interval.

Then the standard error of the curve-fit is given by Eq. (33) as

$$S_Y = \left(\frac{1}{N-2}\sum (Y_i - \hat{Y}_i)^2\right)^{1/2} = 3.86\,\text{W}.$$

We also need S_{xx}, defined by Eq. (34) as

$$S_{xx} = \sum x_i^2 - \left(\frac{1}{N}\right)\left(\sum x_i\right)^2$$
$$= 4.39 \times 10^{-3} - \frac{(0.211)^2}{11} = 3.43 \times 10^{-4}.$$

Then Eq. (34) gives the precision uncertainty of $\hat{Y}$ as

$$P_{\hat{Y}_i} = t_{\nu,\%}\left\{S_y^2\left[\frac{1}{N} + \frac{(x_i - \overline{x})^2}{S_{xx}}\right]\right\}^{1/2}$$

where $\nu = N - 2 = 11 - 2 = 9$, and for a 95% confidence, $t_{9,95\%} = 2.262$. Hence,

$$P_{\hat{Y}_i} = 2.262\left\{15.23\left[\frac{1}{11} + \frac{(x_i - 0.0192)^2}{3.43 \times 10^{-4}}\right]\right\}^{1/2}.$$

The resulting confidence interval is also shown in the figure. The standard error in the slope m is given by Eq. (35) as

$$S_m = \left(\frac{S_Y^2}{S_{xx}}\right)^{1/2} = \left(\frac{14.93}{3.43 \times 10^{-4}}\right)^{1/2} = 209\,\text{W/rad}$$

and the standard error in the intercept is given by Eq. (36) as

$$S_C = \left[S_Y^2\left(\frac{1}{N} + \frac{\overline{x}^2}{S_{xx}}\right)\right]^{1/2}$$
$$= \left[14.93\left(\frac{1}{11} + \frac{0.0192^2}{3.43 \times 10^{-4}}\right)\right]^{1/2} = 4.17\,\text{W}.$$

The corresponding precision uncertainty is given by Eqs. (37) and (38) as

$$\begin{aligned} P_m &= t_{9,95\%} S_m = (2.262)(209) = 473\,\mathrm{W/rad}; \\ P_C &= t_{9,95\%} S_C = (2.262)(4.17) = 9.43\,\mathrm{W}. \end{aligned}$$

Equation (7.90) of BHMT relates the burnout heat load to the angle of inclination as

$$\dot{Q}_{\max} = \left(\frac{\rho_\ell \sigma h_{fg}}{\mu_\ell}\right)\left(\frac{A_w \kappa}{L_{\mathrm{eff}}}\right)\left(\frac{2}{r_p} - \frac{\rho_\ell g L_{\mathrm{eff}} \sin\theta}{\sigma}\right).$$

The wick cross-sectional area A_w is $4.7 \times 10^{-5}\,\mathrm{m}^2$, and the effective length of the heat pipe is $L_{\mathrm{eff}} = 1.40\,\mathrm{m}$. Ammonia properties evaluated at 22 ℃ are

$$\begin{aligned} \rho_\ell &= 609\,\mathrm{kg/m^3}, & \sigma &= 21 \times 10^{-3}\mathrm{N/m}, \\ \mu_\ell &= 1.38 \times 10^{-4}\,\mathrm{kg/m\,s}, & h_{fg} &= 1.179 \times 10^{6}\,\mathrm{J/kg}. \end{aligned}$$

Substituting to obtain $\dot{Q}_{\max}$ with $\sin\theta \cong \theta$ for θ small gives

$$\dot{Q}_{\max} = 3.67 \times 10^{6} \kappa \left(\frac{2}{r_p} - 3.98 \times 10^{5}\theta\right) W$$

where $\kappa[m^2]$ is the wick permeability and $r_p[m]$ is the average pore radius in the wick. Thus, $\dot{Q}_{\max} = 0$ when

$$\frac{2}{r_p} = 3.98 \times 10^{5}\theta \left(\dot{Q}_{\max} = 0\right)$$

and $Y = 0$ when $x = \theta = 147/5061 = 2.905 \times 10^{-2}\,\mathrm{rad}$. Hence,

$$\begin{aligned} \frac{2}{r_p} &= (3.98 \times 10^{5})(2.905 \times 10^{-2}) \\ r_p &= 1.73 \times 10^{-4} = 0.173\,\mathrm{mm}. \end{aligned}$$

Also, the slope of $\dot{Q}_{\max}$ versus θ line is $m = (3.67 \times 10^{6}\kappa)(-3.98 \times 10^{5}) = -1.46 \times 10^{12}\kappa$ and from the data curve fit, $m = -5061$. Hence the permeability is

$$\kappa = \frac{5061}{1.46 \times 10^{12}} = 3.47 \times 10^{-9}\,\mathrm{m}^2.$$

What then are the precision uncertainties in κ and r_p? The answer for κ is straightforward; since

$$\begin{aligned} m &= -1.46 \times 10^{12}\kappa \\ \kappa &= -6.85 \times 10^{-13} m^2. \end{aligned}$$

For $P_m = 473\,\mathrm{W/rad}$,

$$\begin{aligned} P_\kappa &= 6.85 \times 10^{-13} P_m = (6.85 \times 10^{-13})(473) \\ &= 3.24 \times 10^{-10} m^2 (9.4\%). \end{aligned}$$

On the other hand,

$$r_p = -5.03 \times 10^{-6} m/C$$

so P_{r_p} depends on both P_m and P_C. The exact calculation of P_{r_p} proves to be a difficult problem in statistical analysis and is beyond the scope of this manual. However it is of the order of 10%.

12 Inferences

In § 10 and § 11 we have developed useful theory for samples and curve-fitting with normal data distributions. In fields such as the life sciences, medicine, education, sociology and production engineering, the general objective of statistical analysis is to *infer* information about the parent *population* from a limited *sample* of data. Many textbooks are available that present the methodology of statistical inference, but these texts focus on the needs of the above mentioned fields for which statistical inference is of critical importance. The needs of engineering experimentation are usually somewhat different, and the selection of material in § 10 and § 11 recognizes this situation.

In engineering experimentation our concern with statistics is usually only to be able to specify an appropriate precision uncertainty in a result, most often the mean of a sample, or a curve fit. Equations (32) and (34) are the key formulas. We are seldom concerned with parent populations in the sense considered by statistics texts. The situations encountered in engineering experimentation are varied: examples are given below for curve fitting, though similar examples could be given for sample means.

(i) Our linear curve fit is simply a representation (correlation) of data and we wish to specify an uncertainty of the curve-fit, that is, the confidence interval. Then all we are saying is that if we were to repeat the experiment we would be C% confident that the new curve-fit would lie within the confidence interval.

(ii) We may wish to compare our result to the prediction of a theoretical model. Then, if the theoretical prediction lies within the confidence interval, we can say that we are C% confident that the theory is valid for this situation.

(iii) We may have a theoretical model result with unknown parameters that we wish to infer (estimate) from our curve fit, that is, from the slope m and intercept C. Then we find use for the precision uncertainties of the slope and intercept given by Eqs. (37) and (38) (see Example 20).

(iv) There may be a set of data obtained in another laboratory for an allegedly similar situation. We then would ask whether the two situations are identical at a C% level of uncertainty.

(v) There may be an existing correlation of experimental data based on one or more sources. Can we say that we are C% confident that our data is consistent with the correlation? Such a task is usually impractical since seldom are the statistical data available for the existing correlation. The best we can usually do then is to treat the existing correlation like a theoretical model and proceed as in case (ii).

Only case (iv) is of the type of problem dealt with in most statistics textbooks. Of course, there is always the issue that there also are bias errors in our experiments, and that those errors are usually dominant. Following Rule 1 of §2, it is often sufficient to simply calculate the standard

deviation of a sample or standard error of a curve-fit and immediately conclude that precision errors are small and should be ignored.

13 Combining Bias and Precision Uncertainties

In this manual we have attempted to describe the various kinds of errors that occur in engineering experiments. When precision errors are significant we have shown how to use appropriate statistical theory to estimate precision uncertainties. We have described the nature of bias errors, and illustrated their occurrence in real laboratory experiments in various examples. In the case studies of §15 many further occurrences of bias errors in real experiments will be discussed. In the preceding sections of this manual the student has been given material that should facilitate an evaluation and rational discussion of possible uncertainties in their experimental data. In many situations no more can or should be done. Recently, however, there has been a move by research journals and standards organizations to require use of empirical rules for combining precision and bias uncertainties to give a single total uncertainty. In order to discuss and critique such rules, the guidelines given by the Journal of Heat Transfer of the American Society of Mechanical Engineers are reproduced below, as taken from the May 2000 issue of the journal.

An uncertainty analysis of experimental measurements is necessary for the results to be used to their fullest value. Authors submitting papers for publication to the *Journal of Heat Transfer* are required to describe the uncertainties in their experimental measurements and in the results calculated from those measurements. The Journal suggests that all uncertainty evaluation be performed in accordance with a 95% confidence interval. If estimates are made at a confidence level other than 95%, adequate explanation of the techniques and rationalization for the choice of confidence interval should be provided.

For each result presented, the presentation of the experimental data should include the following information:

1. **The precision limit, *P*.** The $\pm P$ interval about a nominal result (single or averaged) is the experimenter's 95% confidence estimate of the band within which the mean of many such results would fall, if the experiment were repeated many times under the same conditions using the same equipment. Thus, the precision limit is an estimate of the lack of repeatability caused by random errors and unsteadiness.
2. **The bias limit, *B*.** The bias limit is an estimate of the magnitude of the fixed, constant error. It is assigned with the understanding that the experimenter is 95% confident that the true value of the bias error, if known, would be less than $|B|$.
3. **The uncertainty, *U*.** The interval about the nominal result is the band within which the experimenter is 95% confident that the true value of the result lies. The 95% confidence uncertainty is calculated from
$$U = \left[B^2 + P^2\right]^{1/2}. \tag{43}$$
4. A brief description of, or reference to, the methods used for the uncertainty analysis.

The estimates of precision limits and bias limits should be made over a representative time interval for the experiment. The following additional information should be presented preferably in tabular form.

(a) The precision and bias limits for each variable and parameter used.

(b) The equations by which each result was calculated.

(c) A statement comparing the observed scatter in results on repeated trials (if performed) with the expected scatter ($\pm P$) based on the uncertainty analysis.

A discussion of sources of experimental error in the body of the text without the above does not satisfy our requirement. All reported data must show uncertainty estimates. All figures reporting new data should show uncertainty estimates of those data either on the figure itself or in the caption. A list of references on the topic is provided below.

Each of the four items in the guidelines will be discussed in turn.

Item 1. The term "precision limit" is similar to our term "precision uncertainty" for a sample mean, and "confidence interval" for a curve fit.

Item 2. The term "bias limit" is loosely equivalent to our term "bias uncertainty." Whereas we chose to simply estimate a "reasonable upper bound" to the bias uncertainty, these guidelines suggest that statistical concepts can be applied to yield a 95% confidence level estimate. But bias errors are *not* governed by the laws of statistics, so that such an approach is without physical basis. Indeed, this dilemma has been recognized by some organizations, e.g. the International Organization for Standardization (ISO), in using the term "coverage" rather than "confidence" in dealing with bias errors. That is, the bias limit gives a 95% *coverage* of the true value of the bias error. But changing the terminology does not really solve the problem of how to actually estimate a 95% coverage. In some cases one can see merit in this approach. For example, consider the very common situation of a sensor with a linear response and a scale factor K. If many sensors are produced, the manufacturer will not calibrate each sensor. Instead, a sample will be calibrated and the mean value given as the nominal value of K, and the 95% confidence level estimate of uncertainty given as the accuracy. Usual calibration procedures are relatively precise, and hence this accuracy can be taken as due to a bias error—each sensor is different. So in this case we have a bias uncertainty estimated by statistical methods: nevertheless, we must remember that it is a bias error and does not change from test to test when using the sensor. Most often, however, we have such a poor understanding of the possible bias errors that to talk about a 95% coverage is meaningless: we simply do our best to quantify the possible error and often our estimate is little more than a guess.

Item 3. If the bias uncertainty truly had a Gaussian distribution, then this combining rule would be valid: it is the same as the rule for combining precision errors given by Eq. (17). But bias errors, by definition, do not have a Gaussian distribution and so the rule has very little meaning.

Example 24 that follows shows how the rule can lead to absurd results. Surely, a statement of the precision uncertainty and an evaluation and discussion of possible bias errors are of more use than a single, possibly meaningless number.

Item 4. Reference to "time interval" is puzzling. Most often errors are relatively larger at extreme values of some of the parameters. It may be important to focus on such situations, rather than "representative" conditions for which errors may have a minor consequence. In reference to item 4(a), our Rule 1 of §2 is surely preferable. Why give details of errors that have negligible impact on the experiment? Item 4(c) violates our Rule 3 of §2. If repeated trials are performed (as is usually the case) or if least squares curve-fits are obtained, the observed scatter is our best source of information for precision errors. If an uncertainty analysis gave a different result it would have to be rejected, or "fine tuned" (fudged) to give the same result. The requirements that all figures reporting new data should show uncertainty estimates of those data is particularly disturbing. In §5 we showed the importance of precision uncertainty of a sample mean, and the confidence interval of a regression line. Very few published papers present this information.

General Comments

1. Implicit in Item 2 is that if there is more than one bias error, these errors should be combined by assuming that they all have Gaussian distributions, then

$$B = \left(B_1^2 + B_2^2 + \cdots\right)^{1/2}. \tag{44}$$

   Again, this practice has no physical basis and can give absurd results. At best it can simply give an indication of the magnitude of the bias uncertainty. In reality with a number of sources of bias error, the true total bias error could be as large as the arithmetic sum of the individual bias errors, and as small as zero if the errors fortuitously cancel. A single number given by Eq. (44) does not allow the user to be aware of such possibilities.

2. If it were relatively simple and quick to follow the guidelines, one could argue pragmatically that it should just be done so that the information is available to interested parties. But, for the usual experiment, a careful and intellectually honest following of all the requirements of the guidelines requires an enormous amount of work, with many difficult decisions to be made. As a result, one seldom sees evidence of a faithful compliance with the guidelines: usually it is obvious that there has been only lip service to the requirements. In the few cases we have seen where such guidelines have been faithfully followed, a careful examination of the details simply demonstrated the futility of the approach. Why expend great effort to estimate small bias errors when the combining rule has no physical basis? Also, the question arises as to who are the interested parties? Editors of journals are unlikely to ever use the results of a paper published in a journal. The interested practicing engineer or research worker is more likely to be interested in (a) the precision uncertainty of the mean (or equivalent), and (b) an intelligent discussion of possible bias errors and their magnitudes. Then they can decide how to use this information for their own specific purposes, which can be quite varied.

Example 19. Errors in a Flow Rate Measurement.

Let us revisit Example 3, which dealt with flow rate measurement using a laboratory burette. It was shown that there was a bias error due to the presence of a liquid film on the burette inside wall. Using a laminar film model it was estimated that the resulting bias error was $B_x \approx 0.093$ ml for the flow rate considered. Let us decide to not make a correction for this bias error. Now suppose that the expected precision uncertainty due to difficulty in reading the scale is $P_x = 0.02$ ml. Then, following the combining rule given by Eq. (43), the total expected error in the flow measurement is

$$U_x = \pm\left(B_x^2 + P_x^2\right)^{1/2} = \pm\left(0.1^2 + 0.02^2\right)^{1/2} = \pm 0.102\,\text{ml}.$$

But clearly the expected total error is rather

$$U_x = +0.1 \pm 0.02\,\text{ml}.$$

In particular, U_x can never be less than +0.08 ml. To suggest that U_x could be –0.12 ml is absurd.

Comments: The bias errors that we are most often concerned with are one-sided (biased!). Thus, use of Eq. (44) can be very misleading.

14 Sampling Time Dependent Data

Examples 6 and 15 dealt with a boiling heat transfer experiment in which the temperature–time response was measured for a copper sphere suddenly immersed in a pool of liquid nitrogen. In principle the resulting data for $T(t)$ can be subjected to an error analysis using the methods described in previous sections of this manual. However, there are special features of this type of problem that are worthwhile considering in greater detail. Some time ago, time dependent data was recorded by using "strip-chart" recorders in which the sensor output was recorded by a pen on a moving chart. But nowadays we almost always use a computer-based data acquisition system in which the sensor analog output is recorded at discrete intervals in digital form: the frequency of sampling the analog output is then a parameter that must be chosen by the experimentor. In Fig. 24 an analog signal is sampled at two different frequencies (rates). Fig. 24(a) shows a situation where the sampling frequency is too low. Because of undersampling, the peaks and valleys are not well resolved by the discrete sampled values. When the sampling frequency

is increased, Fig. 24(b) shows that the signal resolution can

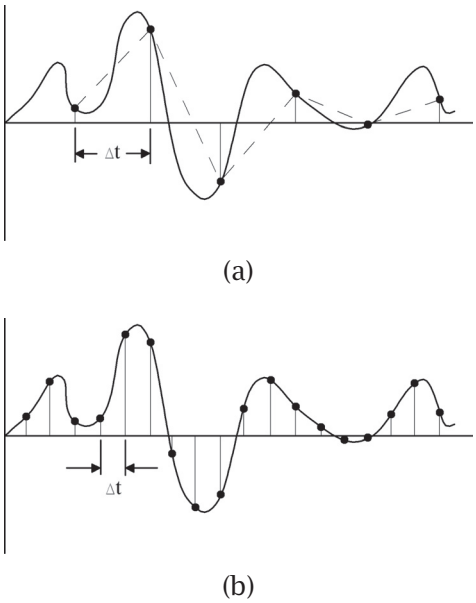

Figure 24 An analog signal sampled at two different rates: (a) Low sampling frequency; (b) High sampling frequency.

be greatly improved. In the situation shown in Fig. 24, it seems obvious that the experimentor must choose a sampling rate high enough to resolve the features of the data that are of interest. Fortunately, even relatively inexpensive modern data acquisition systems can provide sampling frequencies up to 100 Hz (100 samples per second). But there is a complicating factor: the analog to digital signal conversion introduces a precision error (noise) into the digital data. As mentioned in Example 15, the A/D converter replaces the continuous voltage signal by a sequence of discrete values. For example, an 8-bit A/D converter can record $2^8 = 256$ voltage levels. If it is to have a range of 10 mV, then its least count is necessarily $10/256 = 0.04$ mV, which gives a precision error of this order in the digital data. At lower sampling rates the least count can be obtained as shown above. However, some data acquisition systems need to change their mode of operation at higher sampling rates, and a larger least count can result.

If only the actual data values are of concern, and the least count remains constant, increasing the sampling rate will improve the resolution of the signal. However, there can be complications when the signal is further processed, for example, when it has to be differentiated as a key step in the data reduction procedure. Example 20 illustrates this issue.

Since the quantization noise is random in nature, it can be reduced by a process known as *filtering*. A simple filtering scheme consists of replacing the data sequence by a "moving average." For example, three point averaging replaces the 1st, 2nd and 3rd points by their average, the 2nd, 3rd and 4th points by their average, and so on, as shown in Fig. 25. This data *smoothing* process reduces the noise, but must be used carefully because it can distort the true variation of the signal, for example, in the vicinity of a local maximum or minimum. Consider a sequence of data 1, 2, 9, 4, 2, 3. The maximum value is 9± the precision error. Now apply a 3 point moving average to generate a new sequence: $(1 + 2 + 9)/3 = 4$, $(2 + 9 + 4) = 5$, etc. The new sequence is $4, 5, 5, 3$ with a maximum of only 5 (± a reduced precision error).

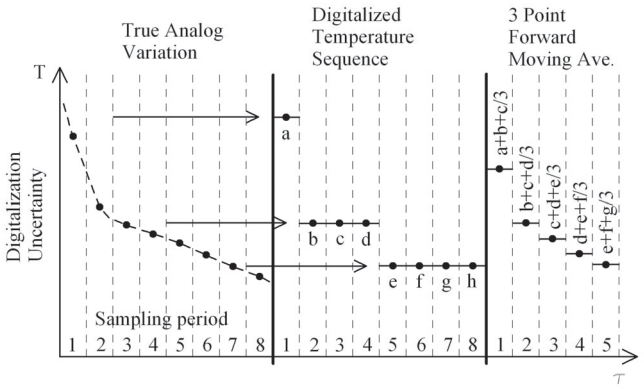

Figure 25 A simple filtering scheme: use of a moving average.

Example 20. Resolution of Boiling Peak Heat Flux.

In Example 15, the precision error introduced into $q(t)$ by the A/D conversion was analyzed by propagating the error in T through the central difference formula used to calculate q. Denoting the precision error in T by P_T, the precision error in q was obtained as

$$P_q = \frac{C}{2\Delta t}\left[P_{T_{n+1}}^2 + P_{T_{n-1}}^2\right]^{1/2}$$

where $C = \rho c D/6$ and $\Delta t = 1/f$ where f is the sampling frequency. In Example 15, this equation was used to predict noise in the film boiling regime. Here we will look into the determination of the peak heat flux (for which data were given in Example 5). For $\rho = 8930\,\mathrm{kg/m^3}$, $c = 250\,\mathrm{J/kg\,K}$, $D = 1.27 \times 10^{-2}\,\mathrm{m}$, $C = 4730\,\mathrm{J/m^2K}$. Also $q_{\max} = 133{,}000\,\mathrm{W/m^2}$. Thus, taking P_T to the least count of the data acquisition system, which at a 50 hz sampling rate was 0.025 K,

$$\begin{aligned}\frac{P_q}{q} &= \frac{0.0178}{\Delta t}\left(0.025^2 + 0.025^2\right)^{1/2} \\ &= \frac{6.25 \times 10^{-4}}{\Delta t}.\end{aligned}$$

For $\Delta t = 0.02$ s,

$$\begin{aligned}\frac{P_q}{q} &= 3.15 \times 10^{-2} \sim 3\% \\ P_q &= 3.15 \times 10^{-2} \times 133{,}000 = 4190\,\mathrm{W/m^2}.\end{aligned}$$

If the sampling rate were 10 Hz, then $\Delta t = 0.1$ s and

$$\frac{P_q}{q} = 6.29 \times 10^{-5} \sim 0.6\%$$
$$P_q = 6.29 \times 10^{-3} \times 133,000 = 840\,\mathrm{W/m^2}.$$

Now let us consider a simple laboratory setup of this boiling heat transfer experiment. For convenience it was decided to process the data in real time, that is, dT/dt and $q(t)$ were calculated as $T(t)$ was recorded and displayed. Then the boiling curve $q(T - T_{\mathrm{sat}})$ was displayed. As q was calculated the highest value was retained and displayed as $q_{\max}$ with the boiling curve. The table below shows some typical results for 8 sample averages.

Δt s	$\overline{q}_{\max}$ $\mathrm{W/m^2} \times 10^{-5}$
0.3	1.18
0.1	1.44
0.05	1.53
0.02	1.67

At first sight one may be one may be tempted to assert that a very small Δt is required to "capture" $q_{\max}$. But this is not true because $q_{\max}$ obtained in this manner is $q_{\max}$ plus the maximum noise: the values in the table are really meaningless. The increase in $\overline{q}_{\max}$ at smaller values of Δt is due to the increase in precision error. Figure 26 shows a set of $q(T - T_{\mathrm{sat}})$ data in the vicinity of $q_{\max}$. The proper way to obtain $q_{\max}$ from the data is to least squares curve fit the data near $q_{\max}$

Comments. Note that the table does show that $\Delta t = 0.3$ s is not small enough to capture $q_{\max}$

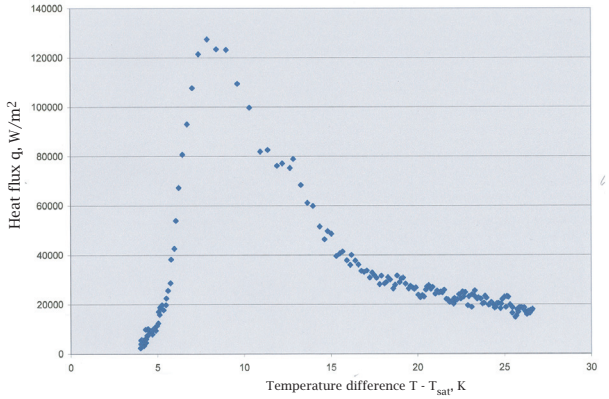

Figure 26 A boiling curve for a sphere in liquid nitrogen.

References

[1] Mills, A.F., *Basic Heat and Mass Transfer, (or Heat Transfer)*, 2nd eds., Prentice-Hall, New Jersey, 1999.

[2] Gopinath, A., and Harder, D.R., "An experimental study of heat transfer from a cylinder in low-amplitude zero-mean oscillating flows," *Int. J. Heat and Mass Transfer* **43**, 505–520 (2000).

[3] Wonnacott, R.J. and T.H., *Introductory Statistics*, 4th ed., John Wiley, 1985.

15 Case Studies

Case Study No 1. Stagnation Line Convective Heat Transfer.

Laminar boundary layer theory is expected to yield a reliable estimate of convective heat transfer at the stagnation line of a smooth circular cylinder in a cross-flow of air. The results of numerical solutions can be correlated as

$$\mathrm{Nu}_D = 1.141\mathrm{Re}_D^{0.5}\mathrm{Pr}^{0.4}, \quad \mathrm{Pr} \approx 1.$$

This equation is a useful benchmark for evaluating experimental methods used to measure local convective heat transfer coefficients. In this case study we describe two methods that were evaluated in this manner.

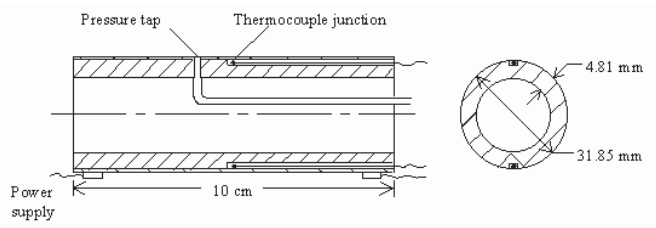

Figure 27 Test cylinder of method 1.

Method 1

This method is based on uniformly heating the cylinder surface and extracting the heat transfer coefficients from the power input to the heater and measured surface and free-stream air temperatures. The test cylinder is shown in Fig. 27. It is 10 cm long, has an outside diameter of 31.85 mm, and consists of 4.81 mm wall thickness, phenolic bonded linen tube, around which is wound a stainless steel heater ribbon 0.0254 mm thick, 12.7 mm wide and 607 mm long. The resistance of the ribbon is approximately 1Ω. The power input to the heater is controlled by a Variac and measured with a wattmeter. Due to the relatively poor peripheral conductance of the composite tube, we can safely assume a uniform heat flux heating in the stagnation region. A 30 gage chromel–alumel thermocouple is located midway across the cylinder just underneath the heater ribbon. A second thermocouple is similarly installed at a displacement of 180 degrees. A third thermocouple measures the free-stream temperature. A digital thermometer provides temperature readouts for the three thermocouples. The cylinder can be rotated to obtain the temperature distribution around the cylinder, and to have either thermocouple at the forward stagnation line. The

wind-tunnel cross-section is 10 cm wide and 40 cm high. The air speed is measured using a pitot tube and an inclined manometer. The test rig was designed to be relatively simple and robust for use in an undergraduate mechanical engineering laboratory course. Accuracy data for the instrumentation are as follows.

1. *Thermocouples/Digital thermometer.* Calibration in a constant temperature bath indicated bias errors that were typically 0.1 K, and never exceeded 0.2 K. Temperature fluctuations were negligible so that the precision errors are no greater than the least count of the digital readout, which is 0.1 K.
2. *Air Speed.* The inclined manometer can be read to 0.005 inches of water which corresponds to 2% and 0.25% of the scale reading at the low and high ends of the range, respectively. Since air speed is proportional to the square root of manometer height, the associated precision error in the air speed is no greater than 1% and 0.1% respectively. Bias errors for the manometer are negligible.
3. *Power Input.* The least count of the wattmeter were of the order of 0.1% of scale readings and fluctuations were negligible. Thus precision errors in the power measurements were negligible, and bias errors in the meters are expected to be less than 0.5%, which is also negligible.

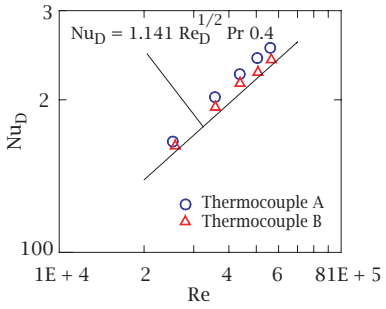

Figure 28 Comparison of stagnation line Nusselt numbers with the theoretical values using method 1.

Results

The local heat transfer coefficient was calculated from

$$h_c = \frac{P/A}{T_s - T_C}$$

where P is the power input to the heater and A is the area of heater ribbon (7701 mm^2). Air properties were evaluated at the mean film temperature to calculate the Nusselt and Reynolds numbers. Sample test data are shown in Table 8 and Fig. 28. The two sets of data for thermocouple A were obtained by first decreasing the tunnel speed and then increasing it back to the maximum. Examination of the result shows two important features.

(i) The precision of the calculated Nusselt numbers is very good—the precision uncertainty is about 1%.

(ii) There is an obvious systematic difference between the results obtained with the two thermocouples.

Table 8 Stagnation line Nusselt numbers obtained using Method 1.

Thermo-couple	Re_D	Nu_D (theory)	Nu_D (exp.)	% difference
A	56,100	233.0	253.4	8.8
A	50,600	221.3	241.4	9.1
A	43,900	206.1	225.5	9.4
A	35,700	185.8	202.5	9.2
A	25,300	156.5	169.5	8.3
A	35,800	186.1	204.0	9.6
A	43,700	205.6	224.8	9.3
A	50,400	220.8	242.0	9.6
A	55,900	232.6	253.3	8.9
B	56,600	234.0	241.7	3.3
B	50,700	221.5	228.2	3.0
B	43,800	205.9	217.0	5.4
B	35,800	186.1	194.8	4.7
B	25,800	158.0	163.3	3.4

Thus, before proceeding further, we can state that precision errors are not an issue in this experiment; the important issue is the bias error in one or both of the surface temperature measurements.

To illuminate this bias error, some information on the history of the test rig is pertinent. The test cylinder used in the experiment was the fourth cylinder that has been built and tested over a period of twelve years. The first cylinder had only one thermocouple installation, and when checked out gave excellent agreement with theory for stagnation-line heat transfer. After successful use by many groups of students over a number of years it was damaged by inadvertent overheating. The second cylinder was essentially identical to the first but, when checked out, there was a significant discrepancy between theory and experiment. After reinstalling the surface thermocouple, the check-out yielded excellent agreement once again. Thus we learned that special care had to be taken to ensure good thermal contact between the thermocouple junction and the under-surface of the heater ribbon. After a few years, cylinder No. 2 started to give poor results, which was attributed to deterioration in the thermocouple installation due to differential expansion over many heating and cooling cycles. Based on this experience, subsequent test cylinders were built with a second surface thermocouple installation to increase the likelihood of having a satisfactory installation, and also to demonstrate the value of redundancy in helping to identify bias errors. Thus it is reasonable to conclude that both thermocouples give biased results due to unsatisfactory installation.

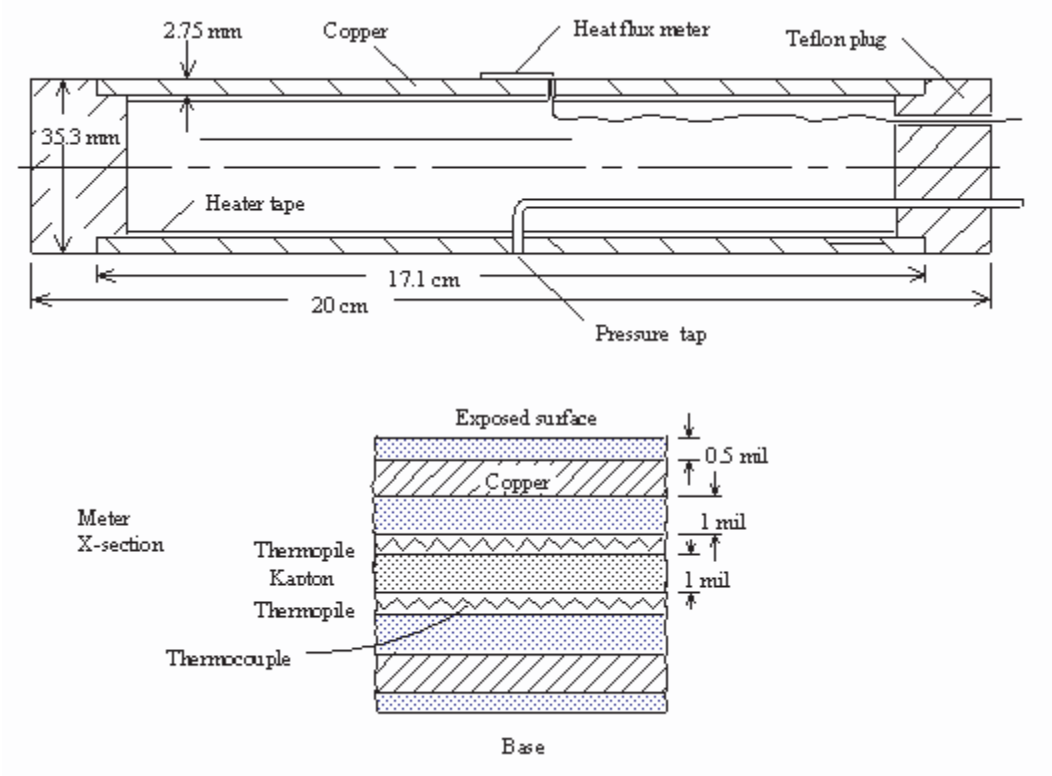

Figure 29 Test cylinder of method 2.

Method 2

This method uses a thin film heat flux sensor bonded to a thick wall copper test cylinder containing an electric heater. The heat transfer coefficient is calculated from the measured heat flux, and surface and free-stream temperatures. The test cylinder is shown in Fig. 29. It has a 35.3 mm outside diameter and 2.75 mm wall thickness. It spans a 20 cm wide, 55 cm high wind-tunnel, and the 15.2 cm long midsection is heated by a heater tape attached on its inner surface. A cross-section of the heat flux meter is also shown in Fig. 29. The sensor is 6.35 mm wide, 15.9 mm long, and approximately 0.1 mm thick, and is bonded to the test cylinder using a contact adhesive. The two thermopiles are located on each side of a 1 mil-thick Kapton film in order to measure the temperature difference across the film. A separate type T thermocouple measures the temperature underneath the film. The manufacturer calibrates the meter by comparing its output to a master sensor, and a calibration constant (in μV thermopile output per unit heat flux) is supplied with the meter. Upstream of the test section is a 4 to 1 area contraction. Pressure taps are located at the ends of the contraction, and the pressure differential to determine the air velocity. An OMEGA PX160 series pressure transducer is used for this purpose. Data acquisition is performed by a Strawberry Tree connection Mini-16 system and the data fed to a PC for display. For convenience, pertinent calculated data are displayed in real time including the Reynolds and Nusselt numbers and the theoretical stagnation-line Nusselt number.

Typical test data is shown in Fig. 30. A significant discrepancy between the experimental stagnation-line Nusselt number and theory was obtained. The measured value is from 8 to 15% too high over the Reynolds number range. The precision of the data is very good: clearly the only issue is an apparent bias error in the measured value. Notice that the bias errors associated with faulty thermocouple installations with Method 1 were never as large as the bias error seen here. Since the wind-tunnel and instrumentation differed to that used with Method 1, all possible sources of error were carefully examined. The velocity profile in the tunnel was checked using a Pitot tube traverse, leading to a high level of confidence in the measured Reynolds numbers. All computer performed calculations were checked by hand. Thermocouples were calibrated. Finally the test cylinder was located in a much larger wind-tunnel with mostly different instrumentation, yielding no significant change in the test results. Thus the conclusion was reached that the heat flux meter calibration was inaccurate.

The manufacturer supplied calibration constant was $0.350 \mu V/(\mathrm{Btu/hr\,ft^2})$, with no accuracy specified. Contacts with the manufacturer were rather frustrating. It was difficult to locate an employee who understood that an accuracy should be specified, and we were not able to obtain such information. One input we received was that our operating heat fluxes were lower than those normally used

and could be affected by an offset error: but no quantitative information was obtained. We decided to replace the heat flux meter with one of the same model, which had a calibration constant of $0.408\mu V/(\text{Btu/hr ft}^2)$. Figure 31 shows the new test data for which the measured value is now from 2.9% to 5.7% too low over the Reynolds number range tested. Since the method of installation of the sensor and the test rig and instrumentation were identical to that used with the first sensor, we concluded that the manufacturer calibration constants were unreliable. Subsequently we noted in the literature a similar complaint concerning the same manufacturer's sensors [1].

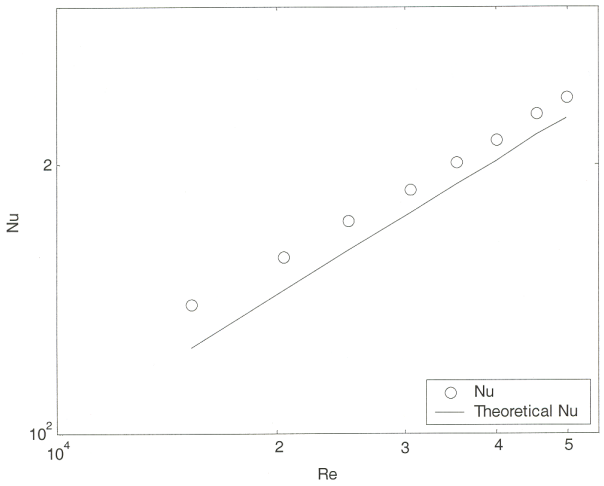

Figure 30 Comparison of stagnation line Nusselt numbers with theory using method 2: first heat flux meter.

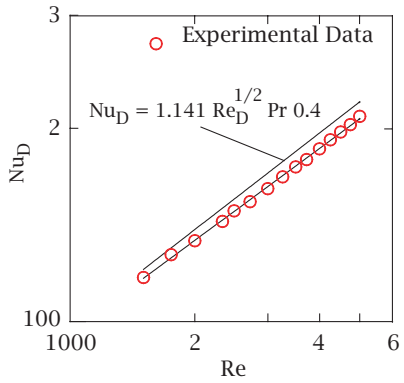

Figure 31 Comparison of stagnation line Nusselt numbers with theory using method 2: second heat flux meter.

To investigate the possible effect of heat flux on sensor accuracy we conducted a series of tests in which the temperature difference $(T_s - T_e)$ was varied from 10 K to 30 K. In order to prevent falsification of these tests by variable fluid property effects, the data was processed according to the recommendation of Kays and Crawford [2]. In this scheme all properties are evaluated at the free-stream temperature with a subsequent temperature ratio correction of applied to the Nusselt number. The results are shown in the Table 9.

Table 9 Nusselt number variation with surface heating.

Re_D	$T_s - T_e$	Nu_{th}	Nu_{exp}	% error
25,190	10.8	156.7	145.6	−7.1
25,190	21.0	157.2	149.6	−4.8
25,190	30.8	157.7	154.5	−2.1
31,100	10.1	174.0	159.3	−8.4
31,100	20.4	174.6	165.2	−5.4
31,100	30.7	175.2	168.8	−3.7
40,490	9.5	198.5	179.1	−9.8
40,490	20.1	199.2	187.3	−6.0
40,490	28.2	199.7	189.7	−5.0

In this table the constant property theoretical Nusselt number is multiplied by $(T_s/T_e)^{0.1}$ to give Nu_{th} and Nu_{exp} is evaluated using free stream properties. Table 9 shows that the accuracy of the experimental results does indeed improve with increasing heat flux, suggesting a zero offset error in the heat flux meter. If this is the case it should be the responsibility of the manufacturer to specify this zero offset error, or at least specify a minimum heat flux for which the calibration constant is guaranteed some tolerance.

References

[1] Scholten, J.W. and D.B. Murray, Heat transfer in the separation and wake regions of a gas–particle flow, *Proc. 10th International Heat Transfer Conference*,Brighton, England, **2**, 375–380 (1994).

[2] Kays, W.M. and M.E. Crawford, *Convective Heat and Mass Transfer*, 3rd ed. McGraw-Hill, New York, 1993.

Case Study No 2. Friction Factor for Flow in a Smooth Tube.

A popular undergraduate laboratory experiment is the measurement of pressure drop for flow of water in a long tube. By varying the flow rate, data are obtained for friction factor as a function of Reynolds number, which can be compared with established correlations or the Moody chart. One such test rig has a flow loop consisting of a high pressure pump, turbine flow meter, control valves to allow one of three different diameter copper tubes to be selected, and a return tank. The pressure differential is measured with a silicon piezoresistive pressure transducer. Type K thermocouples are attached to the walls of the test tubes. The output from the pressure transducer and thermocouples is fed to a data acquisition system connected to a PC. The specifications of the flowmeter and pressure transducer are described in detail in Examples 2 and 5, respectively. Pertinent information about the instrumentation is as follows.

Flowmeter: Maximum bias error ±0.5%

Pressure transducer: "Typical" and "maximum" bias errors due to various sources are arithmetically summed to give the values in the table below.

Pressure,	kPa	200	100	50	20	10	5
Typical	% ±	3.85	3.95	4.15	4.75	5.75	7.75
Maximum	% ±	4.25	4.75	5.75	8.75	13.75	23.75

Data acquisition system: Samples data at 5 Hz and displays 10 sample running averages.

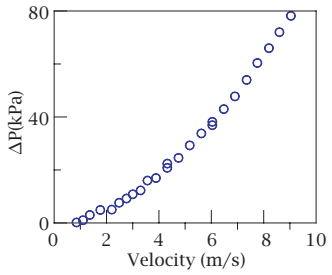

Figure 32 Measured pressure drop versus bulk velocity.

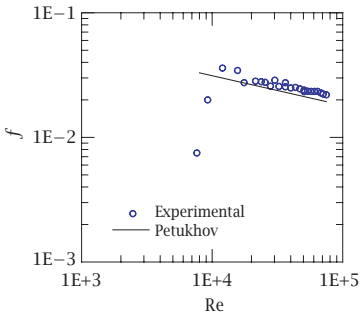

Figure 33 Comparison of measured friction factor with Petukhov's correlation.

The test rig was cleaned and reactivated after a summer vacation, and checked out by obtaining a data set for the smallest diameter tube (7.75 mm I.D., 0.673 m between pressure taps). Plots of pressure drop versus bulk velocity and friction factor versus Reynolds number are shown as Figs. 32 and 33, respectively.

The plot of f versus Re_D shows an erratic behavior at low flow rates that can be easily explained. The plot of ΔP shows that ΔP is less than 5 kPa for the first five data points, and the deviations in f are in line with the possible bias errors given in the pressure transducer specifications. If data is required for $\mathrm{Re}_D < 2\times10^4$ ($\Delta P < 10$ kPa), a pressure transducer with a much smaller full scale span should be used.

Let us discard the data for $\mathrm{Re}_D < 2\times10^4$ and examine the remaining data. Some precision error is in evidence. Observation of the computer screen showed fluctuations of ±0.5 kPa in ΔP. At 13 kPa this is ±4%, which can explain the observed scatter. Further filtering of the data should reduce this precision error. However, the important feature of the results is an apparent bias error: the experimental f values are too high. For example, the discrepancy at $\mathrm{Re}_D \cong 7\times10^4$ is 11%. Since smaller discrepancies had been noted in previous years, it was concluded that some problem had developed causing a systematic error. Fortunately the remedy was fairly simple. By inspecting the system it was found that there was significant residual detergent in water: the system was flushed thoroughly and the table and Fig. 34 shows new results.

Temp. K	ΔP kPa	Flowrate $\times10^4$	Re_D $\times10^4$	f	f_{Petukhov}	Deviation %
294.3	72.2	4.30	7.08	0.0200	0.0194	3.1
294.4	64.1	4.00	6.61	0.0205	0.0197	4.2
294.5	55.8	3.72	6.16	0.0207	0.0200	3.5
294.6	55.9	3.72	6.16	0.0207	0.0200	3.5
294.6	45.0	3.31	5.50	0.0210	0.0205	2.4
294.8	38.1	3.03	5.04	0.0213	0.0209	1.8
294.9	29.9	2.60	4.35	0.0226	0.0216	4.4
295.0	23.7	2.31	3.86	0.0229	0.0223	2.7
295.1	16.6	1.90	3.19	0.0236	0.0233	1.3
295.1	9.8	1.40	2.35	0.0257	0.0251	2.4

Petukhov's formula for friction factor is

$$f = (0.790\ln \mathrm{Re}_D - 1.64)^{-2}; \quad 10^4 < \mathrm{Re}_D < 5\times10^6$$

and gives values essentially identical to those given by the Moody chart in this Reynolds number range. The deviations are now in the range 1.3–4.4%. The scatter indicates a precision uncertainty of the order of ±2% which is very small. Referring to the table of specified bias errors for the pressure drop sensor we see that the deviations in f are less than the "typical" bias error for the sensor. Clearly, there is little more that can be said about errors in these results. For routine engineering purposes the accuracy of the data is certainly adequate. If more accurate data are required, a more accurate pressure sensor must be used. The pressure transducer used here is relatively inexpensive (~ $30): more accurate sensors are widely available but are considerably more expensive.

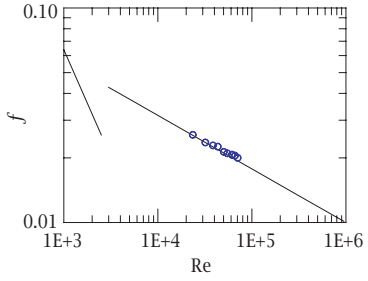

Figure 34 Measured friction factor after eliminating a source of systematic error.

Case Study No 3. Natural Convection in a Circular Cavity.

There have been many experimental studies of heat transfer across horizontal and inclined fluid layers of square or

rectangular cross-sections; corresponding data for a circular cross-section do not appear in the literature. For a horizontal layer the shape of the cross-section should have little effect, but for inclined layers a more significant effect may be expected. An undergraduate laboratory test rig was developed to study heat transfer across a circular layer, partly because it was simpler to construct than a rig for a rectangular layer. For convenience it was decided to use only one test fluid, namely water, and obtain a large range of Rayleigh numbers by varying the thickness of the water layer. A section through the test cell is shown in Fig. 35; the lower plate assembly is fixed and the upper assembly is moved by a screw drive. Sealing of the plates in the container tube is by O-rings. Each plate assembly has a hard rubber layer sandwiched between two copper plates, to serve as heat flux meters. Five 30 gage type-T thermocouples are located on each side of the rubber layers to form the heat flux meters. One plate is heated by hot water from an electrically heated supply; the other plate is cooled by chilled glycol-water coolant. Typically the hot plate is maintained at 45–50 °C and the cold plate at 0–5 °C so that the test liquid is at approximately the ambient temperature of 22 °C. The thermocouples are connected to an ACRO data acquisition system and the digital output transmitted to a PC for display. Pertinent specifications of the instrumentation are as follows.

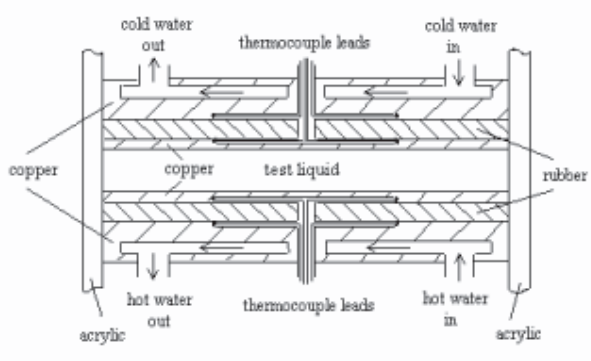

Figure 35 Natural convection cell.

Thermocouples: A bias error of no greater than 0.2 K, possibly no greater than 0.1 K.

Data acquisition unit: Samples at 10 Hz, averages over 2 s, and averages each set of four thermocouples. Displays to 0.1 K which is taken to be the precision error in the temperatures.

Dial-gage: A bias error due to uncertainty in zero reading of 0.1 mm (depends on torque applied to screw to completely close the gap). Least count 0.01 mm.

Heat flux meters: No specification since these are calibrated as part of the experiment procedure.

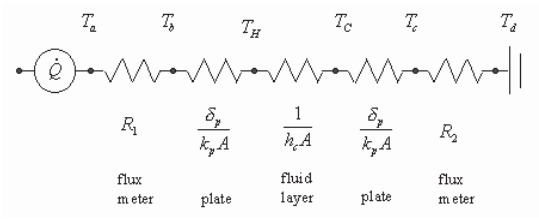

Figure 36 Thermal circuit of the natural convection test cell ($1/h_c A = L/kA$ for calibration).

Heat flux meter calibration. The thermal conductivity and thickness of the rubber layer are not known accurately enough to specify the thermal resistance of the heat flux meters. Calibration is required and is accomplished by rotating the test cell to 180°, for which the cold plate is underneath the hot plate. Then the liquid layer is stable, there is no convection, and heat transfer across the layer is by conduction. Since the thickness of the layer and the thermal conductivity of water are accurately known, the heat flow in the equivalent circuit shown in Fig. 36 can be calculated and used to determine the thermal resistances of the heat flux meters. In principle, calibration at one thickness of water layer should suffice: the meter thermal resistances should be constants. However, calibration at different plate spacings yields a systematic variation with plate spacing, as shown in Fig. 37. The observed precision errors are relatively small and are mainly due to the time required for the system to reach steady state. When more time is allocated to the calibration process, the precision improves.

How should the variation in R_1 and R_2 be viewed? Is this variation a characteristic of the system such that the same variation is obtained in convection experiments with the system inverted? If so, the graphs of R_1 and R_2 can be used to determine appropriate values for the spacings used in the convection tests. Or should we view the variation as a bias error and simply use the average values of R_1 and R_2? The maximum error in so doing would probably be about 5%. But we should not be speculating like this: we should attempt to determine why R_1 and R_2 vary. Some of the hypotheses that have been advanced are as follows.

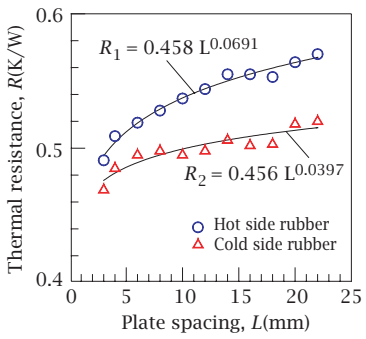

Figure 37 Thermal resistance versus plate spacing.

1. There are spurious convection currents. However, convective effects should increase with plate spacing

to yield a lower resistance and the opposite trend is observed. A quantitative estimate is impossible, but we could perhaps inject some dye to see if the fluid is stationary.

2. There is heat exchange between the water layer and the surroundings. Since the average water temperature is kept close to the ambient temperature, the heat flow will be as shown in Fig. 38. Notice that although the net heat exchange is zero, there is an augmentation of the heat flow recorded by the heat flux meters. For $L = 20\,\text{mm}$, $h_0 = 12\,\text{W/m}^2\,\text{K}$, $k_w = 0.5\,\text{W/m}\,\text{K}$, the heat flow is roughly estimated as

$$\dot{Q}_1 = UA_1\Delta T; \quad \Delta T = 8K; \quad A_1 = \pi D(L/2)$$

$$\frac{1}{U} \approx \frac{Ł_w}{k_w} + \frac{1}{h_0} = \frac{0.0095}{0.19} + \frac{1}{12}; \quad U = 7.5\,\text{W/m}^2\,\text{K}$$

$$\dot{Q} = (7.5)(\pi)(0.15)(0.01)(8) = 0.28\,\text{W}.$$

To explain the variation in R as L goes from 4 to 20 mm we are looking for an augmentation of about 10% in $\dot{Q}$, that is, $(0.1)(15) = 1.6\,\text{W}$. Thus, although $\dot{Q}_1$ has the correct sign, it is only about 18% of the value required to explain the increase in R. To further investigate this hypothesis the test cell was well insulated and additional data obtained, as shown in Fig. 39. The observed effect of the insulation is relatively small.

3. There is a zero-offset bias error in the spacing measurement. A simple calculation shows that a bias error of about $-0.5\,\text{mm}$ would explain the variation in R-values. However, if anything, we could expect a positive bias error due to distortion of the plates preventing tight closure—that is, when the dial gage indicates a plate spacing of 4 mm, the effective layer thickness is larger.

Use of the graphs of R_1 and R_2 to obtain appropriate values for the spacings used in the convection tests has an appealing logic. However, if heat exchange with the surroundings is the main issue, then this approach is flawed. At a given plate spacing, the temperature profiles through the system are very different for calibration versus testing. During calibration the temperature drop across the water layer is much larger than during testing, because convection reduces the thermal resistance of the layer. At the largest plate spacings the Nusselt number h_cL/k was about 10, indicating a temperature drop of 1/10 of that for pure conduction. Thus the temperature distribution in the system is quite different for testing versus calibration at the same layer thickness. To properly account for heat exchange with the surroundings a thermal model of the experimental system must be constructed. A simple model was proposed by Chang and Mills [1] and used with some success. Figure 40 shows a comparison with other experimental studies and the agreement is certainly good enough for engineering purposes. If greater accuracy is desired, then a complete numerical solution of the conduction equations governing heat flow in system components, is required. Alternatively, the test cell could be redesigned to minimize side effects.

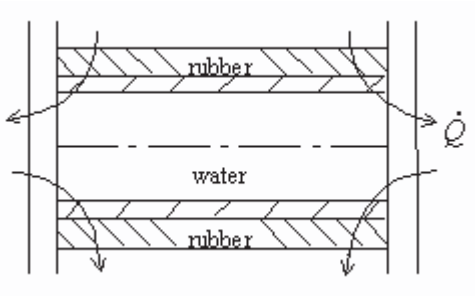

Figure 38 Heat flow sketch.

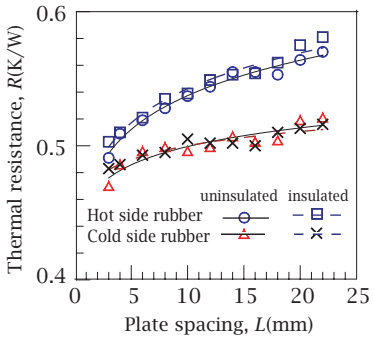

Figure 39 Comparison of thermal resistances for insulated and uninsulated test cell.

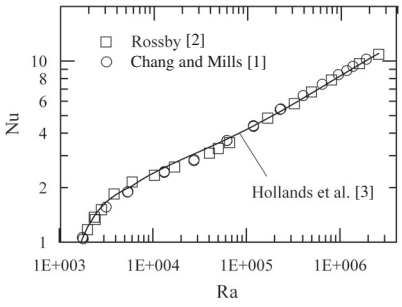

Figure 40 Nusselt number versus Rayleigh number for horizontal water layer.

References

[1] Rossby, H.T., "A studyo of Bernard convection with and without rotation," *J. Fluid Mechanics*, **36**, Part 2, 1309–1336 (1969).

[2] Hollands, K.G.T., Raithby, G.D. and Konicek, L., "Correlations for free convection heat transfer in horizontal layers of water and air," *Int. J. Heat Mass Transfer*, **18**, 879–884 (1975).

Case Study No 4. A Two-Stream Coaxial-Tube Heat Exchanger.

An undergraduate laboratory experiment requires the testing of a coaxial-tube heat exchanger. The unit is 2.50 m long, and has a 6.38 mm O.D. , 4.52 mm I.D. brass tube surrounded by a 9.63 mm I.D. glass tube. Recirculated hot water flows through the inner tube, and cold water from the laboratory supply flows through the outer tube and is dumped to a drain. The hot water is heated by electric heaters that can supply up to 3.5 kW. Flow rates of both streams are controlled by valves, and the direction of the cold stream can be reversed to give parallel or counterflow operation. Inlet and outlet water temperatures are measured by chromel–alumel (type-K) thermocouples connected to a digital thermometer. Flow rates of the two streams are measured by rotometers. Specifications for the instrumentation are as follows.

Flowmeters: 1. Cold stream. Maximum flow rate 0.231 kg/s. Accuracy = 2% of maximum flow rate = 4.62×10^{-3} kg/s. Least count = 2.31×10^{-3} kg/s.

2. Hot stream. Maximum flow rate 0.0976 kg/s. Accuracy = 2% of maximum flow rate = 1.95×10^{-3} kg/s. Least count = 9.76×10^{-4} kg/s.

Thermocouples: Calibration together in a constant temperature bath showed deviations no greater than ±0.1 K.

Digital Thermometer: Accuracy = 0.25 °C. Least count = 0.1 ° C

Notice that the calibration of the thermocouples was done with the digital thermometer: thus the manufacturer claim of a 0.25 K accuracy is conservative to the point of being meaningless in the temperature range of the experiment.

Example 14 presents a conventional propagation of precision error for a single test of the experimental rig. We now examine a comprehensive set of experimental data with a view of obtaining further insight into the precision errors, and, more importantly, to identify possible significant bias errors. Table 10 shows the results of a series of tests in which the capacity rate ratio $R_C = C_{\min}/C_{\max}$ was held constant at 0.496 while the flow rates were varied by more than a factor of 2.

Energy Balance. In Example 14 the data point considered was found to have a 3.7% discrepancy in the exchanger energy balance. In comment No. 3 following the example it was noted that $P_{(\dot{Q}_H - \dot{Q}_C)}$ was about the same as $(\dot{Q}_H - \dot{Q}_C)$, and hence the discrepancy could perhaps be attributed to precision errors. However, to reach a proper conclusion we must examine a set of energy balances and see how the discrepancy varies. The results for the energy balance discrepancies are shown plotted against $C_{\min}$ in Figure 41 (a plot against $C_{\max}$ would yield a similar result). A trend of an increasing discrepancy with decreasing $C_{\min}$ is seen. Also shown is a least squares curve fit

$$100(\dot{Q}_H - \dot{Q}_C)/\dot{Q}_H = -0.0361 C_{\min} + 10.29$$

which has a standard error of 1.03%. From Eq. (12), the midrange precision uncertainty for a single data point is $P_Y \cong 2S_Y = 2.1\%(C = 95\%)$. We can now conclude that the precision uncertainty in the energy balance is in fact relatively small, about ±2%. On the other hand, there is a clear bias error: $\dot{Q}_H$ exceeds $\dot{Q}_C$ by about 2% to 10%, the discrepancy increasing as flow rates decreases.

Effectiveness and Number of Transfer Units. Figure 41 also shows the discrepancies between measured and expected effectiveness and number of transfer units. For these calculations $\dot{Q}$ was taken to be $\dot{Q}_H$: use of $\dot{Q}_C$ gave larger discrepancies. Of course, this choice is somewhat arbitrary. Least square curve-fits and standard errors are

$$\% \text{ discrepancy in } \varepsilon : Y = -0.0396x + 4.756; S_Y = 0.506\%$$

$$\% \text{ discrepancy in } N_{tu} : Y = -0.0817x + 9.927; S_Y = 1.183\%$$

with corresponding precision uncertainties. Since ε and N_{tu} are related by the $\varepsilon - N_{tu}$ relation for a counterflow exchanger, the different values of S_Y for ε and N_{tu} reflect only the fact that $dN_{tu}/d\varepsilon$ is greater than unity in the $C_{\min}$ range tested.

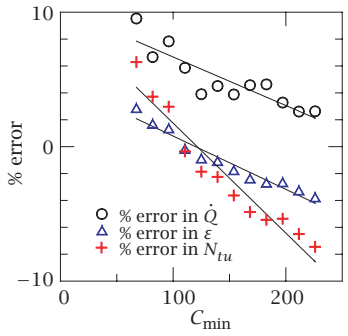

Figure 41 Errors in energy balance, effectiveness, and N_{tu} with variation of flow thermal capacity.

Sources of Bias Error. Figure 41 shows that there are bias errors in the results for $\Delta\dot{Q}$ of 2% to 8%, and for ε of −4% to +3%. Now, the first and most important observation to make is that these errors cannot be considered to be excessive, particularly in view of the relatively simple design of the rig and the robust, inexpensive, instrumentation. Nevertheless, it is of interest to attempt to identify possible sources of the bias errors.

Looking first at the flowmeter we recall that the manufacturer claims an accuracy of 2% of the maximum flow rate. For test No. 10 the resulting possible errors in the hot and cold flow rates are ±8.5% and ±10.0%, respectively. In this light, the corresponding error in the energy balance of 7.83% appears to be about what one may expect. Before proceeding any further to investigate possible sources of bias errors, the flow meters should be calibrated to, say, 0.5% accuracy. Nevertheless we will continue.

Table 10 Test data for a counterflow operation at fixed capacity rate ratio; $\dot{Q} = \dot{Q}_H$.

Test No	1	2	3	4	5	6	7	8	9	10
$T_{H,\text{in}}$(°C)	40.2	40.2	40.2	40.2	40.2	40.2	40.2	40.2	40.2	40.2
$T_{H,\text{out}}$(°C)	25.3	25.1	25	25	25	24.9	24.8	24.9	25	24.9
$T_{C,\text{in}}$(°C)	16.1	16	16.1	16.2	16.4	16.5	16.6	16.9	17.3	17.5
$T_{C,\text{out}}$(°C)	23.3	23.3	23.4	23.4	23.6	23.8	23.9	24.2	24.4	24.5
$\dot{m}_H$ (kg/s)	0.0541	0.0507	0.0472	0.0438	0.0403	0.0369	0.0334	0.0299	0.0265	0.023
$\dot{m}_C$ (kg/s)	0.1089	0.1019	0.095	0.088	0.0811	0.0741	0.0672	0.0602	0.0533	0.0463
Hot, heat loss (W)	3367.2	3195.3	2997.8	2779.3	2558.2	2354.3	2147.6	1913	1680	1471.1
Cold, heat gain (W/K)	3278.5	3111.9	2899.6	2650.6	2441.2	2262.9	2050.7	1838.4	1581.6	1355.9
% difference	2.63	2.61	3.28	4.63	4.57	3.88	4.51	3.9	5.86	7.83
C_H (W/K)	226	211.6	197.2	182.8	168.3	153.9	139.5	125	110.5	96.1
C_C (W/K)	455.3	426.3	397.2	368.1	339.1	310.0	280.9	251.8	222.8	193.7
R_C	0.496	0.496	0.496	0.497	0.496	0.497	0.496	0.496	0.496	0.496
ε, experiment	0.618	0.624	0.631	0.633	0.639	0.646	0.653	0.657	0.664	0.674
ε, expected	0.642	0.645	0.648	0.651	0.654	0.657	0.66	0.662	0.665	0.665
% difference	−3.77	−3.26	−2.65	−2.68	−2.37	−1.75	−1.07	−0.88	−0.16	1.36
N_{tu}, experiment	1.184	1.206	1.232	1.243	1.264	1.293	1.322	1.339	1.37	1.417
N_{tu}, expected	1.28	1.29	1.302	1.314	1.329	1.341	1.352	1.365	1.375	1.376
% difference	−7.45	−6.5	−5.36	−5.44	−4.86	−3.63	−2.25	−1.86	−0.35	2.97
$UA(N_{tu})$ (W/K)	267.6	255.2	243.0	227.2	212.7	199.0	184.4	167.4	151.4	136.2
$UA(\Delta T_{\ell m})$ (W/K)	266.0	253.6	241.1	224.6	210.3	196.8	182.2	165.7	149.1	133.3
% difference	0.6	0.6	0.8	1.1	1.2	1.1	1.2	1.0	1.5	3.8

In discussing the discrepancies in the energy balance, the first cause students suggest is that the cold stream is losing heat to the surroundings. However, the average temperature of the cold stream is 20–21 °C, which is typically the ambient temperature. Thus a net loss to the surrounding is unlikely. Some days the average cold stream temperature is above the ambient temperature and a numerical estimate of heat loss is made. For an extreme case, an average ΔT of 5 K is used, with an outside convective plus radiative heat transfer coefficient of $10\,\text{W/m}^2\,\text{K}$. Then for an outer wall thickness of 1 mm and thermal conductivity of $1.4\,\text{W/m K}$, and a negligible inside convective resistance, the overall heat transfer coefficient is approximately

$$\frac{1}{U} \cong \frac{0.001}{1.4} + \frac{1}{10}; \quad U = 9.9\,\text{W/m}^2\,\text{K}.$$

The heat loss from the outside of the outer tube of area $0.13\ \text{m}^2$ is then

$$\dot{Q} = (9.9)(0.13)(5) = 6.5\,\text{W}$$

clearly this heat loss is negligible compared to the discrepancy in the energy balance. Indeed, the exchanger is not insulated *because* the heat transfer interaction with its surroundings is negligible.

In designing the test rig a decision was made to simply place thermocouples in the center of the flow streams. For turbulent flow the centerline temperature was expected to be a good approximation to the bulk temperature. In checking out the experiment, the initial results were deemed good enough and thermocouple location as a possible source of bias error was not further explored. In the current study the impact of thermocouple location was explored by varying the precise location of the thermocouples. Small changes in the results were seen, but too small to have any significant consequence on the energy balance discrepancy. Turning our attention to the thermocouples themselves, calibration in a constant temperature bath indicated bias errors of the order of 0.1 °C. Recall that the precision error analysis of Example 14 had a precision error of ±0.1 °C for the temperatures. For a quick estimate of the impact of a bias error of 0.1 °C, we note that a worst case for Test 10 would give $\Delta T_C = 6.8\,\text{K}$ instead of 7 K to give an error in $\dot{Q}_C = 2.9\%$. However, this bias error would be essentially the same for all the tests and hence cannot explain the variation of $\Delta\dot{Q}$ with flow rate.

Added insight is obtained if we view UA as the parameter of concern. Then UA can be calculated from either N_{tu}, or the log mean temperature difference $\Delta T_{\ell m}$. In the former case $T_{C,\text{out}}$ is not used, whereas in the latter case it is. A comparison is shown in Table 10, where it is seen that the discrepancy in UA calculated by the two different methods varies from 0.6 to 3.8%, increasing as the flow rate decreases. This results suggests that portion of the bias errors must be attributed to the temperature measurements.

We conclude that both the flow and temperature measurements could be sources of the bias errors noted in the

results. To further explore these issues it would be necessary to calibrate the flowmeter to at least 0.5% accuracy, and to explore variations in the thermocouple installations. Our chief concern should be the energy balance. The discrepancies between experimental and expected ε and N_{tu} values are probably no larger than the accuracy of the heat transfer correlations used to calculate the expected values.

Case Study No. 5 The Evaporation Coefficient of Water

It is usually possible to assume thermodynamic equilibrium at a liquid–vapor interface during phase change. Then the liquid surface temperature can be related to the pressure of the adjacent vapor as $T_s = T_{\text{sat}}(P_v)$, and obtained from thermodynamic vapor pressure tables. However, the assumption of thermodynamic equilibrium is invalid at low pressures and high rates of phase change. A simple kinetic theory model (see, for example [1] pp. 719–722) gives a result that relates P_v and T_S to the rate of phase change $\dot{m}''$,

$$\dot{m}'' = \frac{2\sigma}{2-\sigma}\left(\frac{P_v}{(2\pi RT_v)^{1/2}} - \frac{P_s}{(2\pi RT_s)^{1/2}}\right) \quad [\text{kg/m}^2\text{s}]$$

where P_s is $P_{\text{sat}}(T_s)$, and σ is the *evaporation* or *condensation* coefficient (assumed equal). This coefficient is defined as the fraction of vapor molecules incident on the liquid surface that actually condense: a fraction $(1-\sigma)$ are specularly reflected.

Experiments conducted with water in the 1920's and 1930's obtained very low values of σ, in the range of 0.004–0.04. Such low values would have a serious impact on the design of steam condensers operating with low coolant temperatures, for example, when sea water at extreme latitudes is used as coolant. In succeeding years there have been numerous experimental and theoretical studies of the condensation coefficient for water (about 50 experimental studies have been reported with results ranging from 0.001 to 1.0). A close examination of these experiments is an object lesson on the role played by bias errors in falsifying experimental data. Indeed, it is a lesson on how the scientific literature avoids proper discussion of possible bias errors even when there is evidence that bias errors are a critical issue. In this case study we will examine a few of the most important experiments, from the point of view of bias error. When determining σ the key measurement is T_s, the liquid surface temperature, which is used to obtain $P_s = P_{\text{sat}}(T_s)$ from steam tables. The pressure of the vapor P_v can be accurately measured quite easily, and the vapor temperature T_v can be approximated by T_s with negligible error [2]. The phase change rate $\dot{m}''$ can also be measured quite accurately in most situations. The various experiments to be discussed differ in how T_s was measured.

Hickman [3]

Water was evaporated from a high speed 3.5 mm diameter, 17 mm long jet: the speeds used gave residence times for the water varying from 0.001 to 0.023 s. In a typical run the water entered at 7.5 ℃ and left at a bulk temperature of 7.2 ℃, the test chamber being maintained at 1 mm Hg pressure. In processing the data, P_s and T_s were evaluated at the average bulk temperature along the jet. It was realized that the surface temperature had to be lower than the bulk temperature in order for the enthalpy of vaporization to be transferred to the jet surface. Figure 42 shows the expected temperature profile. Empirical corrections were duly made and estimates of σ between 0.23 and 0.35 reported.

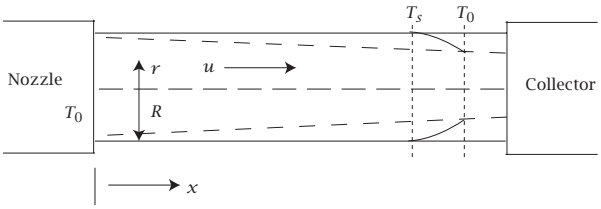

Figure 42 Thermal boundary layer growth in a laminar jet.

However, a proper heat transfer analysis allows the surface temperature to be calculated quite reliably. To model heat transfer in the jet the following assumptions are reasonable:

- Laminar flow.
- The water velocity u is constant across the jet (plug flow).
- The jet cross-sectional area is constant.
- Liquid properties are constant.
- Heat conduction in the axial direction is negligible.

The energy conservation equation for the jet is then

$$u\frac{\partial T}{\partial r} = \alpha\left(\frac{\partial^2 T}{\partial r^2} + \frac{1}{r}\frac{\partial T}{\partial r}\right)$$

with initial condition $T = T_0$, and boundary condition

$$k\left.\frac{\partial T}{\partial r}\right|_{r=R} = h_i\,(T_s - T_C)$$

where h_i is the interfacial heat transfer coefficient,

$$h_i = \frac{2\sigma}{2-\sigma}\left(\frac{2}{\pi RT_s}\right)^{1/2}\frac{\rho_v h_{fg}^2}{T_s} \quad [\text{W/m}^2\,\text{K}]$$

and is derived in Section 7.6 of Reference [1]. It is straightforward to solve this heat conduction problem numerically using finite difference methods. However, the first solution was an approximate one, for which a thin thermal boundary layer was assumed to reduce the problem to an analog of heat conduction in a semi-infinite slab; also h_i was assumed constant at an average value along the jet [2, 4]. The results showed that the surface temperature falls to much lower values than estimated by Hickman, and that $\sigma = 1$ gave a good fit to the experimental data. A value of $\sigma = 0.35$ yields evaporation rates that are only 50% of

those measured, and a value of 0.035 would be impossible. Subsequently, Maa working in Hickman's laboratory [5], and Davies, et al. [6], performed similar experiments, used a heat transfer analysis to obtain the surface temperature, and obtained values of $\sigma = 0.8$ and 1.0, respectively. Thus we can conclude that the original results of Hickman were falsified by a large bias error due to an overestimate of the jet surface temperature T_s: with T_s too high, σ was always too low.

Alty [7]

In this very early study, water was evaporated from a drop forming on the end of a copper pipette, the drop falling into a beaker to sink below a layer of oil to prevent further evaporation. The drop size at detachment was used to infer the surface tension of the water at the pipette, and hence the surface temperature of the water adjacent to the pipette. The droplet surface was assumed to be uniform at this temperature during the evaporation process. The evaporation rate $\dot{m}''$ was inferred from the water supplied to the pipette and the final droplet mass. The vapor phase pressure P_v and temperature T_v were accurately measured, and $P_s(T_s)$ obtained from steam tables. Again the success or failure of the experiment depended on whether the possible bias error in T_s was acceptably small. Yet, nowhere in the paper was this issue ever mentioned!

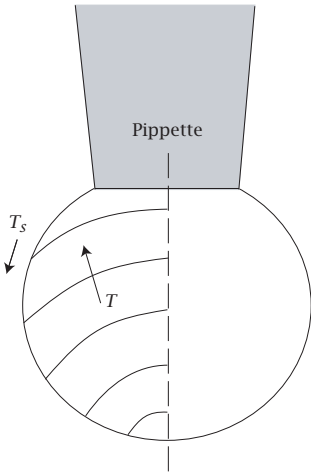

Figure 43 Possible temperature profiles in an evaporating droplet.

The experiment is deceptively simple in appearance: in reality the heat transfer problem is very complex. Copper has a thermal conductivity three orders of magnitude greater than that of water, thus, the temperature deduced from surface tension is the temperature of the copper pipette along the attachment line. Since typically 0.37 of the total drop weight was evaporated, most of the enthalpy of vaporization was supplied by conduction along the copper pipette and in the droplet. Hence there were large temperature gradients in the drop root and across the droplet. Figure 43 shows possible isotherms. The droplet surface cannot be isothermal. In contrast to the configuration of Hickman, a heat transfer analysis is now very difficult. It is a time dependent problem, and there is possibly a surface tension driven flow due to the surface temperature gradient. A simple calculation assuming steady conduction and a uniform surface temperature (as assumed by Alty) shows that temperature gradients of the order of 500 K/mm are required. Since these gradients are impossible, the real heat transfer problem is quite different. Now, 70 years later, it should be possible to use numerical methods to solve a good model of the heat transfer process and obtain the true surface temperature of the droplet: but such an effort is not worthwhile. The experimental technique is essentially impractical and should be discarded. Since the actual droplet temperature must be lower than the pipette temperature, there is a bias error in the value of T_s used, leading to low values of σ. Alty obtained very low values for σ, typically 0.036. In light of the large temperature gradients that must have been present in the drop, such a result is not surprising.

Delaney, et al. [8]

A shallow pool of water was located on top of a copper block as shown in Figure 44. The rate of evaporation was determined by measuring the rate of pressure rise in a known volume of chamber above the pool, and the surface temperature of the liquid was measured using a thermistor probe. The validity of the experimental result of $\sigma = 0.042$ at $T_S \approx 0\,^{\circ}\mathrm{C}$ is dependent on whether the thermistor could measure the true effective surface temperature. At the start of a test run the top edge of the thermistor was at the level of water surface. During the time data was recorded the level dropped about 0.1 mm, which can be compared with a height of the thermistor bead of 0.25 mm. Initially the thermistor can only measure the temperature at a depth below the surface equal to one half its immersion, namely 0.125 mm. Furthermore, as the upper edge of the thermistor breaks the surface it cannot measure a temperature much closer to the surface since the larger underside of the bead will tend to determine the average temperature of the bead. Also, due to the presence of the bead locally preventing evaporation, the temperature underneath the bead must be higher than that water at the same depth below an evaporating surface.

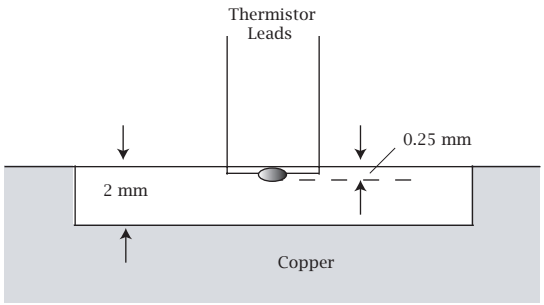

Figure 44 Evaporation from a pool in a copper block [9].

For purposes of estimating a possible bias error it will be assumed that, at best, the bead measures a temperature 0.125 mm below the water surface. To process the data Delaney assumed a uniform surface temperature, which is consistent with one dimensional heat transfer across the pool (by conduction since the Rayleigh number proves to be too small for natural convection to occur). Thus the temperature gradient across the pool is estimated at

$$\frac{dT}{dz} = -\frac{\dot{m}'' h_{fg}}{k_\ell} \text{K/m}$$

and the thermistor temperature is corrected as

$$T_s = T_{th} + \left(1.25 \times 10^{-3}\right) \frac{dT}{dz}$$

to give an estimate of the true water surface temperature. When this was done in reference [4] the corrected values of $(P_s - P_v)$ varied from −0.20 to 0.27 mm Hg—whereas Delaney's uncorrected values varied from 1.66 to 0.66 mm Hg. Since the corrected values straddle zero, and negative values are impossible for evaporation, the only conclusion is that σ is large and cannot be determined using this technique. A subsequent investigation in the same laboratory [9] obtained values ranging from 0.065 to 0.665, which supports the above assessment.

Nabavian and Bromley [10], Mills and Seban [2]

The interfacial heat transfer coefficient is associated with an interfacial heat transfer resistance $R_i = 1/h_i A_S$. From an engineering viewpoint, the issue is whether this interfacial resistance is significant and should be included in the thermal circuit representing the complete heat transfer process. In a steam condenser the circuit includes thermal resistances of the condensate film, tube wall, coolant and noncondensable gas, if present (see, for example, Example 2.9 of reference [11]). We denote the sum of the resistances as $\sum R$; then if R_i is small relative to $\sum R$ it can be ignored. The magnitude of h_i is small at low pressures due to the low vapor density ρ_V, and small if σ is small; correspondingly R_i is then large. If calculations are made for condensers operating with coolant water at about 5 °C, $\sigma = 0.02 - 0.04$ results in values of R_i large enough to have a significant effect on the design. On the other hand, values of σ greater than 0.2 or 0.3 gives values of R_i small enough to be neglected. Thus, although physical chemists might be very interested with the precise values of σ, engineers are only concerned if it is higher than 0.2–0.3. If it is, its precise value is not relevant. It was with this viewpoint that Nabavian and Bromley [10], and Mills and Seban [2], designed experiments that would show unambiguously whether σ was higher than 0.2–0.3. If σ was indeed small then the experiments could yield precise values of σ. If σ was higher than 0.2–0.3, no precise value could be inferred, but then the precise value was irrelevant to the engineering problem.

Associated with the thermal resistances are temperature drops. Figure 45 shows the circuit and temperature profile for the experiment in reference [2]. Low pressure steam was condensed on the front of a 12.7 cm high copper block with coolant passed along the back of the block. An array of thermocouples in the block allowed the surface temperature of the block to be estimated and the heat flow to be calculated. The heat flow was checked by a coolant energy balance and by collecting the condensate. The thermal resistance of the film was calculated using the well known result of Nusselt for film condensation on a vertical surface, given by Eq. (7.16) of BHMT. For a typical test relevant data includes:

$$\begin{aligned} \dot{Q}/A &= 33.9 \times 10^4 \text{W/m}^2 \\ T_{\text{sat}} &= 10.1^\circ\text{C} \\ T_{\text{w}} &= 5.7^\circ\text{C} \end{aligned}$$

Nusselt film condensation theory given $\Delta T_{\text{film}} = 4.2$ K, thus

$$\Delta T_i = (T_{\text{sat}} - T_{\text{w}}) - \Delta T_{\text{film}} = 4.4 - 4.2 = 0.2 \text{ K}.$$

However, the interfacial temperature drop $(T_{\text{sat}} - T_s)$ for $\sigma = 0.036$ is predicted to be 4.2 K. Clearly σ cannot be as low as 0.036.

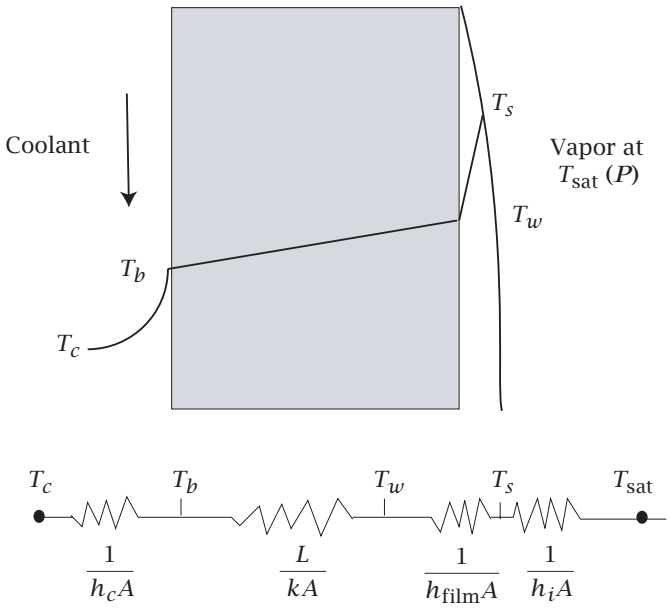

Figure 45 Temperature profile and thermal circuit for the experiment of Mills and Seban [2]

For the 10 tests reported, ΔT_i was measured to vary from −0.6 K to +0.2 K, with a mean value of −0.27 K and a precision uncertainty of the mean $P_{\overline{X}} = 0.26$ K at the 95% confidence level. Of course, ΔT_i cannot be less than zero on physical grounds, but the indicated bias error is small and within the bias errors that may be expected for the key measurements. The results show that the interfacial resistance is indeed negligible, but as a consequence does not yield a precise value of σ. A value of $\sigma > 0.45$ was concluded; similarly, Nabavian and Bromley concluded $\sigma > 0.35$.

Concluding Comments

Case Study 5 illustrates the importance of attempting to quantitatively estimate bias errors. In Hickman's experiment the bias error could be accurately estimated and the technique proves adequate for determining σ when σ is large. On the other hand, in the experiments of Alty and of Delaney (and many others), it can be clearly shown that bias errors in determining the surface temperature are sufficient to give large errors in the measured values of σ. However, the complexity of the heat transfer processes do not allow these bias errors to be satisfactorily estimated, and thus these experiments must be disregarded. The experiments of Nabavian and Bromley, and Mills and Seban were initiated at a time when it was generally accepted that σ was very low for water: Alty's value of 0.036 was usually quoted. These experiments were designed to show unambiguously whether σ could be that low in the actual situation of engineering concern, namely, a low pressure condenser. The results showed that σ could not be lower than about 0.35–0.45, and hence the precise value was of no engineering importance.

In examining the many studies that yielded low values of σ, it is seen that little or no attention was was given to evaluating bias errors. In designing their experiments, the investigators should have asked the question, "How accurately must the surface temperature be measured in order to have a successful experiment?" Then some quantitative estimates of possible bias errors in their measurement technique should have been made. But what is really disturbing is how this situation has been dealt with in the many review articles that have been published up to the present time. There are obvious anomalies in data for σ, yet little or no attempt is made to subject the data to error analysis, and then reject data that cannot be defended. The results of Alty are still displayed prominently. The original results of Hickman at $\sigma = 0.23 - 0.35$ are still given equal weight to the corrected values indicating $\sigma = 0.8 - 1.0$, even when some of the corrected values are in reports from Hickman's own laboratory!

This case study certainly illustrates the statement made in §2, namely, "Precision errors can be a nuisance, a gross bias error can be a catastrophe!"

References

[1] Mills, A.F., *Heat Transfer*, Prentice-Hall, New Jersey, 1999.

[2] Mills, A.F. and Seban, R.A, "The condensation coefficient of water," *Int. J. Heat Mass Transfer* **10**, 1015–1827 (1967).

[3] Hickman, K.C., "Maximum evaporation coefficient of water," *Ind. Engrg. Chem.* **46**, 1442–1446 (1954).

[4] Mills, A.F., The Condensation of Steam at Low Pressures, Ph.D. Thesis, Technical Report Series No. 6, Issue No. 39, Space Sciences Laboratory, University of California, Berkeley (1965).

[5] Maa, J.R., "Evaporation coefficients of liquids," *Ind. Eng. Chem Fund* **6**, 504–518 (1967).

[6] Davies, E.J., Chang, R., and Pethica, B.D., "Interfacial temperatures and evaporation coefficients with jet tensimetry," *Ind. Eng. Chem. Fund.* **14**, 27–33 (1975).

[7] Alty, T., "The maximum rate of evaporation of water," *Phil. Mag.* **15**, 82–103 (1933).

[8] Delaney, L.J., Houston, R.W., and Eagleton, L.C., "The rate of vaporization of water and ice," *Chem. Eng. Sci.* **19**, 105–114 (1964).

[9] Bonacci, J.C., Myers, A.S., Norgbi, G., and Eagleton, L.C., "The evaporation and condensation coefficient of water, ice and carbon tetrachloride," *Chem. Eng. Sci.* **31**, 609–617 (1976).

[10] Nabavian, K., and Bromley, L.A., "Condensation coefficient of water," *Chem. Eng. Sci.* **18**, 651–660 (1963).

[11] Mills, A.F., *Mass Transfer*, Prentice-Hall, New Jersey, 2001.

Case Study No. 6. Average Heat Transfer for a Cylinder in Cross-Flow

Case Study No. 5 dealt with bias errors that resulted from faulty measurements of the surface temperature of evaporating water. In this case study we deal with bias errors that result from an incomplete understanding of the physical phenomena being investigated. In Case Study No. 1 we looked at measurements of stagnation line heat transfer on a cylinder in cross-flow of air. We now look at average heat transfer for the cylinder, as well as local heat transfer distributions around the cylinder. In particular we will examine the role played by "nuisance" variables, that is, variables that may not be identified or controlled, and yet have significant effects.

All standard heat transfer textbooks present correlations for the average heat transfer coefficient for a single cylinder in cross-flow. For example, BHMT gives the correlations recommended by Churchill and Bernstein [1] in the form

$$\overline{\mathrm{Nu}}_D = f(\mathrm{Re}_D, \mathrm{Pr}). \tag{45}$$

BHMT Section 4.2.3 also describes how an experiment to obtain $\overline{\mathrm{Nu}}_D$ might be performed in a wind tunnel. It is used to specify the range of Reynolds number over which the correlation is valid (although an accuracy is almost never specified). The Reynolds number is an obvious variable that affects the flow field, and hence the Nusselt number. But are there other variables that affect the flow? All the experimental data has been obtained in wind tunnels and in first instance, three variables can be identified:

1. The level of turbulence in the oncoming flow.
2. The aspect ratio of the cylinder, i.e., width of tunnel divided by cylinder diameter, $AR = L/D$ assuming the cylinder spans the tunnel.
3. The blockage ratio, i.e., the cylinder diameter divided by tunnel height, $B = D/H$.

Average heat transfer tends to increase with increases in these three parameters. In the limit of zero turbulence, infinite AR and zero B we have the situation of a very long cylinder moving through the undisturbed atmosphere, and it is this situation that is imagined by most readers of these texts. But the data has been obtained in real wind tunnels so we must ask whether these limiting conditions effectively existed in the experiments. Another variable is the surface condition of the cylinder—is it smooth or rough? Again it is usually imagined that the surface is smooth though no quantitative assessment is given. Then there are variables related to thermal issues:

1. The effect of variable fluid properties.
2. The effect of the wall thermal boundary condition.

The larger the temperature difference between the wall and free-stream, the more important are the effects of fluid property variations across the flow, particularly viscosity variation. However, this issue is common to all convective situations and is usually adequately handled in these texts. Either properties are evaluated at the mean film temperature, or property ratio correction factors are specified (see BHMT §4.2.4). It is usual to have either an approximately uniform wall temperature or uniform heat flux around the circumference of the cylinder. The local heat transfer coefficient variation around the cylinder depends on this wall boundary condition. Furthermore, it is not meaningful to calculate an average heat transfer coefficient in the usual manner for a uniform wall heat flux (see BHMT Eq. (4.82)).

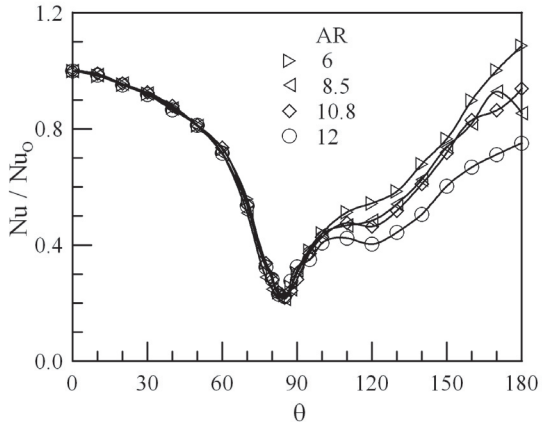

Figure 46 Centerline local Nusselt number around a cylinder in crossflow. $Re_D = 33,740$, aspect ratios AR from 6 to 12 [1].

These secondary or "nuisance" variables greatly complicate what appeared to be a rather simple convective heat transfer situation. They were not discussed in Case Study No. 1 because, except in more extreme situations, they have no effect on stagnation line heat transfer: it is the local distribution around the cylinder and the resulting average value that is affected. In the case of aspect ratio, the characteristic feature is a significant increase in local heat transfer coefficients on the rear of the cylinder, and a resulting increase in the average heat transfer. Figure 46 shows distributions of the local Nusselt number, normalized by the stagnation line value, at the centerplane for aspect ratio varying from 12 to 6. (For $AR < 12$ the aspect ratio effect is essentially negligible.) A number of experimental studies have been reported in the literature giving data taken at small aspect ratios, without the investigators being aware of the effect of aspect ratio. It is this type of bias error that can greatly reduce the value of an experimental study. Researchers are not infallible—we all make errors due to a less than complete understanding of our work. The important lesson is to critically examine all aspects of a problem so as to minimize the risk of having an unknown bias error.

J.

Case Study No. 7 Single-Phase Flow in Microchannels.

Microchannel heat sinks have received much attention owing to their promise for effective heat removal from space constrained electronic devices. Channels of hydraulic diameters in the range of 50–1000 μm are considered. Smaller sizes have higher heat transfer coefficients but the associated large pressure drops cannot satisfy pumping constraints. BHMT [1], Exercises 8-88 to 8-91 illustrate design considerations for microchannel heat sinks. The designer requires appropriate correlations for friction factor and Nusselt number, and physical considerations suggest that the usual continuum correlations should apply: see, for example, the correlations given in Section 4.3.1 of BHMT [1]. Research to confirm the validity of these correlations for microchannel flow commenced in the 1980's and numerous studies were reported in the 1990's and to the present time. A review of this work provides a striking example of how bias errors can cause utter confusion and considerable waste of time and money.

Early experimental studies, e.g. Wu and Little [2] and Choi, et al. [3] showed large deviations from the conventional theory and correlations for both laminar and turbulent flow. Such results led to a commonly held view that there were physical phenomena peculiar to microchannel momentum and heat transfer. In their 1999 review article, Ho and Tai [4] state "…the unique features in micromechanics are perhaps the most intriguing ones for the researchers in basic fluid mechanics." In 2004 Nakayama [5] introduced a special issue of *Heat Transfer Engineering* devoted to microscale technologies for electronics cooling and wrote "…but there remains controversy as to possible involvement of some novel physical processes in microscale dimensions."

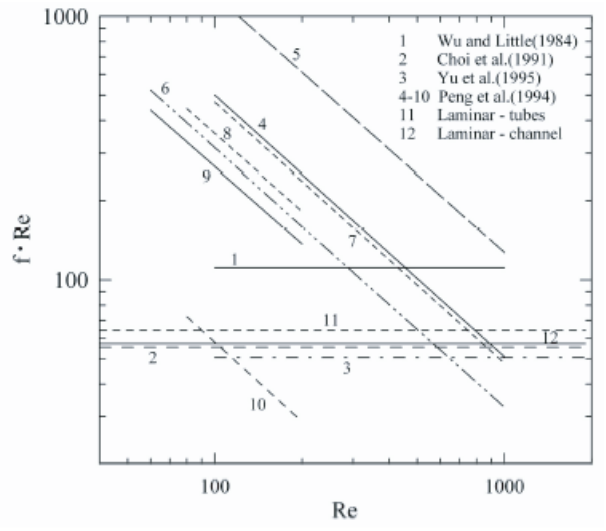

Figure 47 Comparison of experimental and theoretical friction factors for laminar flow in microtubes and microchannels [6].

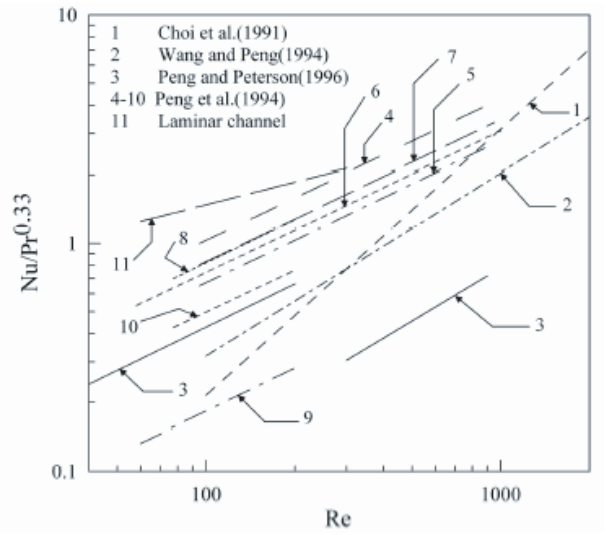

Figure 48 Comparison of experimental and theoretical Nusselt numbers for laminar flow in microchannels and microtubes [6].

These anomalous experimental results encouraged other workers to perform more experimental studies, and to do analytical and numerically modeling that might shed light on the observed behavior. However, the new experimental results did not agree with earlier results: each new study gave different results! Figures 47 and 48 show a comparison of experimental results for friction factor and Nusselt number for laminar flow presented by Garimella and Singhal [6]. There is no agreement with respect to absolute values, or trends with Reynolds number: the experimental friction tends to be much higher than theory, whereas the heat transfer is lower. If one looks at data from any particular study, it will be seen that the scatter (random error) is much smaller than the discrepancies shown in Figs. 47 and 48. Figure 49 shows a sample. Thus we must conclude that the experimental data is falsified by a variety of bias errors. Random error is simply not an issue and need not be discussed further.

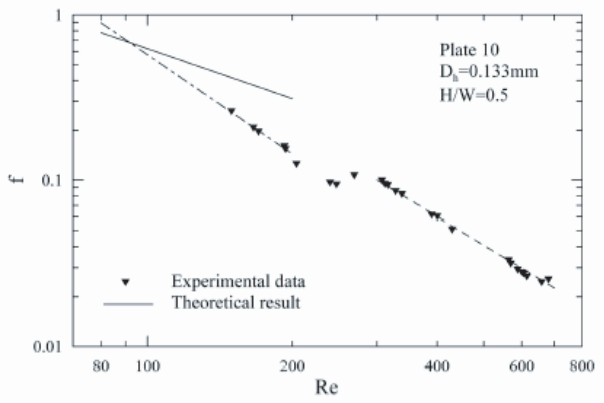

Figure 49 Comparison of experimental and theoretical friction factors for laminar flow in a microchannel with a hydraulic diameter of 0.133 mm [12].

How should one proceed to resolve such anomalous behavior? One should not just try another experimental study. What is needed is a critical examination of the reported studies in an attempt to identify possible sources of bias error. The most fortunate of situations is when a bias error is identified and the original experimental data can be reprocessed or reinterpreted to give the suspected true result. Herwig and Hausner [7] did just this for experimental heat transfer data reported for laminar flow in microtubes by Tso and Mahulikar [8]. They showed that axial conduction in the fluid and the block containing the microtubes could not be ignored. Using a standard CFD code to solve the conjugate heat transfer problem they found that the experiment indeed gave Nusselt numbers close to the theoretical value of 4.36 over the central part of the tubes: deviations at each end resulted from axial conduction effects. Often experimental studies are poorly reported and identification of possible bias errors is difficult: such studies should be discarded as unverifiable. Sometimes the manner in which the experimental work was carried out suggests that the results should be viewed with some skepticism. For example, in the series of papers by Peng, et al. [9, 10, 11, 12] key definitions change from paper to paper without any explanation for these changes. Also how some key measurements were made is not explained. Again such studies should be discarded. In contrast, there have been some carefully designed and performed experiments that show good agreement with accepted theory and correlations. Figure 50 shows a sample of friction factors taken for laminar flow reported by Garimella and Singh [6].

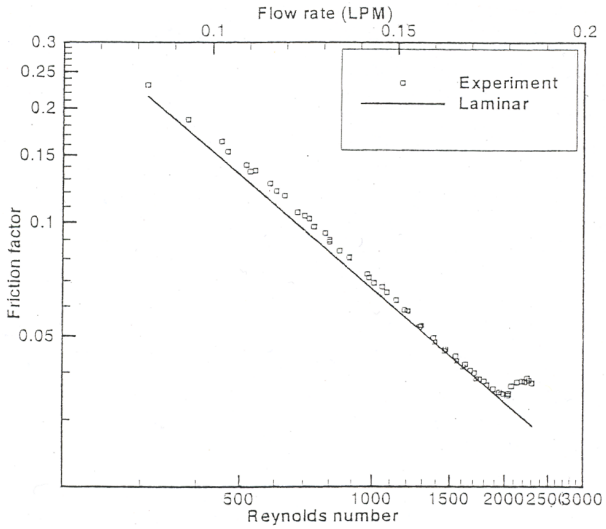

Figure 50 Friction factor versus Reynolds number. Hydraulic diameters of 974 μm and 324 μm.

In the foregoing experimental work the objective was to obtain friction factors and Nusselt number data for flow in microchannels: the experimental apparatus was usually designed to facilitate this objective. The idea was that such data could be used to design optimal heat sinks, as shown in Exercise 89 of BHMT [1]. Given the difficulties encountered one could argue that it would have been cost effective to test a range of prototypes of expected near optimal configuration (in particular, channel widths). Such tests would be relatively simple. The only key measurements are power dissipated by the electronic device on the heat sink, its temperature, the coolant flow rate and coolant inlet temperature. In this manner bias errors introduced through the configuration of the experimental apparatus, for example in the Tso and Mahulikar experiment [8] are avoided.

References

[1] Mills, A.F., *Basic Heat and Mass Transfer*, Prentice-Hall, New Jersey, 1999.

[2] Wu, P.Y. and Little, W.A., "Measurement of friction factor for the flow of gases in very fine channels used for microminature Joule–Thompson refrigerators" *Cryogenics*, **23**, 273–277 (1983).

[3] Choi, S.B., Barron, R.F., and Warrington, R.O., "Fluid flow and heat transfer in microtubes" *Micromechanical Sensors, Actuators and Systems*, ASME DSC **32**, 123–134 (1991).

[4] Ho, C-M., and Tai, Y-C., "Micro-electro-mechanical systems (MEMS) and fluid flows" *Annu. Rev. Fluid Mech.* **30**, 579–612 (1998).

[5] Nakayama, W., "Micro-scale technologies for electronics cooling" *Heat Transfer Engineering* **25**(1), 1–3 (2004).

[6] Garimella, S.V., and Singhal, V., "Single-phase flow and heat transport and pumping considerations in microchannel heat sinks" *Heat Transfer Engineering* **25**(1), 15–25 (2004).

[7] Herwig, H., and Hausner, O., "Critical view on new results in micro-fluid mechanics" *Int. J. Heat Transfer* **46**, 935–937 (2003).

[8] Tso, C.P., and Muhulikar, C.P., "Experimental verification of the role of Brinkman number in microchannels using local parameters" *Int. J. Heat Mass Transfer* **43**, 1837–1849 (2000).

[9] Wang, B.X., and Peng, X.F., "Experimental investigation on liquid forced convection heat transfer through microchannels" *Int. J. Heat Mass Transfer* **37** Suppl. 1, 73–82 (1994).

[10] Peng, X.F., Wang, B.X., Peterson, G.P., and Ma, H.B., "Experimental investigation of heat transfer in flat plates with rectangular microchannels" *Int. J. Heat and Mass Transfer* **38**, 127–137 (1995).

[11] Peng, X.F., and Petersen, G.P., "The effect of thermofluid and geometrical parameters on convection of liquids through rectangular microchannels" *Int. J. Heat and Mass Transfer* **38** 755–758 (1955).

[12] Peng, X.F., and Peterson, G.P., "Convective heat transfer and flow friction in microchannel structures" *Int. J. Heat Mass Transfer* **39**, 2599–2608 (1996).